

CHAPTER ONE

INTRODUCTION

1.1 Overview

Aluminium alloys are conventional materials that are widely used in diverse applications such as aviation, marine, transport, electrical equipment, automotive. The advantages of using aluminium alloy are their relative low cost, light weight material and easily machined by both traditional and non-traditional machining processes [1]. Aluminium alloy 6061 (Al 6061) was used in this research as a benchmark material due to its good machinability.

The machinability of 30% (by volume) of alumina (Al_2O_3) reinforced aluminium metal matrix composite using electro-discharge machining is assessed in comparison with Al 6061.

Aluminium metal matrix composites (AMMC) are aluminium-based metal matrix reinforced by metal, ceramic or polymer. AMMC offer a number of advantages compared to their base metal, such as higher specific strength, modulus of elasticity and good resistance at elevated temperature. However, they are more expensive and have lower toughness compared to their base metals [1]. AMMCs have been applied in aviation, marine, automotive parts as diesel engine pistons, cylinder and brake components though their use is limited due to difficulty in machining, which is due to high abrasiveness of the reinforcing constituents present in composite material [2]. The AMMC being investigated in this research is 30% of Al_2O_3 reinforced aluminium metal matrix composite machined by electro discharge machining (EDM). The difficulty in machining AMMC using non-traditional machining methods motivates the investigation for other feasible alternative such as non-traditional machining

methods using EDM. EDM is a thermal machining process that generates electrical spark between the workpiece and tool to remove material from the workpiece with no mechanical cutting force, [3]. EDM is known as an effective process for machining of hard materials which are good electrical conductors.

EDM can be mainly categorized as die-sinking EDM and wire-cut EDM. In die-sinking EDM, a three dimensional electrode creates its own reverse image in the workpiece. In wire-cut EDM, a long thin metal travelling through workpiece serves as an electrode to machine the workpiece. According to the preliminary test conducted on the wire-cut and die-sinking EDMs, the feasibility of die-sinking EDM machining on 30% Al₂O₃ reinforced aluminium metal matrix composite is better compared to that wire-cut EDM. Key process parameters of EDM such as the peak current, ON-time (pulse duration) and OFF-time (pause duration) are varied to analyze their influences on 30% Al₂O₃ reinforced AMMC. The affect of these parameters on 30% Al₂O₃ reinforced AMMC are compared with those of Al 6061. The outputs analyzed are the surface roughness (Ra), material removal rate (MRR), tool wear ratio (TWR), overcut (OC), surface morphology and thickness of affected layer.

The significance of this research is to study the machinability of AMMC using EDM and the information can be used in the research and also in the industries for machining of AMMC.

1.2 Problem Statement

EDM has been successfully applied for machining conventional aluminium alloy but its application to 30% alumina reinforced AMMC yet to be explored. This research is to investigate the machinability of AMMC using EDM with copper electrode by analyzing the surface roughness, material removal rate, tool wear and overcut, surface morphology and affected layer.

Few researches done on EDM for machining AMMC could be found from the literature review regarding the effects and optimum EDM parameters such as peak current, ON-time and OFF-time for machining 30% Al₂O₃ reinforced AMMC.

The presence of the hard reinforcement material in aluminum metal matrix composite (AMMC) results in poor machinability and short tool life when material is machined by conventional machining process such as lathe and milling, which leads to tool breakage, surface and subsurface damage of the material such as metallurgical alterations and micro-crack.

Diamond the hardest of all materials, has long been employed as a cutting tool, although its high cost has restricted its use to operations where other tool materials cannot perform effectively. It is hypothesized that non-traditional machining using EDM can address this problem if the correct machining parameters are identified.

1.3 Objectives

This research has been conducted to meet the following specific objectives:

- To study the machinability of 30% Al₂O₃ reinforced AMMC using electro discharge machining with copper electrode.
- To analyze the effects of the EDM parameters namely peak current, ON-time, OFF-time on the machining performance in terms of surface roughness (Ra), material removal rate (MRR), tool wear ratio (TWR), overcut (OC), surface morphology and thickness of affected layer.
- To identify the optimum EDM parameters for machining 30% Al₂O₃ reinforced AMMC in order to obtain the minimum surface roughness (Ra), maximum material removal rate (MRR), low tool wear ratio and minimum overcut.

1.4 Scope

The scope of this research is as follows:

- The machining process used is die-sinking EDM Mitsubishi EA8 for machining 30% Al₂O₃ reinforced aluminium metal matrix composite using copper electrode.

- The effects of three parameters on the 30% Al₂O₃ reinforced AMMC are investigated. The three parameters are:
 - Peak current,
 - ON-time ,
 - OFF-time.
- The investigated outputs are surface roughness (Ra), material removal rate (MRR), tool wear rate (TWR), surface morphology and thickness of affected layer.
- Determine EDM optimal parameters and establish the mathematical model of output responses using response surface methodology by employing Design Expert software.

1.5 Thesis Organization

This thesis is organized into five chapters to present the different stages of work that have been carried out to achieve the research objectives.

Chapter One describes general overview of the research, problem statement, research objectives, the scope of work and organization of thesis.

Chapter Two describes the background of aluminium alloy and composite materials; electro-discharge machining, design of experiment and a review of previous works are included.

Chapter Three presents the materials, the equipments and procedures used in this study.

Chapter Four covers the results and discussion. The results are actual statement of observation, including tables and graphs.

Finally, Chapter Five presents the conclusions drawn from the experimental observations.

CHAPTER TWO

LITERATURE REVIEW

In this chapter, the materials under study and the EDM process are described with recent research works in this area.

2.1 Aluminium Alloys

Aluminum alloys are divided into two categories such as wrought alloys, those that are worked to shape and cast alloys and those that are poured in molten state into a mold that determines their shape [4]. Both wrought and cast aluminium alloys are grouped into different series depending on the percentage of the alloying elements. According to the classification of aluminum alloys established by the International Alloy Designation System (IADS) [5] both wrought and cast alloys group series are designated by four digits.

Wrought aluminium alloy series are referred collectively by assigning three digits after the first digit ranging from 1 to 8. The first digit of the alloy number indicates the series to which that alloy belongs: 1xxx: Aluminum 99.0% minimum; 2xxx: Copper (1.9% to 6.8%); 3xxx: Manganese (0.3% to 1.5%); 4xxx: Silicon (3.6% to 13.5%); 5xxx: Magnesium (0.5% to 5.5%); 6xxx: Magnesium and Silicon (Mg 0.4% to 1.5%, Si 0.2% to 1.7%); 7xxx: Zinc (1% to 8.2%); 8xxx: Others [5]. The second digit indicates modification of the alloy or impurity limits. The last two digits identify aluminum alloy or indicate the alloy purity.

The casting aluminium alloy series are referred by fourth digits with a decimal between the third and fourth digit. The first digit indicates the alloy group according

to the major alloying element: 1xx.x: Aluminum 99.0% minimum; 2xx.x: Copper (4% to 4.6%); 3xx.x: Silicon (5% to 17%) with added copper and/or magnesium; 4xx.x: Silicon (5% to 12%); 5xx.x: Magnesium (4% to 10%); 7xx.x: Zinc (6.2% to 7.5%); 8xx.x: Tin; 9xx.x: Others. The second two digits indicate aluminum alloy or indicate the alloy purity. The last digit indicates the product form: casting (designated by “0”) or ingot (designated by “1” or “2” depending on chemical composition limits). Sometimes a slightly modified version of an existing alloy is registered, in which case an ‘A’ may be added to distinguish it from the original [4], [5].

Aluminium alloy 6061 is used in this research as a benchmark workpiece material. In this group of alloys, magnesium and silicon are the main alloying elements. Aluminium alloy 6061 has good machinability when subjected to conventional or non-conventional machining. It is one of the most used alloys in the 6xxx series. This standard structural alloy is popular for medium to high strength requirements and has good toughness characteristics. Their applications range from components of transportation and machinery equipments to recreational products [6]. The first digit in aluminium alloy 6061 indicates the group the alloy belong to with magnesium and silicon as main alloying. The second digit indicates the modifications made to the original alloy; “0” specify that the alloy is original. The two last digits specify the alloy purity contents meaning that the alloy 6061 contents minimum 61% of aluminium (Figure 2.1).

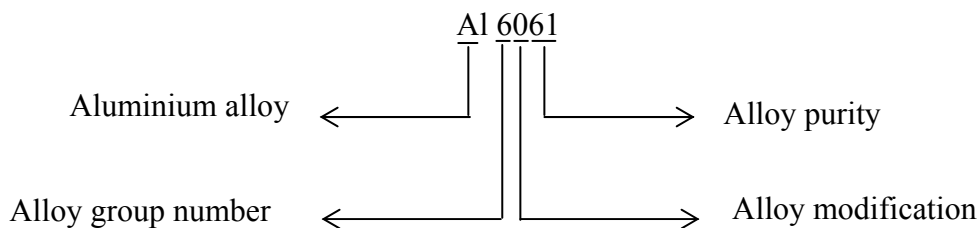


Figure 2.1: Aluminium Alloy Designation [4]

2.2 Composite Materials

Composite material is composed of two or more distinct materials (matrix phase and reinforcing phase) to form a new material with enhanced strength, stiffness, corrosion resistance and low weight [7]. The material that makes up the matrix is usually more

ductile and less hard than the reinforcing phase. The role of matrix in composite is to hold the reinforcing phase, to transfer the load to the reinforcing phase and to protect it from environment [7], [8]. The reinforcing phase is imbedded in the matrix and is usually stronger than the matrix. The role of reinforcing phase is to improve the properties of the composite system [7], [9].

The physical and mechanical properties of composites depend on the concentration and properties of their constituents. The strength and stiffness of a composite material can be increased by increasing the volume content of reinforcing constituent [10].

There are two classification systems of composite materials. The first is based on the matrix material and the second is based on the reinforcement phase.

2.2.1 Classification of Composite Material Based on Matrix

The first level of classification is usually made with the matrix. The major composite classes include:

- Metal Matrix Composites (MMCs),
- Ceramic Matrix Composites (CMCs),
- Polymer Matrix Composites (PMCs).

The metal matrix composites are composed of a metallic matrix which could be aluminum, magnesium, iron, cobalt, copper etc., and a dispersed phase such as ceramics which can be oxides, carbides or metallic such as lead, tungsten, or molybdenum. High strength, fracture toughness and stiffness are some of the advantageous offered by metal matrices compared to those offered by their polymer counterparts. Metal matrices have better resistance at elevated temperature than polymer composites [11]. Metal matrix composites (MMCs) contain a certain amount of hard and abrasive reinforcements to give high strength, hardness and stiffness. Machining of MMCs using traditional tool materials is difficult due to the presence of the abrasive nature of reinforcing phases, which cause faster tool wear. The greater

reinforcement in composite material causes faster the tool wear ratio. Thus non-traditional machining like electro-discharge machining (EDM) can be used to perform the precision machining of MMCs [12], [13].

Ceramic matrix composites are composed of a ceramic matrix and imbedded fibres of other ceramic materials (dispersed phase). High melting points, good corrosion resistance, stability at elevated temperatures and high compressive strength, render ceramic-based matrix materials a favourite for applications requiring structural materials that do not give way at temperatures above 1500°C [11], [14].

According to literatures, [15], [16], EDM of ceramics may create a damaged surface layer with poor surface integrity including unfavourable residual stresses, cracks and craters.

Polymer matrix composites (PMC) are composed of a polymer matrix combined with a fibre reinforcing dispersed phase. Polymer matrix composites are popular due to their low cost and simple fabrication methods [14], [17].

Electrical discharge machining of carbon fibre composite materials can be done at low current because high current can cause the epoxy resin to coat over the surface then leading to minimize material removal rate and rapid deterioration of the EDM surface [18].

2.2.2 Classification of Composite Material Based on Reinforcement

The second level of classification refers to the reinforcement form. The main types of reinforcements are:

- Particles,
- Fibres and,
- Whiskers.

Particulate composites consist of a matrix reinforced by a dispersed phase in the form of particles. The effect of the dispersed particles on the composite properties depends on the particles dimensions. Large dispersed phase particles have low

strengthening effect, but are capable to share load applied to the material, resulting in increase of stiffness and decrease of ductility. The hard particles dispersed in a softer matrix can increase the wear and the resistance of abrasion. There are two sub-classes of particulates such as flake (composites with random orientation of particles) and filled (composites with preferred orientation of particles) [17], [19].

Dispersed particles in the form of fibres (fibre composites) improve strength, stiffness and fracture toughness of the material. The increase in strength becomes much more significant when the fibres are arranged in a particular direction (preferred orientation) and a stress is applied along the same direction. The strengthening effect is greater in long-fibre (continuous-fibre) reinforced composites than in short-fibre (discontinuous-fibre) reinforced composites. Short-fibre reinforced composites consist of a matrix reinforced with a dispersed phase in the form of discontinuous fibres and have a limited ability to share load [19], [20].

A whisker composite has essentially the same near-crystal-sized diameter as a fibre, but generally is very short. Naturally, fibres and whiskers are of little use unless they are bonded together to take the form of a structural element that can carry loads [19], [20].

2.2.3 Aluminum Metal Matrix Composite

AMMCs offer many advantages over conventional aluminium alloys including high specific strength and stiffness, lightweight, enhanced fatigue resistance, increased elevated temperature strength, improved wear resistance, control over thermo-physical properties (thermal expansion and conductivity) through variations in reinforcement. The disadvantages of AMMC include decreased ductility and high cost; AMMCs cost is about three times more than conventional aluminium alloys. AMMCs have been applied in aviation, marine, automotive parts as diesel engine pistons, cylinder and brake components [21].

Among the AMMC materials, there are the type of reinforcement and matrix, the geometric arrangement and volume fraction of each constituent.

2.2.3.1 Matrix

Aluminium alloys are the most used matrix for metal matrix composites due to their high ductility in order to provide strain accommodation around the brittle reinforcements; low melting point in order to permit liquid-phase fabrication processes without making imperfect the reinforcements' properties; low density in order to achieve high specific properties [22]. American aluminum association standard designation system for AMMC identifies the material of the matrix, abbreviation of the reinforcement's designation/arrangement and volume fraction in percentage [8], [23] and [24]. In this research, the AMMC is designated as A242/Al₂O₃/30p. The matrix A242 is designated according to the B108 - 03a standard (ANSI).

2.2.3.2 Reinforcement

AMMCs can be reinforced with metallic, carbon, or most commonly ceramic reinforcement (especially silicon carbide (SiC) and alumina (Al₂O₃)) in either continuous or discontinue fibrous or particulate forms.

Continuous fibre of filament reinforced designated by letter "f" include graphite, silicon carbide (SiC) and aluminium oxide (Al₂O₃). Discontinuous reinforcement include SiC whisker designated by letter "w", SiC or Al₂O₃ particles designated by letter "p", or short designated by letter "c" [8], [24].

2.2.3.3 Fabrication

AMMC can be formed from both solid and molten states by forgings, extrusions, or casting. There are three viable processes for fabrication of AMMCs, which can be classified into solid-state, liquid-state and deposition processes.

- **Solid-State Processes**

The most frequently used method in this category is powder metallurgy, which is usually used for high melting point matrices. It prevents segregation effects and

brittle reaction product formation that is prone to occur in liquid state processes. Using this method, it is possible to obtain discontinuous particle reinforced AMMCs with the highest mechanical properties. These AMMCs are used for military applications [9], [24] and [25]. Figure 2.2 shows the solid state process.

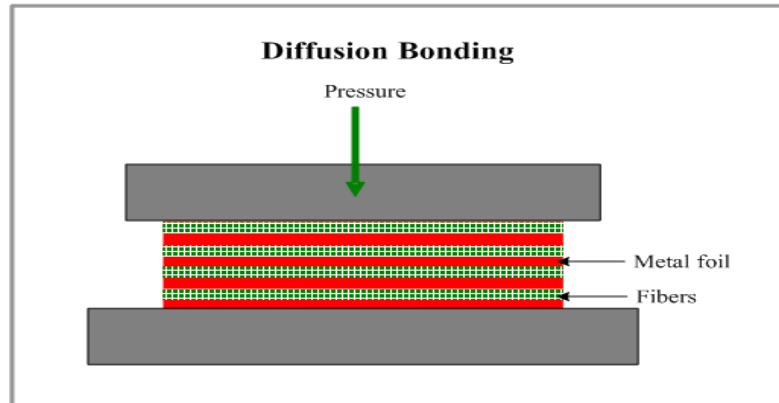


Figure 2.2: Solid state process [5]

- **Liquid-State Processes**

One can distinguish the infiltration processes where the reinforcements form a preform and are infiltrated by the alloy melt with pressure applied by a piston or by an inert gas (gas pressure infiltration) or without pressure. In the case the inert gas is without pressure, one can distinguish the reactive infiltration processes using the wetting between reinforcement and melt obtained by reactive atmosphere, elevated temperature, alloy modification or reinforcement coating (reactive infiltration) and the dispersion processes, such as stir-casting, where the reinforcements are particles stirred into the liquid alloy. Process parameters and alloys are to be adjusted to avoid reaction with particles [9], [24] and [25]. Figure 2.3 shows the liquid state process.

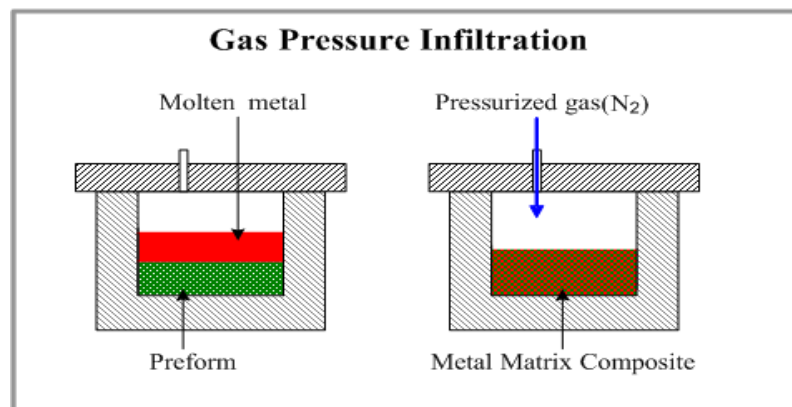


Figure 2.3: Liquid state process [5]

▪ Deposition Process

Droplets of molten metal are sprayed together with the reinforcing phase and collected on a substrate where the metal solidification is completed. The advantage of this technique is that the matrix microstructure exhibits very fine grain sizes and low segregation, but it has several inconveniences. The technique can only be used with discontinuous reinforcements, the costs are high and the products are limited to simple shapes obtained by extrusion, rolling or forging [9], [24] and [25].

The 30% Al₂O₃ used in this research was cast using solid state process fabrication.

2.2.3.4 Machining

Machining a composite material depends on the properties and relative content of the reinforcement and matrix materials. In general, composite materials are difficult to machine due to the high abrasive nature of the reinforcing constituents [2], [26].

The mechanical and thermal properties of composite materials and their poor machinability have been the handicap to their substitution for conventional materials. The hard abrasive reinforcement phase causes rapid tool wear during machining by conventional processes. F Muller et al. [27] mentioned that particle reinforced metal matrix composites have proved to be extremely difficult to machine using conventional manufacturing process due to heavy tool wear caused by the presence of the hard reinforcement.

From the review, it can be deduced that the morphology, distribution and volume, fraction of the reinforcement phase, as well as the matrix properties, are all factors that affect the overall cutting process. The machining of composites materials by conventional machines causes series of brittle fracture, shearing and the cracking of matrix materials, brittle fracture across the fibre, dust type chip and poor surface roughness [28]. Figure 2.4.a and Figure 2.4.b present metal and composite machining using conventional process. It shows the continuous plastic deformation in metal machining and series of brittle fractures on workpiece and tool wear in composite machining.

2.3 Electro-Discharge Machine (EDM)

2.3.1 Background

EDM was found by two Soviet scientists, B. Lazarenko and N. Lazarenko who studied why electrical breaker and contact points degraded from material transfer. They discovered that material transfer could be controlled by varying the electrical properties of the materials. With this understanding, they made the first attempts to remove material with the cutting action of electricity. B. and N. Lazarenko were credited for the invention of both the pulse circuit and a simple servo controller that helped in maintaining the gap width between the tool and the workpiece. This greatly reduced direct current arcing (short circuits) and made the EDM cut more effective. This was the turning point in the history of the electro-discharge machining process [3], [29] and [30]. In this research, the focus is on die-sinking EDM.

EDM has advantage in precision machining that not found in other technologies and conventional tools. The average surface roughness (Ra) produced by EDM on sample can be ranging from 12.5 to 0.8 μm [31]. On the other hand, the disadvantages are that it only works on conductive materials, both the tool and the surface being drilled are worn down, there are costs associated with creating the electrodes and time wasted removing the debris [3], [32].

2.3.2 EDM Machines

EDM is a thermal process during which the material is removed by a series of electrical discharge between electrode (tool) and workpiece in a presence of a dielectric fluid. A series of voltage of magnitude about 30 to 300 V and frequency in the order of 5 kHz is applied between the two electrodes, which are separated by a small gap, typically ranging from 0.01 to 0.5 mm [3].

2.3.2.1 Die-Sinking EDM

Die-sinking EDM (Figure 2.5) is a repeated battering of the electrode tool against the workpiece. The tool is the opposite shape of the sample to be machined. Die-sinking EDM is traditionally performed vertically, but it could also be performed horizontally [3].

In die-sinking EDM machines the workpiece must be inside a tank and covered with dielectric fluid. The electrode is lowered to a distance of few millimeters from the workpiece. Die-sinking EDM machine has the ability to produce complex cavities out of a solid piece of metal.



Figure 2.4: Die-sinking EDM machine EA8 [UTP workshop]

Die-sinking EDM machines vary in sizes and operating mode from manual operating table top systems to large automatic computer numerical control (CNC) [3]. Die-sinking EDM is made up of a number of main subsystems:

- Power supply,
- Dielectric fluid,
- Tool,
- Servo system.

2.3.2.2 Wire-Cut EDM

Wire-cut EDM (Figure 2.6) uses an ultra-thin conductive material like copper or brass as a full-surface electrode to cut through the hard metal. Sparking takes place from the electrode wire-side to the workpiece [3].

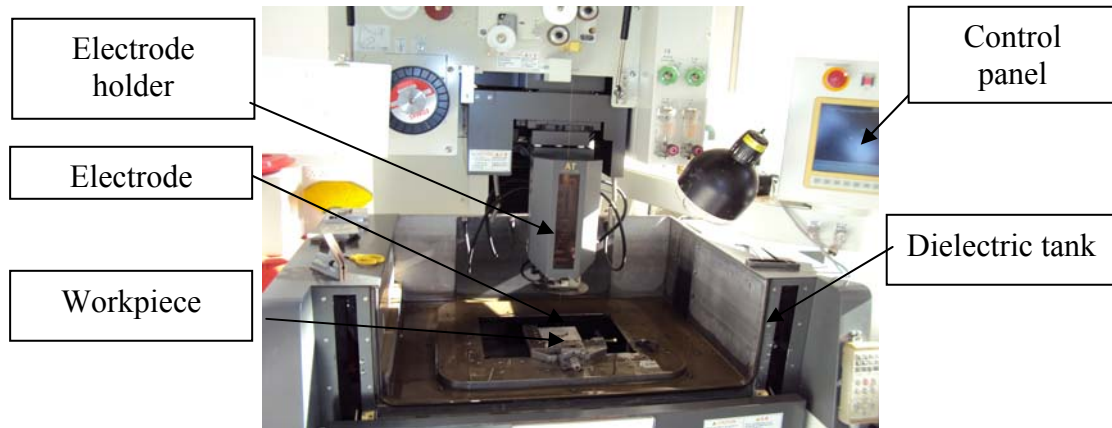


Figure 2.5: Wire-Cut EDM machine FA10 [UTP workshop].

The wire die system continuously delivers wire at constant tension to the work area guided by a set of guides or diamond wire guide. They can run unattended for long periods including overnight and weekends [3]. The four basic subsystems of wire-cut EDM include:

- Power supply,
- Dielectric system,
- Wire feeding system,
- Positioning system.

2.3.2.3 EDM Drilling

Drilling EDM (Figure 2.7) is effective on boring holes into a long bronze piece of metal, depending on consistent pressure and rotation of the electrode [32].



Figure 2.6: Drilling EDM machine [UTP workshop]

Drilling EDM machines is used for drilling small holes and slots of round and regular shapes. This machine uses long rounded electrode which rotate with speed about one hundred revolutions per minute [30].

2.3.3 EDM Principles

Basically, EDM is performed by means of electrical sparks that jump between two electrodes, which are subjected to a given voltage and are submerged in an insulating liquid (Figure 2.8).

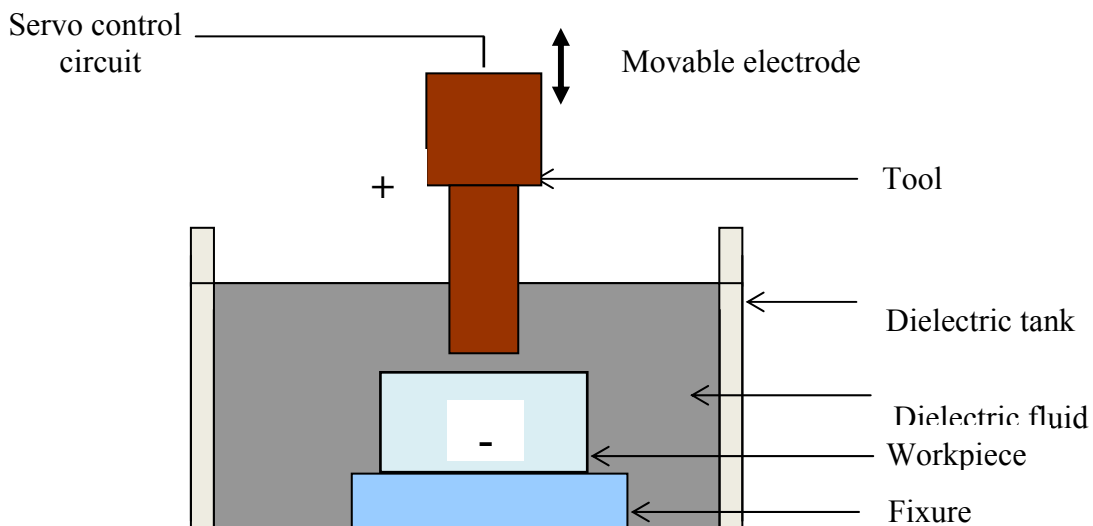


Figure 2.7: Basic components of Die-sinking EDM [3]

Since the two electrodes are in a dielectric or insulating medium, the voltage applied to them must be sufficient to create an electric field which is greater than the

dielectric rigidity of the fluid. As a result of the action of this electrical field, free positive ions and electrons are accelerated creating a discharge channel which becomes a conductor and it is precisely at this point where the spark jumps. This causes collisions between the ions (+) and the electrons (-). A channel of plasma is thus formed (Figure 2.9) [3]. These collisions create high temperatures in both poles and a ball of gas is formed around the plasma channel, which begins to grow. At the same time, the high temperature at the two poles causes the both workpiece to melt and vaporizes part of the material, while the electrode itself suffers. The plasma channel breaks down and the spark disappears. The dielectric fluid then breaks the ball of gas making it explode inwards. This creates forces which force the molten material to be flush away [3], [33].

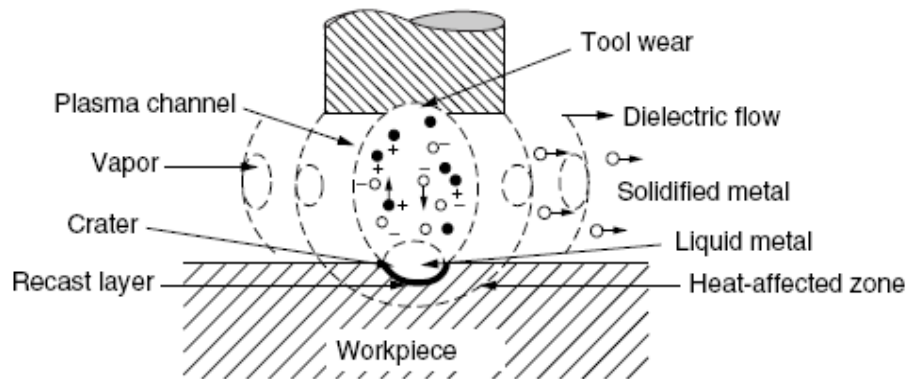


Figure 2.8: EDM spark description [30]

2.3.4 Components of EDM System

2.3.4.1 Dielectric Fluids

The main functions of the dielectric fluid are to insulate the gap before high energy is accumulated, to concentrate the discharged energy to a thin area, to recover the gap condition after the discharge, to cool the electrodes (workpiece and tool) and to flush away the discharge products. The two commonly used dielectric fluids are petroleum-based hydrocarbon mineral oils and deionized water. The oil should have high flash points and the right viscosities. High insulation, high density and high viscosity oils have the positive effects of concentrating the discharge channels and the discharge energy, but they may have difficulty flushing away the discharged products [34].

Figure 2.10 presents the different methods of flushing: injection flushing in which a slight taper is produced on the sides of the cavity due to lateral discharges as debris pass up the side of the tool (Figure 2.10a); suction flushing through which the side taper is avoided (Figure 2.10b); side flushing in which a slight taper is produced on the side of the cavity at the outlet (downstream) of the dielectric direction (Figure 2.10c) [33], [35].

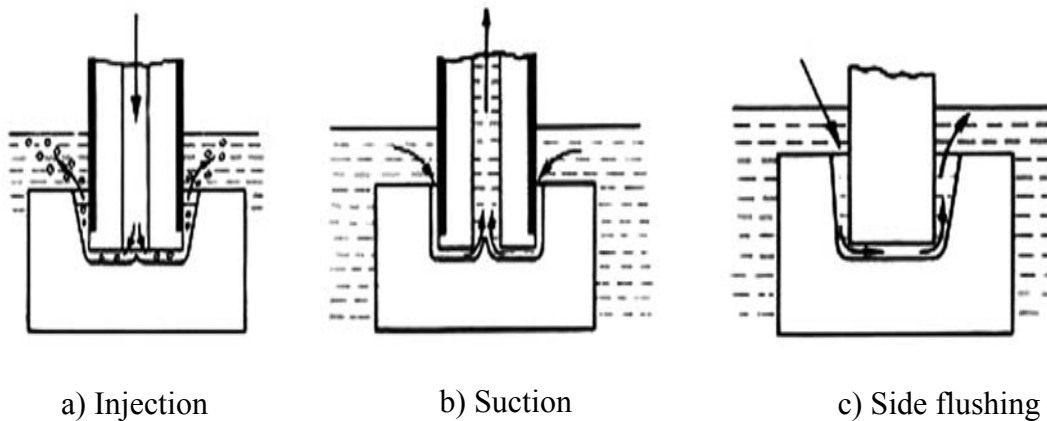


Figure 2.9: Dielectric flushing modes [36]

Flushing generates a force on the workpiece and this force can be detrimental for the thin-section or micro-feature machining due to bending and possibly fracturing the miniature Workpiece during EDM. Increasing the dielectric fluid pressure will reduce the surface roughness. The flushing is to clean the debris from the gap between the electrode and workpiece and consequently can improve the material removal rate [37].

2.3.4.2 Tool Materials

In EDM die-sinking, the tool is used to convey an electric current, which can either leave or enter the electrode. EDM machines create an electric sparks between an electrode and the workpiece.

The basic requirements for a tool material are:

- High electrical conductivity: Since electric current is the “cutting tool”, higher conductivity (or conversely, lower resistivity) promotes more efficient cutting [34],

- High melting point: Since EDM is a thermal process, it would be logical to assume that the higher the melting point of the electrode material is, the better the wear ratio will be between the electrode and workpiece [34],
- High thermal conductivity: Since the tool has a higher range of thermal conductivity, the heat from the EDM process will quickly spread through the electrode. As the temperature of the electrode increases, the electrical resistance also increases and much of the energy needed to create the EDM spark is turned into heat within the electrode [34].

The above properties of electrode determine the tool spark-resisting capability. The material for the electrode tool also should be easy to be machined and inexpensive. The most frequently used materials are graphite, copper and bronze for machining steels and copper tungsten for machining carbide. Other materials include brass and tungsten [38].

2.3.4.3 Power System

An EDM power system transforms the AC power into pulsed DC power with 30V to 300V and several milliamperes of peak current. The power system provides series of DC current electric discharges between the electrode and the workpiece. It also controls the voltage, current, frequency and electrode polarity [3]. Figure 2.11 illustrates an electrical circuit during charging and discharging duration.

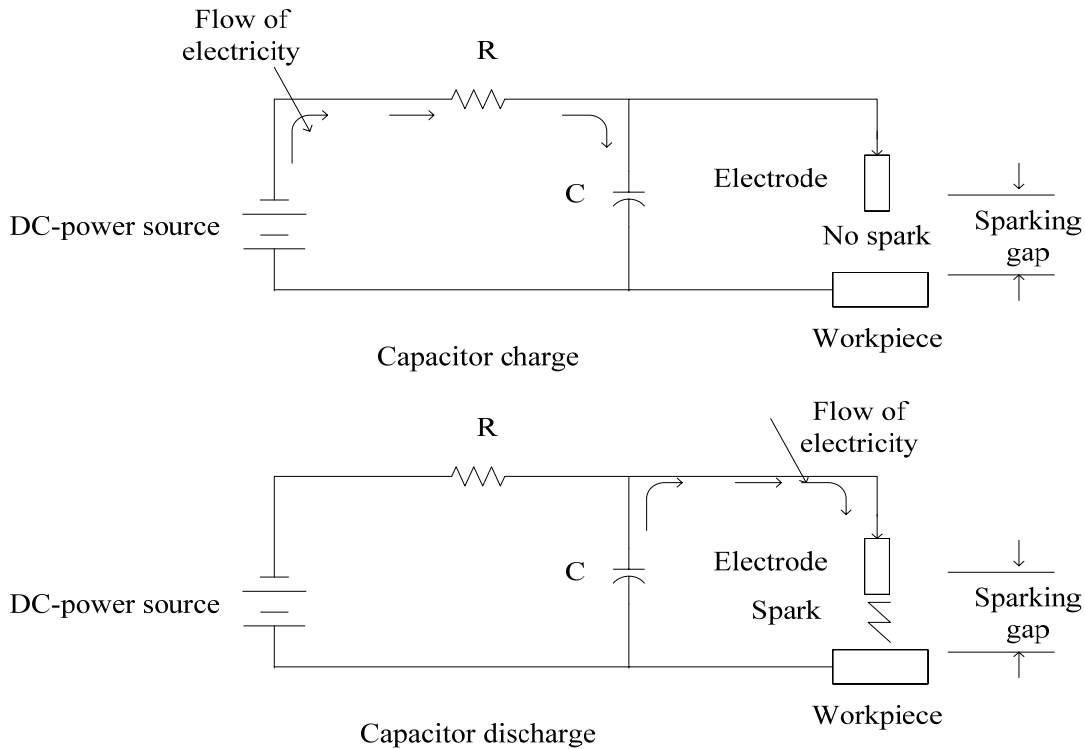


Figure 2.10: Power supply system for capacitor charge and discharge [3]

The capacitor stores the electricity received from the resistor and discharges it through the electrode, the workpiece and through the spark gap in the form of spark. The time the capacitor is being charged is the OFF-time (pause duration) and discharging time is ON-time (pulse duration) [3].

2.3.4.4 Servo Control System

The servo control system is used to keep the inter-electrode gap within a small distance during machining and machining duration. The gap size control is vital in EDM machining because it maintains efficient spark [3]. The requirements for an EDM servo control system are:

- The electrode must not touch the workpiece.
- The electrode must advance toward and retract from the workpiece to maintain the voltage between the electrode and workpiece [3].

2.3.5 EDM Parameters

Electro-discharge machining performance is influenced by a large number of parameters and their interactions. In die-sinking EDM, the material removal, tool wear and resulting surface integrity depend on pulse characteristics (peak current, ON-time, OFF-time voltage etc.), workpiece and material properties (electrical conductivity, melting point, thermal conductivity), dielectric flushing conditions (dielectric flushing pressure, dielectric flushing direction, etc.), dielectric properties (dielectric flushing point and viscosity, etc.), electrode geometry and working depth [30]. Figure 2.12 illustrates the pulse train for a controlling generator.

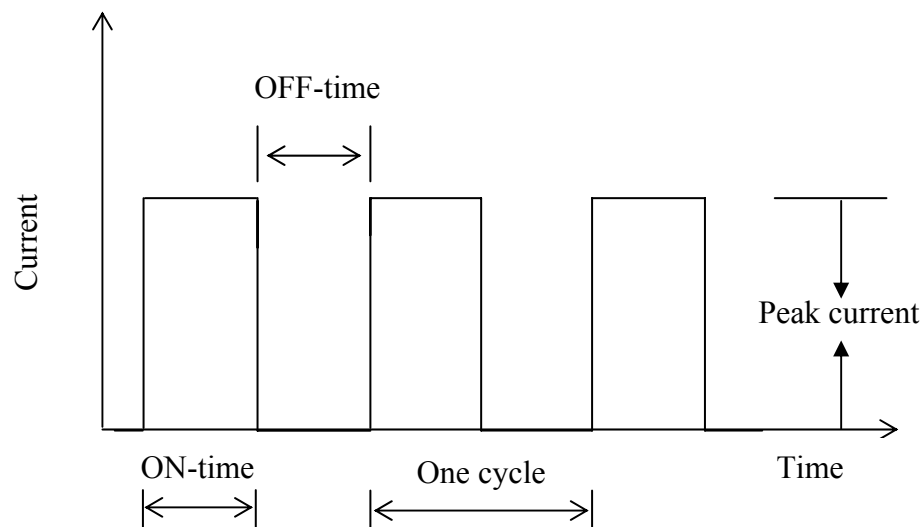


Figure 2.11: Pulse current train for controlling generator [3]

2.3.5.1 Peak Current

The "Peak Current" is the intensity of the electricity flow into the workpiece forming the craters and cracks. The peak current is capable of determining the energy size of an electrical discharge. By getting higher value on peak current setting, a larger electric discharge can be generated [34]. During ON-time the current increases until reaching a preset level, which is expressed as the peak current [39]. Norassettekul et al. mentioned that the energy input in EDM depends directly on discharge voltage, peak current and ON-time [40]. Kathiresan et al. observed that higher peak current and ON-time resulted in higher material removal rate and surface roughness due to higher thermal loading into the electrodes (workpiece and tool) [41].

2.3.5.2 ON-time

The “ON-time” is an amount of time when current runs into the gap before it is turned off. ON-time influences the discharge energy. Machining increases by increasing the value of ON-time, due to an increase of the discharge energy. However, the surface accuracy decreases because the gap discharge becomes wider [42].

2.3.5.3 OFF-time

The “OFF-time” is the amount of time when the current is off after making a single crater. As the OFF-time is shorter, the number of discharge within a given period becomes more; leading to a faster machining but the machined surface becomes rougher [43]. Material removal rate and surface roughness are proportional to the amount of energy applied during the machining duration (ON-time) [44].

2.3.5.4 Voltage

The voltage is the setting parameter that determines the supply of electricity to the gap. Increasing the voltage will cause more discharge energy to be produced, thus giving the similarly effect as peak current and ON-time; and with the decrease of voltage, the values of cutting speed and surface roughness slowly drop [43]. In general, the machining surface becomes rougher and MRR slightly increases as a result of using higher voltage [45].

2.3.6 Performance Characteristics

EDM performance, regardless of the type of electrode material and dielectric fluid, is usually measured by the main following criteria:

- Surface Roughness (Ra),
- Metal removal rate (MRR),
- Resistance to wear or tool wear ratio (TWR),

- Overcut (OC),
- Surface integrity.

2.3.6.1 Surface Roughness

Surface roughness is a critical parameter for evaluating machining product. The specified principal parameter mostly used for surface roughness is the surface roughness average value (Ra). It measures the average roughness value by calculating all the peaks and valleys to the mean line and then averaging them all over the entire the measuring length. Cut-off length is the length that the stylus is dragged across the surface. The surface roughness characterizes the quality of machined surface. Voltage, peak current and ON-time are parameters that have the most influence on surface roughness because they are responsible of spark energy. High peak current and longer ON-time increases spark energy creating larger craters [41].

According to Delpreti [46], Motoki and Lee [47] the average surface roughness can be expressed in terms of pulse current i_p (A) and pulse duration t_p (μ s) by the Equation (2.1):

$$Ra = 0.0225 i_p^{0.29} t_p^{0.38} \quad (2.1)$$

The surface roughness tester is used in this research to measure the surface roughness average.

2.3.6.2 Material Removal Rate

In EDM the metal is removed mainly from the workpiece and some from the tool. The material removal rate (MRR) depends not only on the workpiece material but also on the material of the tool and the machining variables such as pulse setting conditions, electrode polarity and the machining medium [34]. Typical removal rates for EDM die-sinking machining can range from 0.1 to 400 mm³ /min (about 0.002 to 10.8 g/min) [25], [30].

Many methods for determining the MRR exist in literature. Singh et al. [48], F. Kolahan et al. [49] and M Shabgard et al. [50] expressed in Equation (2.2) that the MRR in grams per minutes is the ratio of the difference of the mass in grams of the workpiece before and after machining to the machining time in minutes.

$$MRR = \frac{\text{Mass loss of workpiece}}{\text{machining time}} \quad (2.2)$$

A. Hascalik et al. defined the material removal rate in cubic millimeters per minutes as a measure of removed material volume per minute and it is expressed in Equation (2.3) [51].

$$MRR = \frac{\text{Electrode Cross – Sectional Area} \times \text{Depth of cut}}{\text{Machining time}} \quad (2.3)$$

The material removal rate, or volumetric removal rate (VRR), in mm³/min, was also described in equation (2.4) by Delpreti [46], Motoki and Lee [47]:

$$MRR = (4 \times 10^4) IT_w^{-1.23} \quad (2.4)$$

Where I is the EDM current (A) and T_w is the melting point (°C) of the workpiece material.

The Equation (2.2) was widely used and reported in literatures and it is selected for this research.

2.3.6.3 Tool Wear Ratio

The tool wear ratio is the ratio at which the cutting edge of tool wears away during machining process. Electrode wear is specified in one of four ways, including corner wear, end wear, side wear and volumetric wear. Figure 2.13 illustrates the different kinds of electrode. In this research, the electrode wear is express in term of mass loss.

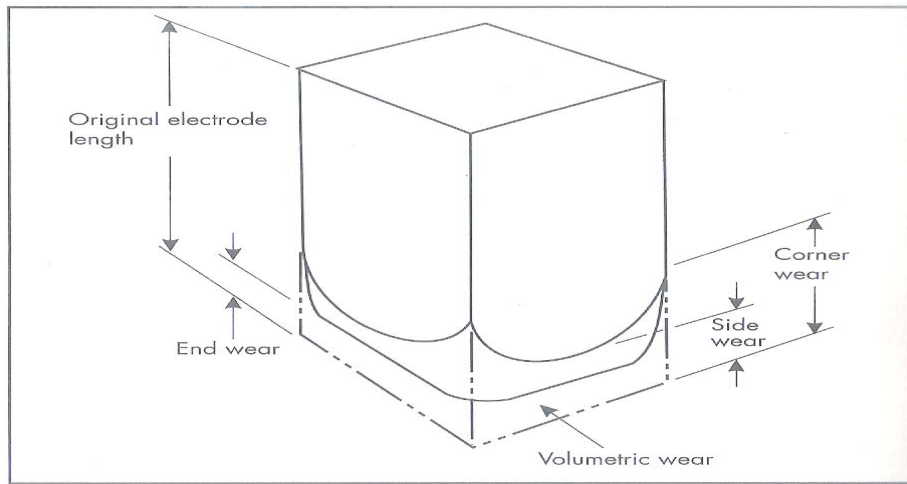


Figure 2.12: Different types of electrode wear [3]

Narender et al. [48], Kolahan et al. [49], Shabgard et al. [50] and Hascalik et al. [51] expressed the tool wear ratio (TWR) using Equation (2.5) as mass difference of the electrode before and after machining:

$$TWR = \frac{w_{eb} - w_{ea}}{w_b - w_a} \times 100 \quad (2.5)$$

Where:

w_{eb} is the mass of electrode before machining,

w_{ea} is the mass of electrode after machining,

w_b is the mass of workpiece before machining,

w_a is the mass of workpiece after machining,

TWR is the ratio of the electrode mass loss to the material loss in percentage.

The ideal wear ratio is less than fifty percent (50%) relative to the amount of material removed tool [52].

2.3.6.4 Overcut

Overcut (OC) is expected in EDM machining and is a result of sparking gap erosion and the value of overcut can be used for determining the size of the electrode [3].

Overcut or overburn is the gap distance between the electrode and workpiece. The amount of overcut varies according to the amount of peak current, ON-time, OFF-time, voltage, type of electrode and the workpiece material properties. Figure 2.14 presents the schematic of overcut. Overcut in EDM machining can be ranged from 0.020 to 0.63mm [53].

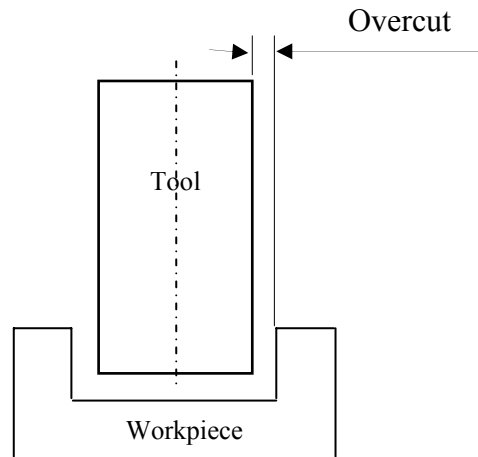


Figure 2.13: Schematic of overcut [3]

According to Narender et al. [48], the overcut is expressed in Equation (2.6) as half of the difference of diameter of workpiece cavity to the electrode diameter.

The determination of overcut (OC) is by using the following Equation (2.6) [48]:

$$OC = \frac{D_1 - D_2}{2} \quad (2.6)$$

Where: D_1 is the tool diameter and D_2 is cavity diameter.

2.3.6.5 Surface Integrity

Machining process produces a surface consisting of topography and metallurgy. These will influence the surface functional performance during applications. If the surface is rougher, it is likely that the resulting functional performance will be poor [42], [54]. The term surface integrity has been described as:

- The inherent or enhanced condition of surface produced in a machining or other surface generation operation or;

- The topographical (roughness and waviness), mechanical (residual stress and cracks), chemical and metallurgical (phase change, hardening and softening) quality of a manufactured surface and its relationship to functional performance [54].

In the schematic of Figure 2.15, three regions can be seen. Firstly, there is an upper region which has reacted with the air and consisting of deposit and oxide materials. Secondly, there is the region beneath this where the material that has been influenced and affected in some way by the manufacturing unit event (i.e. the affected material zone). Thirdly, there is the bulk material that remains unchanged by the unit event. Usually the bulk material transformation is gradual and often there is no clear demarcation line. For example, if the machining process involves plastic deformation, the affected material zone (AMZ) will be workpiece hardened. The hardness will be a maximum at the surface and it will gradually decay to the bulk value [42].

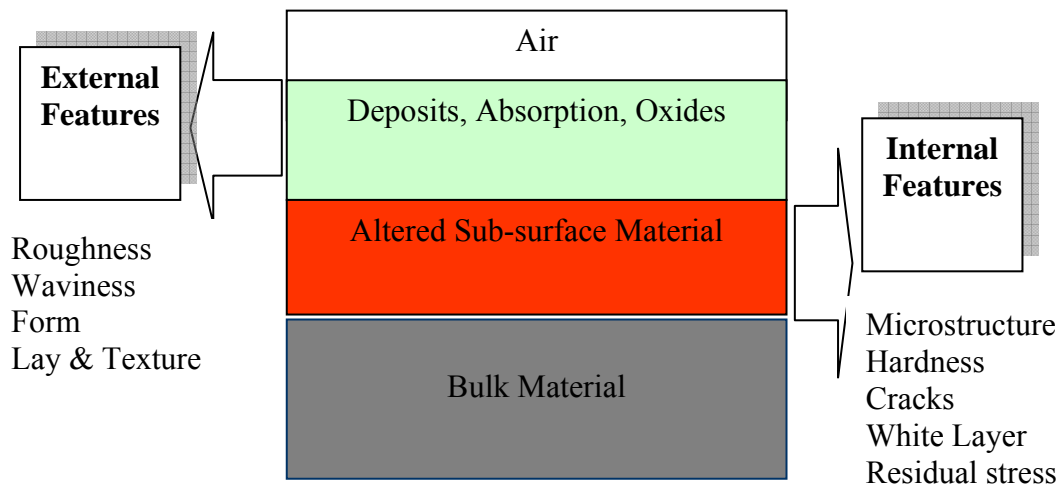


Figure 2.14: Schematic section through a machined surface [42]

With the temperature of the discharges reaching 8000°C to 12,000°C, metallurgical changes occur in the surface layer of the workpiece. Additionally a thin recast layer of 1µm to 25µm is formed. Delpretti [46], Levy and Maggi [55] claimed that the heat-affected zone adjacent to the resolidified layer reaches 25µm.

2.3.7 Application and Limits

Because the EDM process uses high energy for electric-thermal erosion (instead of mechanical cutting forces) to remove material, it is capable of machining difficult-to-cut materials such as hard steels, carbides, high strength alloys and even the ultra-hard conductive materials like polycrystalline diamond and some ceramics. Also EDM is effective in machining brittle but electrically conductive materials because the tool does not contact the workpiece and no substantial mechanical force is expected on the workpiece. EDM can machine complicated shapes with prefabricated tools. The process is particularly well suited to sinking cavities and drilling irregularly (complex) shaped holes. The limit in EDM process is the electrical conductivity of the workpiece material. The conductivity of $0.1 (\Omega^{-1}\text{Cm}^{-1})$ is considered as the minimum value for EDM to be effective. The electrical conductivity of AMMC under study is $344.827\Omega^{-1}\text{Cm}^{-1}$. The other problems in EDM include tool wear and the irregularity of tool wear as well as limitation of EDM to machine sharp corners because of existing gap between the tool and the workpiece [34]. The surface layers of workpiece machined by EDM will be altered metallurgically and chemically after going through the extremely high thermal energy process (up to $12,000^{\circ}\text{C}$) accompanied by the dielectric cooling process. The layer usually differs significantly from the base in the metallurgical structures due the recasting and it also contains gas holes, tool material particles and other impurities from the dielectric [34].

The main disadvantages of this process are:

- This process can only be employed in electrically conductive materials,
- Material removal rate is low and the overall process is slow compared to conventional machining processes,
- Unwanted erosion and over cutting of material can occur,
- Rough surface finish when machining at high of MRR [34].

2.4 Design of Experiment

2.4.1 Design of Experiment Principle

Design of Experiment (DOE) is a test referring to a plan, design, analysis and interpreting of experiment. DOE performs some changes to input variables called factors (parameters) of process and the corresponding changes to output called responses. The factors can be either continuous or categorical variables. Mathematical and statistical techniques are incorporated in DOE for modelling and interpretation and establishing a relationship between input variables and output responses [56]. This method has been well established in various applications and disciplines. Experimental design methods also plays a major role in engineering design activities [57], where new products are developed and existing products are improved.

Available examples of system for design and analysis of associated to DOE are Design Expert, Statistica, Minitab, Systat, SPSS and JMP. Design Expert, commonly reported in literature review and available, is used in this research for design and simulation.

2.4.2 Terms and Concepts

2.4.2.1 Data

The factors that can be varied in experiment can be divided into process variables, such as peak current, ON-time of EDM machining which can be either continuous, categorical or mixture variables [57], [58].

2.4.2.2 Mathematical Models

In analyzing an experiment, the models are fitted relating a response or quality characteristic to a set of controllable variables. For continuous control variables, the model often used can be linear, factorial or quadratic [57], [58].

- Linear mathematical model:

$$Y = \beta_0 + \beta_1 X_1 + \beta_2 X_2 + \beta_i X_i + \varepsilon: \quad (2.8)$$

Average effect of varying a control and $\beta_i X_i$ is the linear term;

Factorial mathematical model:

$$Y = \beta_0 + \beta_1 X_1 + \beta_2 X_2 + \beta_{12} X_1 X_2 + \beta_{ij} X_i X_j + \varepsilon: \quad (2.9)$$

This allows the effect of changing a control to vary with the setting of another control and $\beta_{ij} X_i X_j$ is the factorial term;

- Quadratic mathematical model:

$$Y = \beta_0 + \beta_1 X_1 + \beta_2 X_2 + \beta_{12} X_1 X_2 + \beta_{11} X_1^2 + \beta_{22} X_2^2 + \beta_{ii} X_i^2 + \beta_{ii} X_i^2 + \varepsilon: \quad (2.10)$$

This allows for curvature in the effect of a control on the response and $\beta_{ii} X_i^2$ is the quadratic term.

2.4.3 Selecting a Design Class

According to the type of model, DOE offers a large number of different classes of design such as Response Surface Methodology (RSM) in which there are sub-classes called Central Composite Design (CCD: each of factor is varied over five level), Box-Behnken (each of factor is varied over three level) etc.; Factorial containing the sub-classes called 2-Level Factorial (2FI) which is design for 2 to 21 factors where each factor is varied over 2 levels, Taguchi Orthogonal Array (explore two-level factorial and general factorial designs as alternative), etc; Mixture containing sub-class named Simplex Lattice (design for 2 to 30 components where components must have same range and are no constraints on the design space), Simplex Centroid (design for 3 to 8 components where components must have same range and are no constraints on the design space) etc and Combined containing D-Optimal (for systems with both mixture and process factors) etc [57], [58].

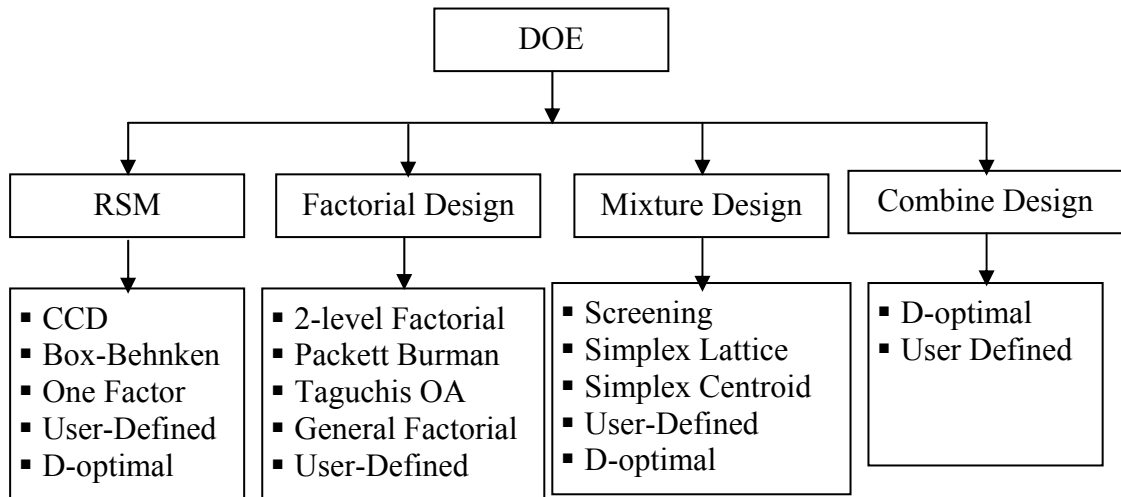


Figure 2.15: Types of DOE class [57]

Response surface methodology is used in this research and central composite design (CCD) is chosen to explore the relationships between parameters and output responses and to obtain an optimal response.

2.4.4 Analysis

The following are main steps to analyze the experiment.

2.4.4.1 Analysis of Variance

Analysis of variance (ANOVA) allows researcher to test for differences in the means of several different groups or populations. ANOVA evaluate the null hypothesis that the means for all of the groups are the same. In order to test this hypothesis, a Fisher statistic is calculated which compares the variation among the groups with the variation [57], [58].

2.4.4.2 Diagnostics Plots

Diagnostic option provides graphical summaries for case study by selecting the Diagnostics button. Most of the plots display residuals, which show you how well the model satisfies the assumptions of the analysis of variance [57], [58].

2.4.4.3 Model Graphs

Model graph provides the plot of one factor, two and three dimensional, interaction of parameters of results [57], [58].

- One factor plot: Main effect plot showing the average effect of shifting a single control, while holding the other controls constant,
- Interaction plot: Plot showing how the effect of changing one control varies with changes in a second control,
- Contour plot: Plot showing the effect of two parameters on output response,
- 3-D Surface plot: Plot showing the effects of three parameters on output response.

2.5 Previous Works

Machining a composite material depends on the properties and relative content of the reinforcement and matrix materials [2]. In general, composite materials are difficult to machine using conventional process due to the anisotropic and non-homogeneous structure of composites and the high abrasiveness of their reinforcement constituents [2].

Although composite materials are superior in mechanical and thermal properties, their poor machinability is deterrent to their substitution for conventional materials [59]. The hard abrasive reinforcement phase causes rapid tool wear during machining of AMMC by conventional process and, consequently, high cost. The morphology, distribution and volume, fraction of the reinforcement phase, as well as the matrix properties, are all factors that affect the overall cutting process [60]. The machining of composites materials by conventional machines causes series of brittle fracture, shearing and cracking of matrix materials, brittle fracture across the fibre, dust type chip and poor surface roughness [2].

In this research project, aluminum metal matrix composite (30% Al₂O₃ reinforced aluminium composite) has been used as the workpiece material and electrolytic copper material is used as electrode (tool).

Previous research in diverse materials for EDM electrode on influence of EDM parameters on varying workpiece materials while others focus on optimization of EDM parameters.

Research in the area of electro discharge machining of Titanium alloy (Ti6Al4V) using three different electrode materials such as graphite, electrolyte copper and aluminum includes work from Hascalik et al. [51]. Results showed that the surface integrity of EDM of Ti6Al4V includes roughening because of decomposition of recast layer on the surface, surface micro-cracks, debris and melted drops. The average white layer thickness is increasing with EDM parameters. Graphite electrode gives the highest material removal rate, followed by electrolytic copper and aluminum. Graphite exhibits the lowest wear rate due to higher melting point at all the applied condition. Aluminum electrode exhibits the best performance with regard to surface finish.

Kiyaka et al. [61] worked on examination of machining parameters on surface roughness in EDM of steel (40CrMnNiMo864) of sizes 20mm x 70mm x 315mm using a cylindrical pure copper. The results showed that the surface roughness increased with increasing peak current and ON-time. Low peak current and ON-time with high OFF-time produced minimum surface roughness that means good surface finish quality. High peak current and ON-time provide low surface roughness finish quality. However, this combination would increase material removal rate.

Effect of electrical discharge machining on surface characteristics and machining damage of AISI D2 Tool steel was carried out by Y. Guu et al. [62]. Results showed that the recast layer becomes thicker with increase of peak current and ON-time. An excellent machined surface can be obtained by setting the machining parameters at low peak current, short ON-time and longer OFF-time leading to low energy. Low energy reduces the frequency of burst of dielectric fluid and melt expulsions.

Examination of wire-cut electrode discharge machining of Al₂O₃p/6061Al composites was studied by Hwa et al. [63]. Three kinds of work materials were machined particularly 0, 10 and 20 vol % Al₂O₃ particles using brass wire with a diameter of 0.25mm. The results showed that wire-cut EDM of Al 6061 composite obtained the highest cutting speed than the two Al₂O₃p/6061 composites. Additionally, increasing the volume fraction of reinforcing Al₂O₃ particle facilitated wire breakage. Increasing the percentage of reinforcement Al₂O₃ particle deepened and widened discharge craters of the wire surface, promising WEDM.

Mehta et al. [64] did research on review of the development of conductive ceramic materials followed by the progress of EDM technology in this context from its initiation to present state. They found that the manufacturing conditions can be explained in terms of work-tool combination, electrode polarity, peak current, ON-time and OFF time, duty cycle factor, flushing pressure and process stability. The tool wear process (TWP) is similar to the material removal mechanism as the tool and workpiece are considered as a set of electrodes in EDM. Generally, for EDM machining copper, graphite or copper-tungsten electrodes are used. Electrode polarity, thermal properties of electrode and flushing pressure are significant parameters responsible for electrode wear. The electrical discharge machined surface is made up of three distinctive layers consisting of white layer (recast layer), heat affected zone and unaffected parent metal.

B. Mohana et al. [65] investigated the Electric discharge machining of Al–SiC metal matrix composites using rotary tube electrode. Results indicated that the MRR is proportional to the product of energy transferred per pulse frequency. The MRR was high for all rotating modes of the electrodes than for the stationary modes. This is possibly due to the superior debris removal effect of the rotating electrode. The EWR was more when the electrodes were kept at positive polarity than at negative irrespective of the volume percentage of SiC. This is due to the increase in MRR with the positively connected electrode. It was also observed that increase in discharge current resulted in an increase in Ra value. These events can results in larger discharge energy, subsequently causing a larger crater on the surface of the workpiece.

Y. Guu et al. [62] worked on effect of machining parameters on surface textures in EDM of Fe-Mn-Al alloy. They observed that the morphology of the EDM surface was dependent on the applied peak current and ON-time; moreover, the EDM surfaces abound with the craters and ridged surfaces. Higher peak current and a longer ON-time caused a poorer surface finish. The EDM-treated surface is covered with micro-cracks and micro-voids. The depth of the EDM damage layer is affected by the process parameters of peak current and ON-time.

P. Narender et al. [48] studied EDM of Al-10%SiCp as-cast metal matrix composites. MRR was found to increase with increase in current and pulse ON-time. It is also evident that the surface roughness value increases with increase in peak current and ON-time. It was observed that the flushing has influence effect on MRR and TWR. When the dielectric fluid is forced at low velocity into the spark gap, short-circuiting becomes less pronounced as a result of the accumulated particles.

P. Cichosz and P. Karolczack [66] studied EDM of aluminium matrix composites and they gave particular attention to the thickness of defected layer, surface roughness, EDM surface machined. Higher EDM spark energy parameters resulted in changes to the machined surface.

G. Chrisna et al. [67] showed in influence of machining parameters on EDM of maraging steel that the cracks are formed with the results of high thermal stresses prevailing at the specimen surface as latter was cooled at fast rate after the discharge.

Khanra et al. [68] in Application of new tool material for EDM showed that when the energy increases the electron bombardment from the side wall of tool increased, which led to more overcut.

Janmanee [69] studied the performance of different electrode materials on tungsten carbide workpiece with EDM process. The results show that the electrode negative polarity performs very well; Poco EDM-3 gives higher Material Removal Rate (MRR). Both powder electrodes give the better MRR and EWR. They conclude that the suitable duty factor is 11%. The Surface Roughness of copper-tungsten gives the best when current peak intensity not over 20 amperes.

Kumar et al. [70] developed the modelling of machining parameters namely pulse current, discharge time and pause time for MRR in EDM using response surface methodology. They found that all three machining parameters and some of their interactions have made significant effect on the output response.

Researches in the domain of effects of EDM parameters on the machined surface by using different types of workpiece materials and various machining conditions have been done. The results showed that the effects of EDM occur on any types of workpiece material. Ra, MRR, TWR and overcut vary due to change in EDM parameters. The affected surface layer occurs under different spark erosion conditions and it contains numerous, cracks and craters.

CHAPTER THREE

METHODOLOGY

In order to test the machinability of aluminium metal matrix composite (AMMC) using electro-discharge machine, research methodology needs to be defined before running the experiment.

In this chapter the methodology, output responses, machines, instruments and procedures used for EDM machining of AMMC and aluminium alloy (Al 6061) in this research are described.

The research was started by reviewing literatures on AMMC, aluminium alloy and the EDM process. A short training on the operation of the EDM machine was conducted to familiarise the researcher on the process and the machine parameters settings. Experiments were planned to conduct the experiment based on design of experiment (DEO). Samples were prepared and the experiments were conducted as planned. The data collection collected were analysed and interpreted.

3.1 Research Methodology

According to experiment plan, 21 runs with different parameters setting were done on 30 % Al₂O₃ reinforced aluminium metal matrix composite and Al 6061. The research methodology is summarized in a flowchart shown in Figure 3.1.

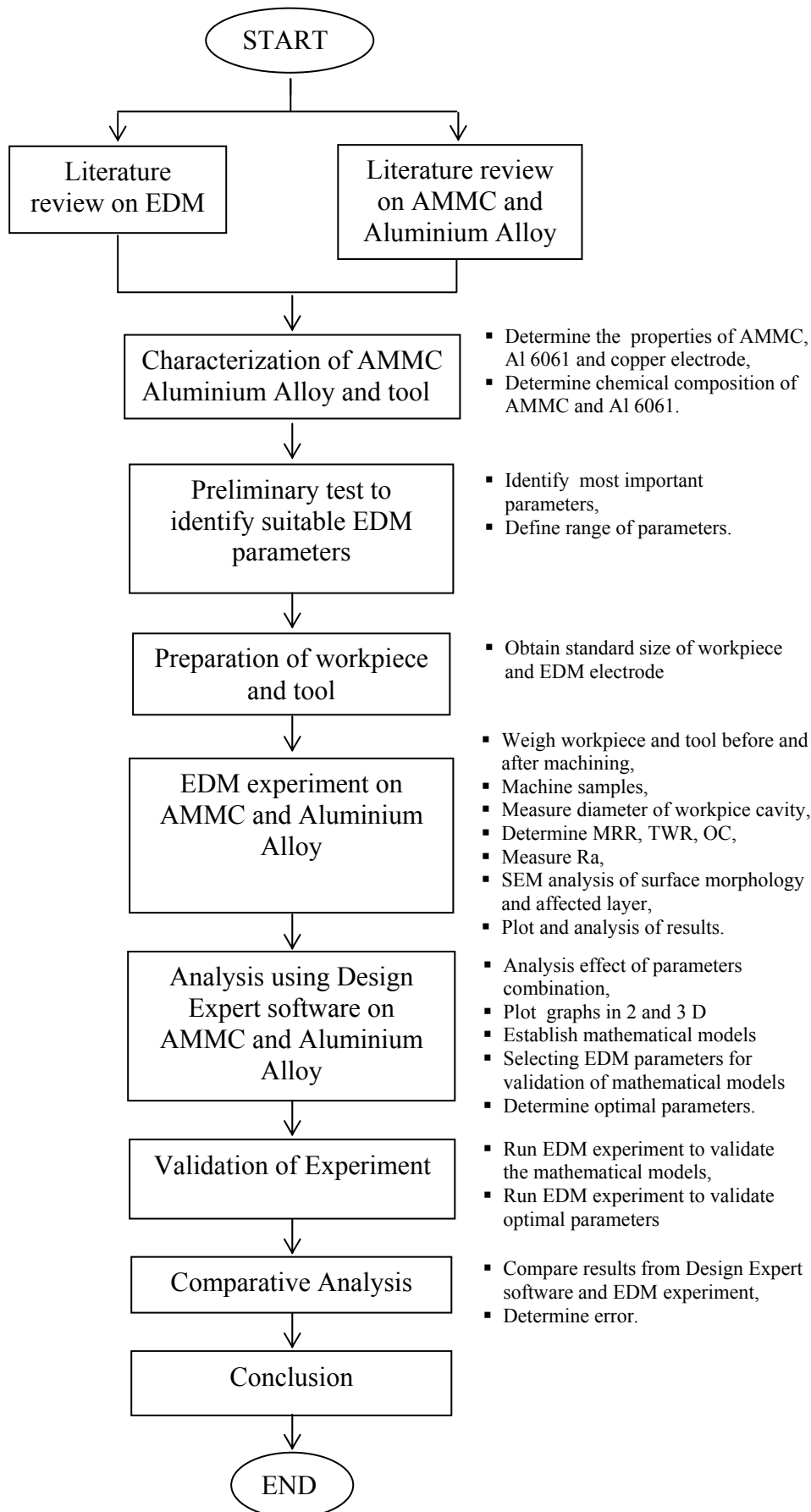


Figure 3.1: Research methodology chart

For the characterization of workpieces and tool materials, a test was done in order to determine the main properties and chemical composition and the results are presented in Table 3.3 to Table 3.6.

The preliminary test and EDM manual permit to identify the most important EDM parameters and to establish the parameters range. Table 3.1 presents the parameters setting.

For the workpiece preparation, CNC Mazak milling machine is used to cut the raw material into block shape required for clamping on EDM. Die-sinking EDM is used to machine the workpiece into samples. Two steps were used to machine the samples. Firstly, a hollow electrode was used to machine the first side up to 10mm (Figure 3.2a) and secondly, the bottom side is returned (Figure 3.2b) to be machined by using rectangular solid electrode. From the second step, the sample (Figure 3.2c) dropped and collected. After machining each sample, the wear part of electrode is cut off before proceed for machining the next sample from the actual workpiece (Figure 3.2d). The hollow cylindrical shape of electrode is chosen to produce cylindrical samples for testing which has yet been done and it might provide for more efficiency dielectric flushing.

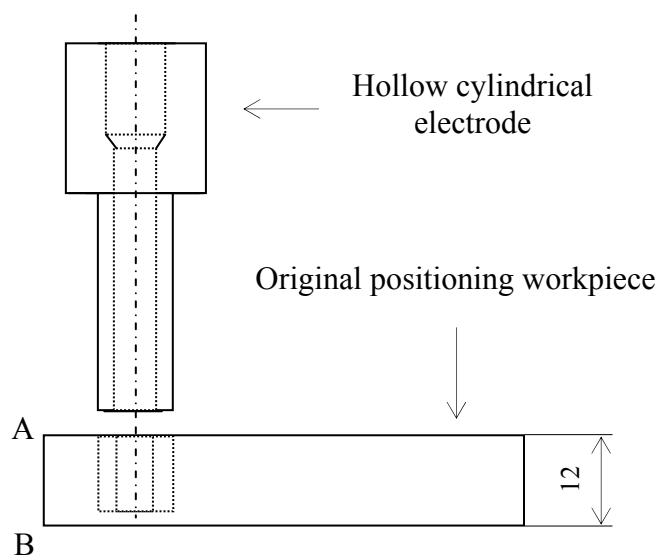


Figure 3.2a: Step 1 for machining the samples

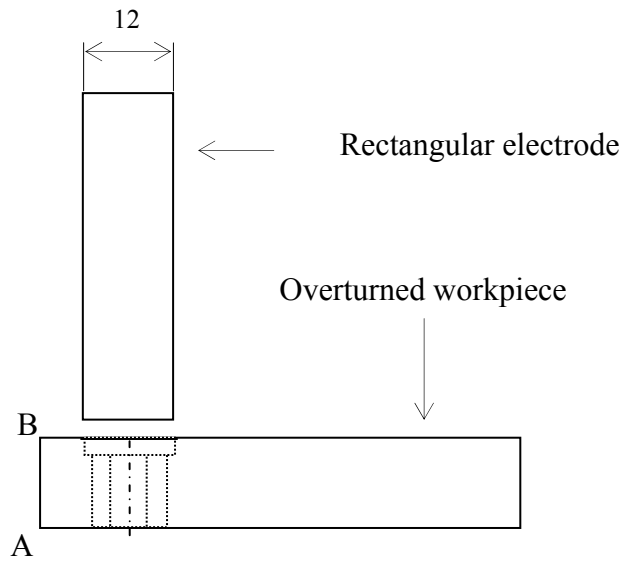


Figure 3.2b: Step 2 for machining the samples

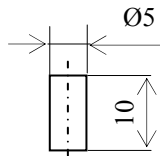


Figure 3.2c: Actual sample

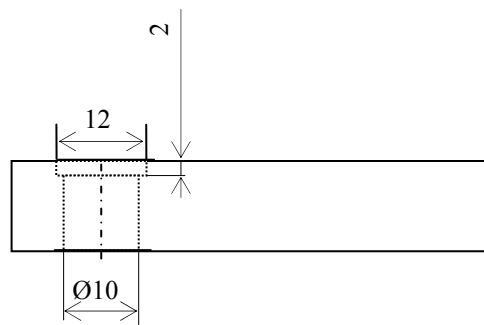


Figure 3.2d: Actual workpiece

The electrode was turned using lathe machine and finishing using Wire-cut EDM. After EDM each sample, the electrode is cut to remove the wear shape.

For the weighing, the workpiece was weighed before and after the machining in order to calculate the loss of mass for the workpiece and electrode during EDM machining.

For data collection and analysis, the mass loss for workpiece and tool are used to determine material removal rate and tool wear ratio. The surface roughness is determined using surface roughness tester. Scanning electron microscope (SEM) is used to examine the machined surface in order to investigate the surface morphology and affected layer. Design Expert 7.1 system is used to generate data based on analysis of variance (ANOVA), to optimize the output responses and to establish the mathematical models. Validation tests are run to evaluate the accuracies of the models.

3.2 Input Machining Parameters

The EDM machining parameters and their range of values used in this research are presented in Table 3.1. Three parameters namely peak current, ON-time and OFF-time were varied as the input parameters. The EDM parameters ranges have been selected according to EDM manual [71] and preliminary tests.

Table 3.1: Machining parameters

Parameters	Setting
Peak current (A)	3 - 55
ON-time (μ s)	3 - 192
OFF time (μ s)	3 - 96
Voltage (V)	220
Depth of cutting (mm)	10

The experiments were conducted by varying only one parameter at a time, while keeping all other parameters at constant values as planned in Table 3.2.

Table 3.2: Experimental plan for EDM of AMMC and Al 6061

Parameters			
Run No	Peak current (A)	ON-time (μ s)	OFF-time (μ s)
Peak current varies, ON-time and OFF-time are constant			
1	3	16	8
2	5.5	16	8
3	10	16	8
4	15	16	8
5	25	16	8
6	35	16	8
7	55	16	8
ON-time varies, peak and OFF-time are constant			
8	15	3	8
9	15	6	8
10	15	12	8
11	15	24	8
12	15	48	8
13	15	96	8
14	15	192	8
OFF-time varies, peak current and ON-time are constant			
15	15	16	3
16	15	16	4
17	15	16	6
18	15	16	12
19	15	16	24
20	15	16	48
21	15	16	96

3.3 Workpiece Material

Workpiece used for this research is aluminum metal matrix composite prepared and supplied by material technology laboratory, Ottawa, Canada (Figure 3.3).

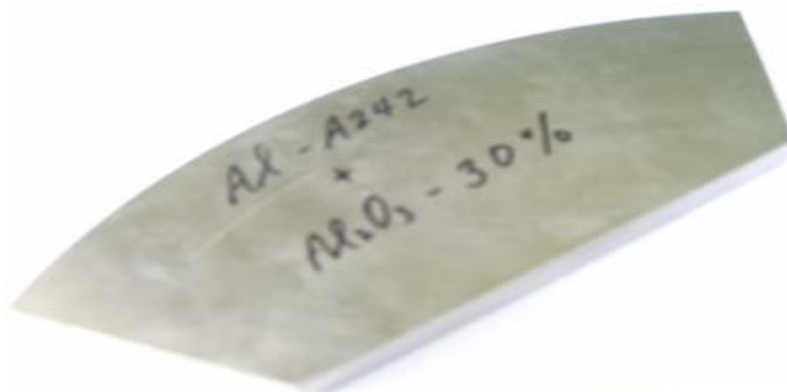


Figure 3.3: AMMC material used in this study

The chemical composition of 30% Al₂O₃ reinforced AMMC and Al 6061 tested using inductively coupled plasma (ICP) are listed in Table 3.3 and Table 3.4.

Table 3.3: Chemical composition of 30% Al₂O₃ reinforced AMMC (in % weight)

Al	O	Cu	Ni	Fe	Ti	Cr	Mn	Zn	Mo	Co
89.47	6.67	2.2	1.1	0.3	0.1	0.09	0.03	0.02	.008	0.008

Table 3.4: Chemical Composition of Al 6061 (in % weight)

Al	Mg	Fe	Si	Cu	Zn	Cr	Ti	Mn
96.5	1.0	0.7	0.6	0.3	0.25	0.2	0.15	0.15

The properties of 30% Al₂O₃ reinforced aluminium metal matrix composite and Al 6061 are presented in Table 3.5. The hardness is determined by hardness tester,, tensile and Young's modulus are determined by using universal testing machine; melting point is tested using differential scanning calorimetry (DCS); electrical resistivity is measured using resistivitimeter.

Table.3.5: Workpiece properties

	Hardness (HRB)	Melting point (°C)	Tensile strength (MPa)	Young's modulus (GPa)	Electric resistivity (Ωm)
AMC	91	710	434.1	85	2.96x10 ⁻⁵
Al 6061	60	660	328.0	68.9	3.99x10 ⁻⁷

3.4 Electrode Material

In this project, electrolytic copper (EC 99) was used as the electrode material. The electrode dimensions are indicated in Figure 3.5. Copper and certain power supply settings enables low wear burning. Also, Copper is compatible with the polishing circuits of certain advanced power supplies [34].

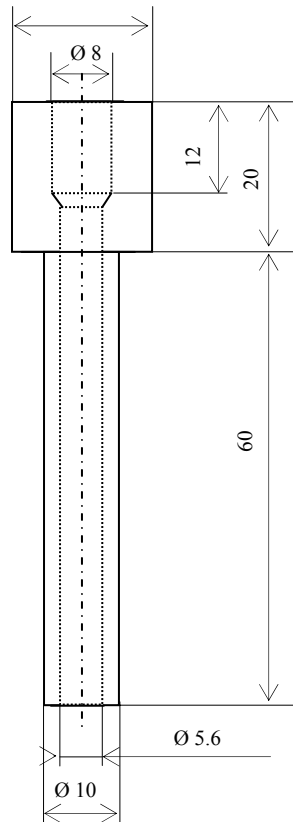


Figure 3.4: Schematic of copper electrode - all units are in mm

The properties of this electrode are presented in Table 3.6.

Table 3.6: Electrode properties

Density	8.96
(g/cm ³)	(°C)
Melting Point	1060
Young's	130
Hardness	100

3.5 Performance (Output Responses)

The output responses investigated in this research are surface roughness, material removal rate, tool wear ratio, overcut, surface morphology and thickness of affected layer.

3.5.1 Surface Roughness Measurement

The surface roughness average (Ra) was adopted and measurements were performed on all samples using a Mitutoyo SV3000 surface roughness tester presented in Figure 3.5.

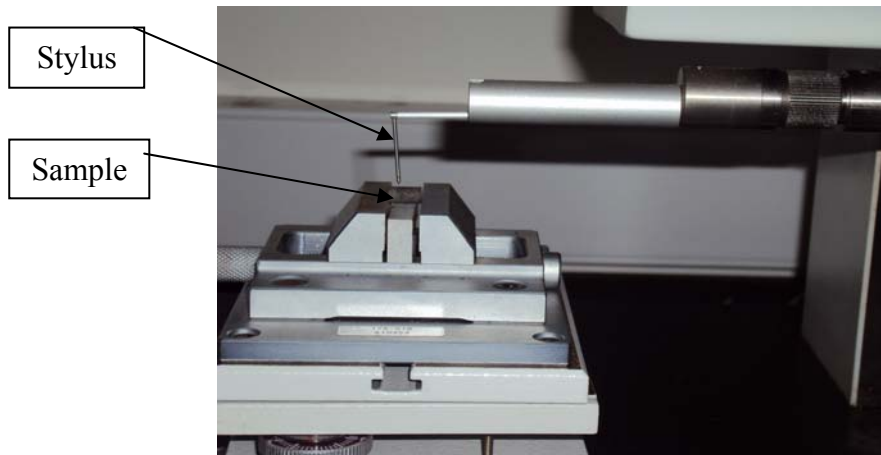


Figure 3.5: Surface roughness tester Mitutoyo SV3000 [UTP workshop]

One of main surface roughness tester part is stylus. The stylus traverses the surface peaks and valleys (Figure 3.6) and the vertical motion of the stylus is converted by the transducer into an electrical signal which may be analyzed by digital or analogue techniques. In many kinds of modern instruments, the signal undergoes analogue-to-digital conversion. The result in digital profile is stored in a computer and can be analyzed [42].

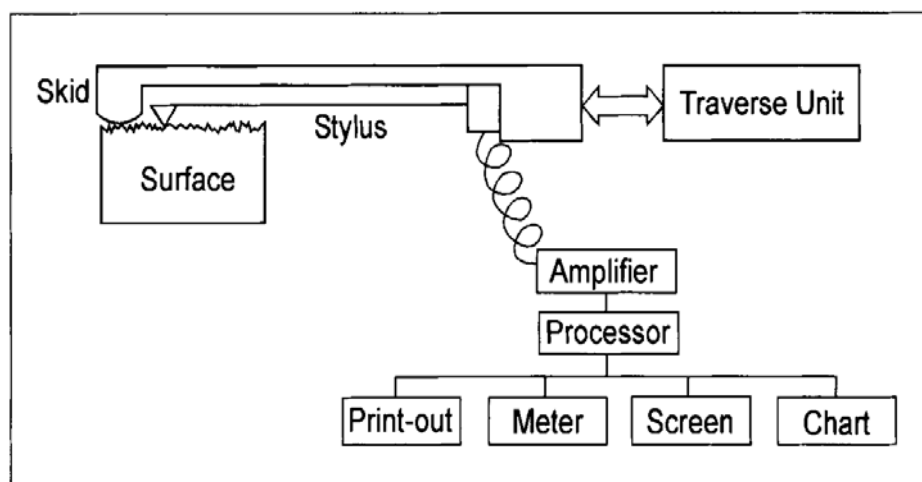


Figure 3.6: Schematic diagram of stylus instrument [42]

Since the samples are solid cylindrical, the measurement was taken longitudinally on four different locations. An average of four reading was calculated. Before conducting the measurement, all the samples were cleaned with ethanol.

3.5.2 Material Removal Rate (MRR)

The material removal rate in g/min was determined by using Equation (2.2) in chapter two which by dividing the mass loss of workpiece against the machining time.

The mass loss is measured by weighing the workpiece before and after machining using the electronic balance machine presented in Figure 3.7. Electronic balance machine is from branch Mettler Toledo AX. The maximum weight that can be measured is 500g with the resolution of 0.1mg.



Figure 3.7: Electronic precision balance machine [UTP workshop]

3.5.3 Tool Wear Ratio (TWR)

The present study defines the Tool wear ratio according to ratio in mass of the electrode and the workpiece which is expressed as percentage in Equation (2.5) in chapter two. This definition is the most commonly used among the researchers [48], [49], [50] and [51]. The mass loss of tool and workpiece are measured using electronic balance.

3.5.4 Overcut (OC)

Overcut is the gap distance between the electrode and the workpiece produced by sparking. It is determined by the half difference of cavity diameter from workpiece and the electrode diameter using Equation (2.6) in chapter two. Coordinate measuring machining (Figure 3.8) was used to determine the diameter of cavity. The coordinate measuring machine (CMM) from Beyond Crysta 707-Mitutoyo branch is a machine used for measuring physical geometrical characteristics of an object. This machine can be manually controlled by an operator or it may be computer controlled. Probe attached to the third moving axis defines the measurement. The probes can be mechanical, optical, laser.



Figure 3.8: Coordinate measuring machine [UTP workshop]

3.5.5 Microscopy

3.5.5.1 Morphology of Machined Surface

Samples were machine during EDM process at various machining parameters setting. Examination of surface morphology of machine surface was done on selected samples. Scanning electron microscope Leo 1430VP model (Figure 3.9) was used to examine the longitudinal machined surface of cylindrical solid samples.



Figure 3.9: Scanning electron microscope [UTP workshop]

3.5.5.2 Affected Layer

Scanning electron microscope (SEM) was used to determine the thickness of affected layer on the cross-section area of samples. The samples were ground using grinder machine from Buehler Metasser Aser V2000 model Figure 3.10 with silicon carbide paper starting from 240 up to 1000 grits following by polishing process using polishing cloth and diamond 6μ and 3μ grit.



Figure 3.10: Grinder machine [UTP workshop]

3.6 Response Surface Methodology Procedure

Response surface methodology (RSM) is a tool in design of experiment (DOE) for designing, mathematical modelling and analysing the experiment. RSM is mainly

applied in industry, engineering and sciences [72], [58]. The objective of RSM is to find the optimum response, to understand how the response changes in a given parameters and to visualized graphically the response. The software associated to DOE and used in this research is Design Expert. The version 7.1 of Design Expert software helps to conduct the design, analysis and interpreting of multi-factor experiments [58]. It analyzes the data and graphically displays the results, permits the user to see how an output such as Ra, MRR, TWR and OC vary with changes in EDM parameters [73]. During the RSM, central composite design (CCD) is set up. After the experiment completed, the output responses must be entered into the template created during the design plan. The following steps are used to analyse the data [74]:

- Choose a transformation if desired. Otherwise, leave the option at “None”.
- Fit Summary option to fit all of the polynomial models to the selected response. Model Summary Statistics presents the regression-squared (R^2) which measures the amount of variation around the mean explained by the model, statistical measure of how well a regression line approximates real data.
- Select the appropriate model (linear, quadratic or cubic) suggested in fit summery to be used,
- Perform the analysis of variance (ANOVA). Analysis of variance (ANOVA) permits to test for differences in the means of several different groups. ANOVA tests the null hypothesis that the means for all of the groups are equal,
- Inspect various diagnostic plots,
- Generate the model graph (2-D, 3-D, interaction graph),
- Optimize the multi-responses after analysis of each response.

A good model must be significant and the various coefficient of determination, R^2 value should be close to one.

CHAPTER FOUR

RESULTS AND DISCUSSION

Results from the experimental work on machining of 30 % vol alumina reinforced aluminium metal matrix composite and on aluminium alloy (Al 6061) are presented in this chapter. The results involve the effect of EDM parameters on surface roughness (Ra), material removal rate (MRR), tool wear ratio (TWR), overcut (OC), surface morphology and affected layer. The experimental results have been obtained using diverse instruments and methods as described in chapter three. Design Expert software was used to establish a relationship between output responses and the parameters and to determine the optimum response. Validation test was done to evaluate the accuracy of mathematical models.

During EDM experiment, three EDM parameters namely peak current, ON-time and OFF-time were varied and they are respectively labelled as A, B and C. The parameter values were varied in the specified range. Peak current (A) ranges from 3A to 55A; ON-time (B) ranges from 3 μ s to 192 μ s and OFF-time (C) ranges from 3 μ s to 96 μ s as scope of this research.

4.1 Effects of EDM Parameters on Surface Roughness

Machining process operation leaves characteristic evidence on the machined surface. Roughness consists of surface irregularities which result from the machining process. The effects of EDM parameters on surface roughness of both AMMC and Al 6061 are recorded and presented in appendix A-1, A-2 and A-3.

4.1.1 Effects of Peak Current on Surface Roughness

The influence of the peak current supplied to the electrode on Ra was observed by keeping the ON-time and OFF-time constant at 16 μ s and 8 μ s, respectively. As the current is increased from 3A to 55A, the Ra of both AMMC and Al 6061 increases, but at different rates as it can be seen from Figure 4.1 with regression squared (R^2) 0.9788 and 0.9852 for AMMC and Al 6061 respectively. As the peak current is increased to 55A, the Ra of AMMC is about three times higher than that of Al 6061. To achieve a certain value of Ra less than 12.5 μ m of AMMC, peak current can be set below 8A with keeping ON-time and OFF-time at 16 μ s and 8 μ s respectively. Although peak current can be increased to maximum value and achieve Ra less than 12.5 μ m for Al 6061.

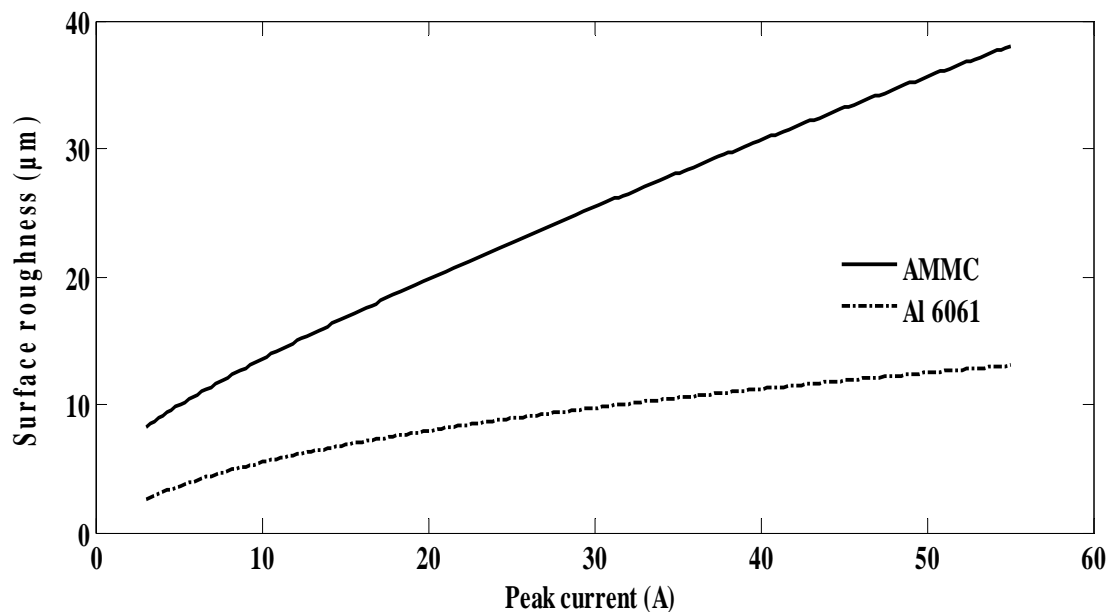


Figure 4.1: Variation in surface roughness due to change of peak current (ON-time: 16 μ s, OFF-time: 8 μ s)

Higher peak current caused a poorer surface finish of AMMC. The peak current determines the size of spark energy. By increasing the peak current, the spark energy increases which create more craters and cracks leading to increasing surface roughness. Narender et al. observed that higher peak current resulted higher surface roughness due to higher thermal loading into the workpiece and electrode [48]. The less sensitive effect of peak current on surface roughness of Al 6061 compared to that of AMMC is due to the superior thermal and electrical conductivities of Al 6061 than that of AMMC and the hard of the reinforcement particle present in AMMC.

Materials with high thermal conductivity dissipate heat rapidly through the workpiece resulting in low value of Ra. Since the EDM process uses electrical current as a tool, the high electrical conductivity of Al 6061 promotes more machining efficiency compared to that of AMMC.

4.1.2 Effects of ON-time on Surface Roughness

The effect of ON-time applied to the electrode on surface roughness is observed by keeping constant the peak current and the OFF-time at 15A and 8 μ s respectively. As the ON-time is increased from 3 μ s to 192 μ s, the Ra of both AMMC and Al 6061 increased but at different rates as it can be seen from Figure 4.2 with R^2 0.9821 and 0.9906 for AMMC and Al 6061 respectively. As the ON-time is increased, the Ra of AMMC is about two and half times higher than that of AMMC. Ra less than 12.5 μ m can be achieved at ON-time set below 18 μ s, while peak current and OFF-time are kept at 15A and 8 μ s respectively. Although ON-time can be increased to maximum value and obtain the acceptable Ra.

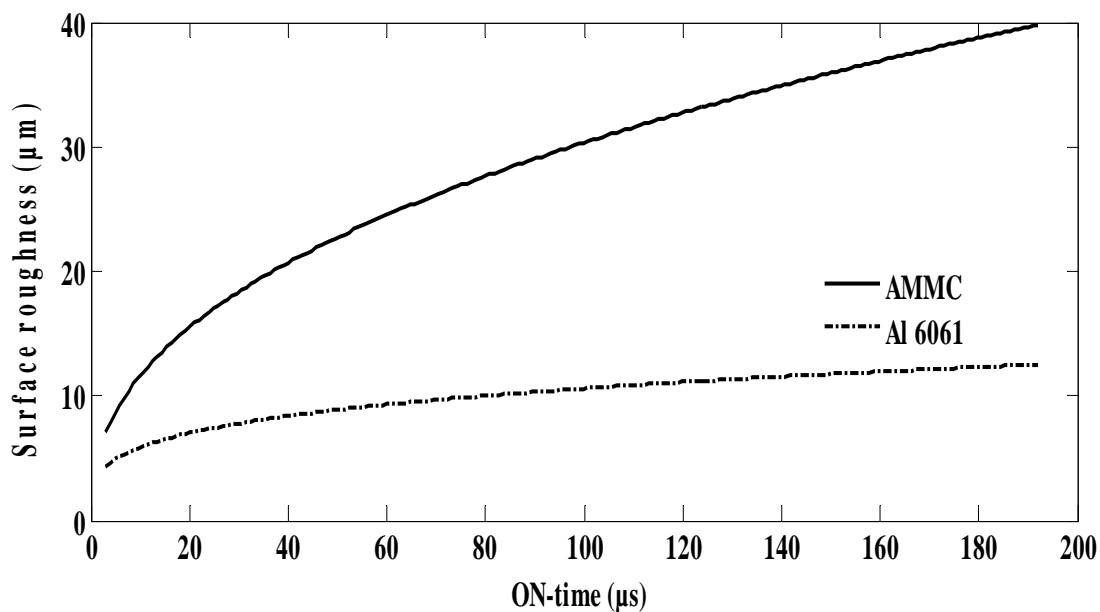


Figure 4.2: Variation in surface roughness due to change in the ON-time (Peak current: 15A, OFF-time: 8 μ s)

Higher ON-time caused a poorer surface finish. Spark energy is also a function of ON-time. Increasing ON-time leads to increase the spark energy, which increases crater and crack sizes. Due to the good aptitude of Al 6061 to be machined using by

non-conventional machining compared to AMMC, the surface roughness of AMMC becomes comparatively worse than that of Al 6061. This concurs with observation by Guu et al. [62] that the higher discharge energy caused more frequent melting expulsion, leading to the formation of deeper and larger crater on the machined surface and consequently resulted in poor surface finishing.

4.1.3 Effects of OFF-time on Surface Roughness

The effect of OFF-time applied to the electrode on Ra is observed by keeping the peak current and ON-time at 15A and 16 μ s respectively. As the OFF-time is increased from 3 μ s to 96 μ s, the Ra of both AMMC and Al 6061 decreases but at different rates as it can be seen in Figure 4.3 with R^2 0.9600 and 0.9885 for AMMC and Al 6061 respectively. At very low OFF-time, Ra of AMMC is about four times higher than that of Al 6061 due to the presence of alumina. For OFF-time beyond 24 μ s, the Ra of AMMC decreases rapidly while Ra of Al 6061 remains closely constant. When OFF-time is set at higher value, the Ra of both AMMC and Al 6061 tends to be closer. To achieve a Ra value of less than 12.5 μ m for AMMC, the OFF-time need to be set higher than to 15 μ s, while keeping constant peak current and ON-time at 15A and 8 μ s respectively.

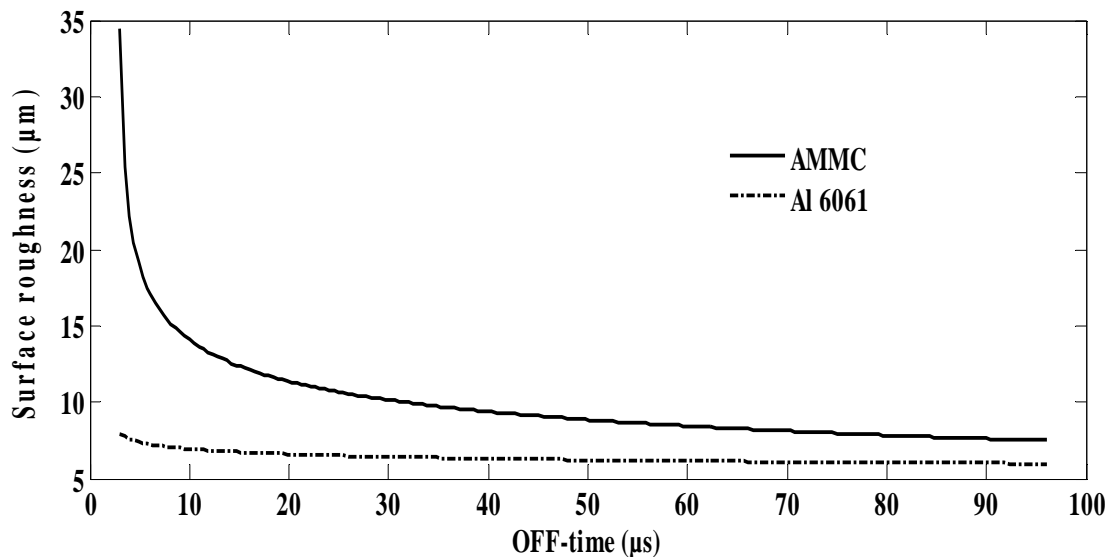


Figure 4.3: Variation in surface roughness due to change in the OFF-time (Peak current: 15A, ON-time: 16 μ s)

As the OFF-time is shorter, the number of discharge within a given period becomes more which leads to a faster machining but the surface roughness becomes worse. The increase of OFF-time leads to decreasing of gap voltage. Fine machined finish can be observed by setting the machine parameters at a longer OFF-time. This can be due to the fact that as the OFF-time increases, the discharges strike the surface of the sample less intensely and the resulting finer erosion effect leading to a smoother surface finish. Furthermore, as the OFF-time increases, the amount of heat energy transferred to the sample surface decreases and so less material melts.

4.1.4 Analysis of EDM Parameters on Ra using Design Expert Software

The output responses were analyzed using response surface methodology (RSM) in Design Expert software. Appendix B-1, B-2, B-3 and B-4 present the sequential and ANOVA tables for Ra of AMMC and Al 6061.

4.1.4.1 Analysis on AMMC

Figure 4.4 shows the perturbation (influence on the system that causes it to deviate slightly) plot, from which the effects of the three parameters on MRR can be observed. The results indicate that peak current (A), pulse On-time (B) and OFF-time (C) have influence on Ra. The value of Ra increases when peak current and ON-time increase. Though, Ra decreases when OFF-time increases.

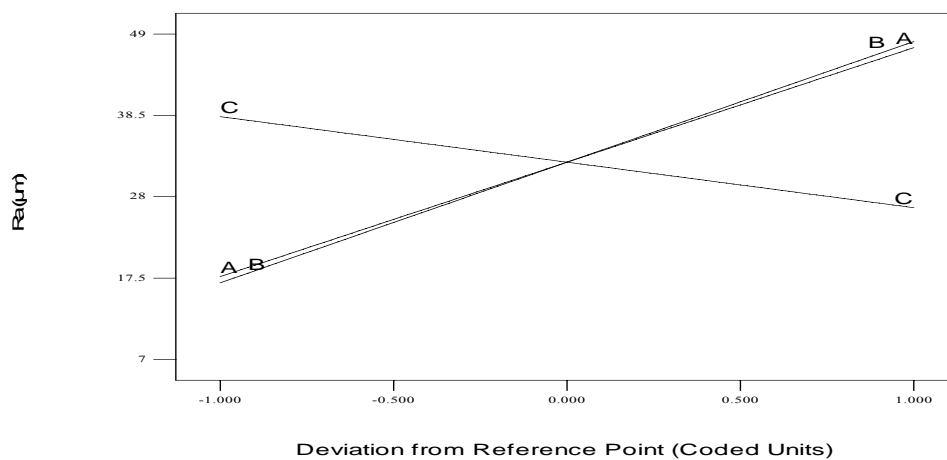


Figure 4.4: Perturbation plot Vs. deviation from reference point for Ra of AMMC

Figure 4.4 compares the effect of all three parameters at the particular point in the design space. Curves Peak current (A) and ON-time (B) grow, which indicates the increasing of surface roughness with increasing of peak current and ON-time. The curve OFF-time (C) indicates the decreasing of surface roughness when OFF-time increases.

Figure 4.5 shows the contour plot of surface roughness versus peak current and ON-time, while keeping OFF-time constant at 25.5 μ s. It is a two-dimensional representation of surface roughness for the selected parameters. As it can be seen, the surface roughness becomes worsen with increasing of peak current and ON-time.

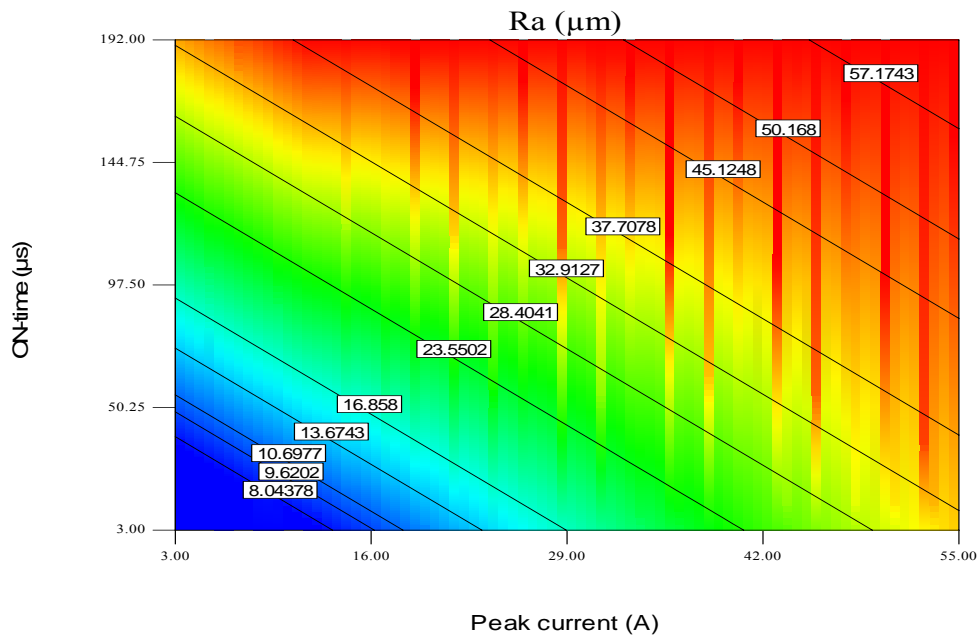


Figure 4.5: Contour plot Vs. parameters for Ra of AMMC

Figure 4.6 shows a three-dimensional graph for surface roughness. The increase in surface roughness with increasing peak current and ON-time can be seen clearly from this graph.

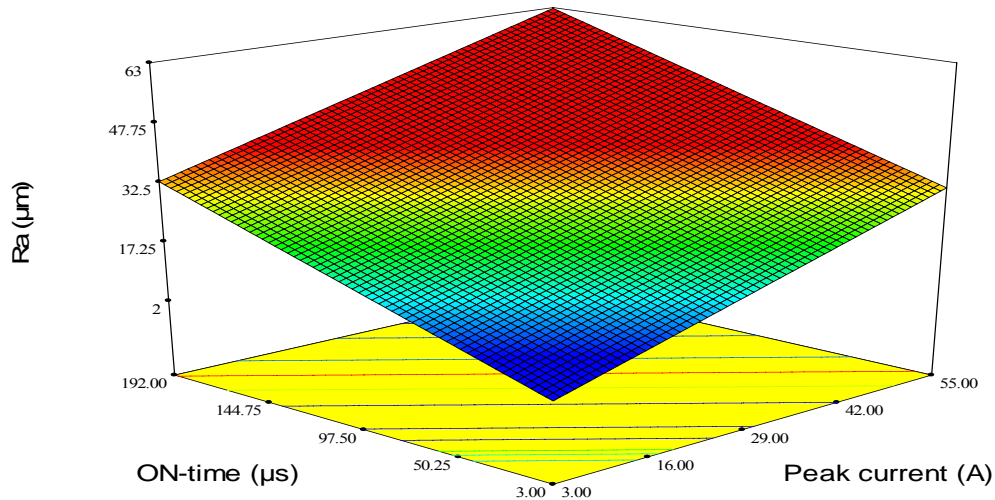


Figure 4.6: 3-D graph for Ra of AMMC

A mathematical model of the collected data was obtained by performing a linear regression analysis of the data using Design Expert software. The final equation with regression squared (R^2) equals 0.7868 for surface roughness is:

$$Ra = 6.196 + 0.626A + 0.124B - 0.171C \quad (4.1)$$

Where, Ra is surface roughness, A is peak current, B is ON-time and C is OFF-time.

4.1.4.2 Analysis on Al 6061

Figure 4.7 shows a perturbation plot showing a comparison of the effects of the three parameters on Ra. The intersection of the three lines is known as the reference point and the actual conditions for the parameters at the reference point as indicated on the graph. The result indicates that peak current (A), On-time (B) and OFF-time (C) have a significant effect on Ra. The value of Ra increases when either peak current or ON-time leading to an increase. However, Ra decreases when OFF-time increases.

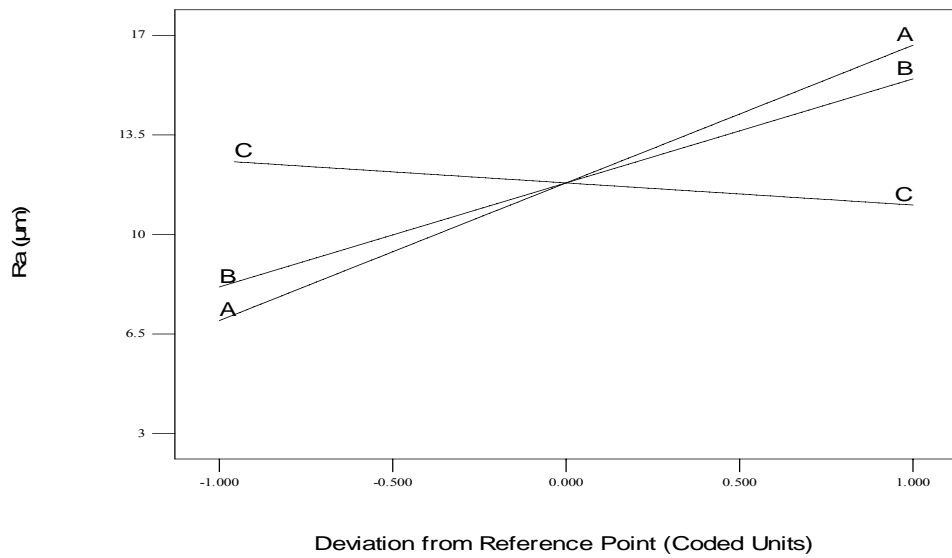


Figure 4.7: Perturbation plot Vs. deviation from Reference: point for Ra of Al 6061

Figure 4.8 shows the effect of peak current and ON-time on Ra, while OFF-time remains constant at 25.5µs. It can be observed that increasing the peak current and ON-time leads to an increasing of Ra.

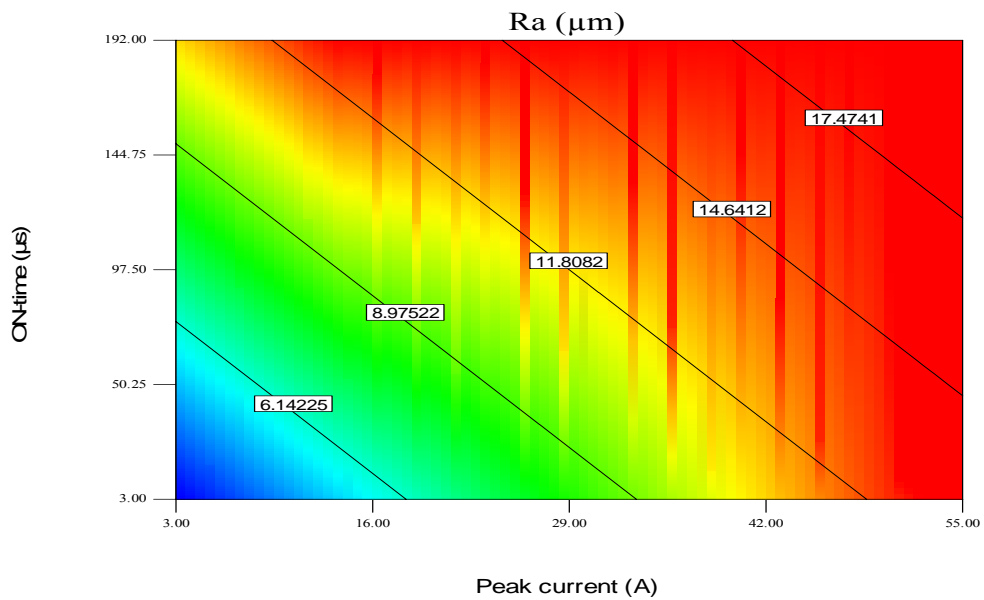


Figure 4.8: Contour plot Vs. parameters for Ra of Al 6061

Figure 4.9 presents the 3-D graph for Ra of Al 6061. It shows the effects of peak current and ON-time, while OFF-time is kept constant at 25.5 μ s. As it can be seen, the Ra increases when peak current and ON-time increase.

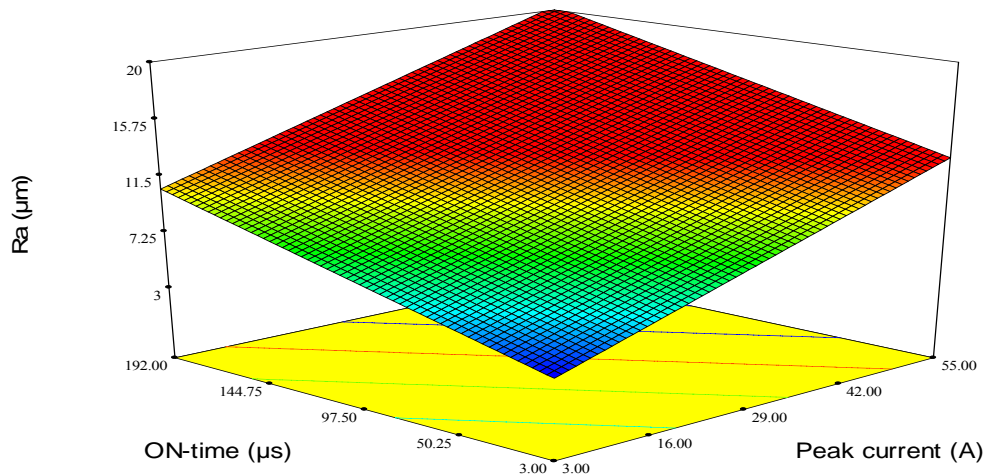


Figure 4.9: 3-D graph for Ra of Al 6061

Based on linear regression analysis of the experimental data, the mathematical model with R^2 equals 0.8676 for surface roughness of Al 6061 is:

$$Ra = 3.394 + 0.187A + 0.032B - 0.020C \quad (4.2)$$

Where, Ra is the surface roughness, A is peak current, B is ON-time and C is OFF-time.

4.2 Effects of EDM Parameters on Material Removal Rate

Material removal rate (MRR) in EDM process is an important factor because of its effect on the industrial economy. The effects of EDM parameters on material removal rate are recorded and presented in Appendix A-4, A-5 and A-6.

4.2.1 Effects of Peak Current on Material Removal Rate

The influence of peak current supplied to the electrode on MRR is observed by keeping the ON-time and OFF-time at 16 μ s and 8 μ s respectively. As the current is

increased from 3A to 55A, the MRR of both AMMC and Al 6061 increased but at different rates as it can be seen in Figure 4.10 with R^2 0.9552 and 0.9963 for AMMC and Al 6061 respectively.

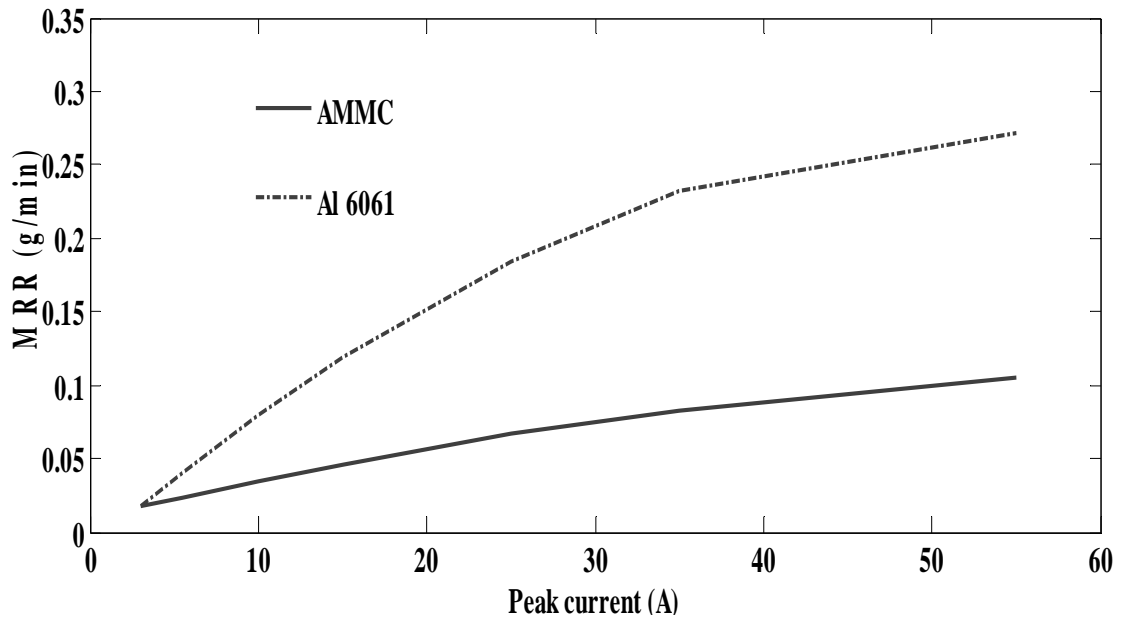


Figure 4.10: Variation in MRR due to changes in peak current (ON-time: 16 μ s, OFF-time: 8 μ s)

At very low peak current, MRR of AMMC and Al 6061 are almost similar, but for peak current greater than 15A, the MRR of Al 6061 is about three times higher than that of AMMC. As the peak current is increased to the maximum value, the rate of increase of the MRR for both materials appeared to taper off at 0.28g/min for Al 6061 and 0.11g/min for AMMC. This is due to the good electrical and thermal conductivities of Al 6061 than that of AMMC. The increase of MRR when peak current increase is due to the increase in spark discharge energy which facilitate the action of melting and vaporization and advancing the large impulsive force in the spark gap, so increasing the MRR. Higher peak current results in a higher thermal loading on both the cathode and anode, followed by a higher amount of material being ejected. This results in a larger crater size lead to rougher machine surface. Kumar et al. showed also that the MRR tends to increase significantly with increase in peak current due to their dominant control over their input energy [70].

Figure 4.11 with R^2 0.9370 and 0.9649 for AMMC and Al 6061 respectively presents the result of effect of peak current on machining time. When peak current increases from 3A to 55A, the machining time of AMMC and Al 6061 decreases but at different rate. The machining time of AMMC is about two times greater at low peak current and about five times at higher peak current than that of Al 6061. This is due to the increase of spark energy by increasing peak current. Higher spark energy removes more materials.

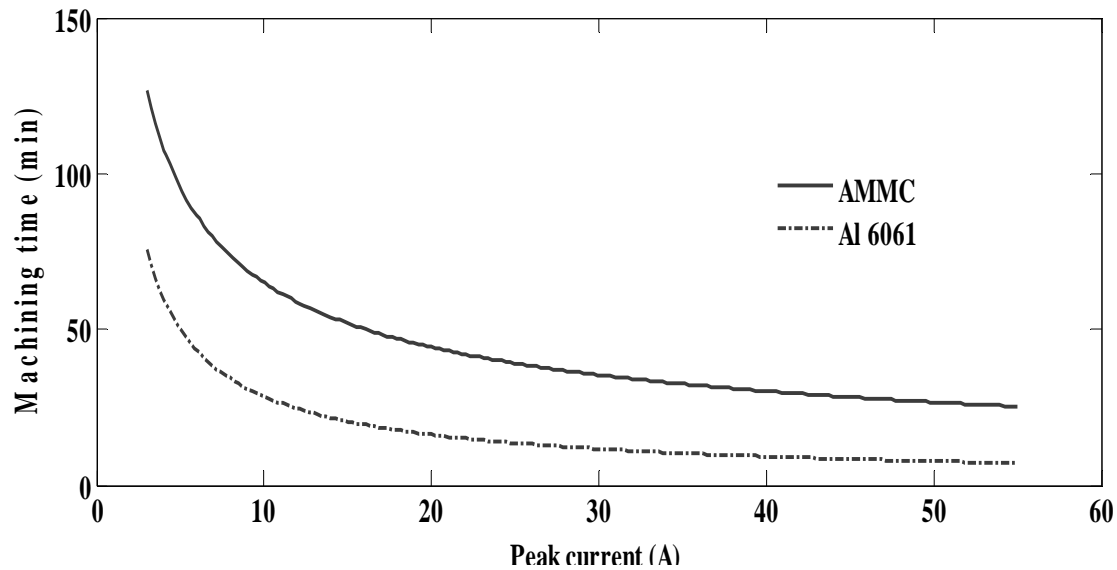


Figure 4.11: Variation in machining time due to changes in peak current (ON-time: 16 μ s, OFF-time: 8 μ s)

4.2.2 Effects of ON-time on Material Removal Rate

The effect of varying ON-time on MRR is observed by keeping peak current and OFF-time constant at 15A and 8 μ s respectively. The effect of ON-time is similar to that of peak current. As the ON-time increased from 3 μ s to 192 μ s, the MRR of both AMMC and Al 6061 increased as it can be observed from Figure 4.12 with R^2 0.9838 and 0.9548 for AMMC and Al 6061 respectively. For the same reasons described previously for the effect the peak current on MRR, ON-time increases of spark energy size leading to increase MRR.

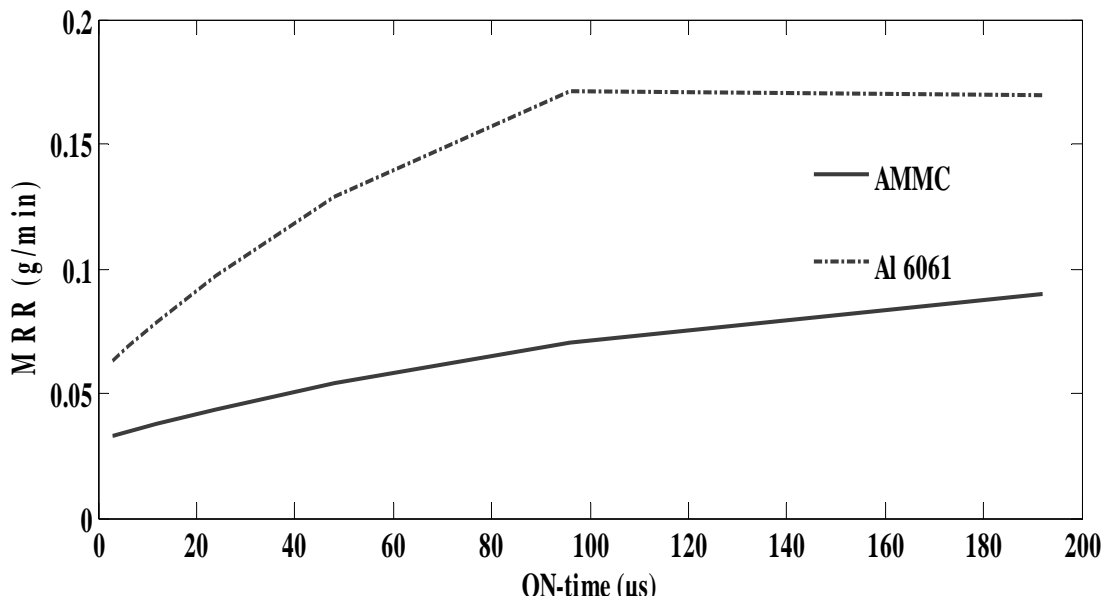


Figure 4.12: Variation in MRR due to changes in ON-time (Peak current: 15A, OFF-time: 8 μ s)

The MRR of Al 6061 increases rapidly and in greater amount than that of AMMC and is about two times greater than that of AMMC. The increase in ON-time increases the spark energy leading to faster material removal. Kumar et al. have shown that the MRR tends to increase significantly with increase in ON-time due to their dominant control over the input energy [70]. Maximum MRR of AMMC and Al 6061 can be achieved at longer ON-time but Ra becomes worse for AMMC.

Figure 4.13 with R^2 0.9767 and 0.9415 for AMMC and Al 6061 respectively shows the effect of ON-time on machining time of both AMMC and Al 6061. As it can be observed from Figure 4.11, the machining time of Al 6061 is greater than that of AMMC when ON-time increases from 3 μ s to 192 μ s. The machining time of AMMC is about two times greater at short ON-time and about three times greater at longer ON-time greater than that of Al 6061. The increase in ON-time increases the spark energy and it has similar effect on machining time as peak current.

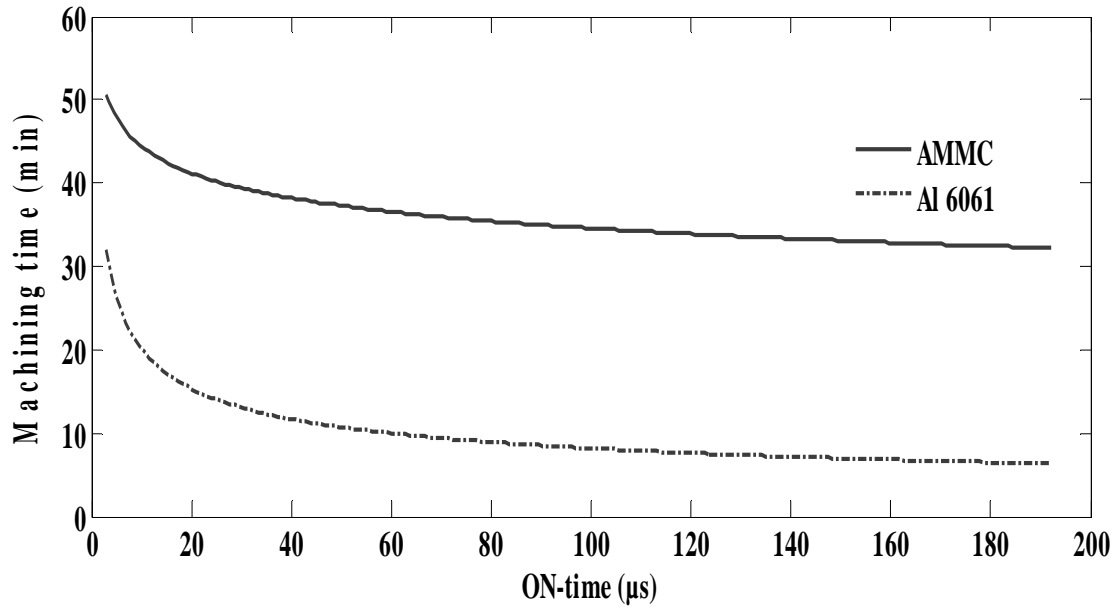


Figure 4.13: Variation in machining time due to changes in ON-time (Peak current: 15A, OFF-time: 8 μs)

4.2.3 Effects of OFF-time on Material Removal Rate

The effect of varying OFF-time on MRR is observed while keeping peak current and ON-time at 15A and 16 μs respectively. The OFF-time is varied from 3 μs to 96 μs as shown in Figure 4.14 with R^2 0.9918 and 0.9872 for AMMC and Al 6061 respectively.

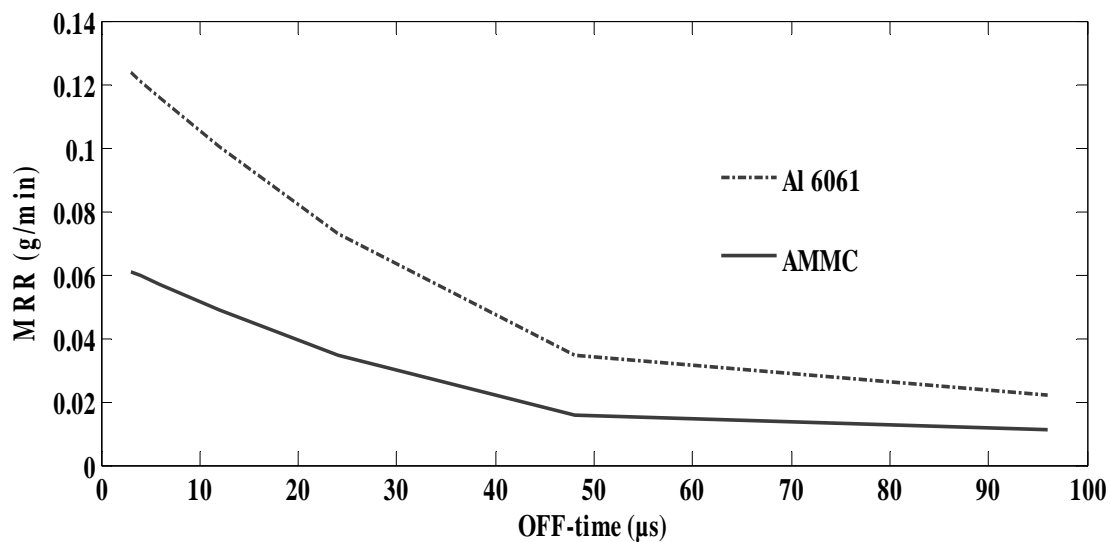


Figure 4.14: Variation in MRR due to changes in OFF-time (Peak current: 15A, ON-time: 16 μs)

For OFF-time below $15\mu\text{s}$, MRR of both AMMC and Al 6061 are higher but the MRR of Al 6061 is about two times greater than that of AMMC. For OFF-time beyond $15\mu\text{s}$, MRR of both materials decreases rapidly. Longer OFF-time causes longer cooling time of workpiece and electrode. The melted workpiece part has sufficient time to be solidified before reheated at next ON-time leading to low machining speed resulting in low MRR. Short OFF-time give more sparks energy per unit of time and thus more material removal. Singh et al. also showed that MRR decreases with OFF-time [75]. As the ON-time is increased, the Ra of AMMC is about two and a half times higher than that of AMMC. Ra less than $12.5\mu\text{m}$ can be achieved at ON-time set below $18\mu\text{s}$, while peak current and OFF-time are kept at 15A and $8\mu\text{s}$ respectively. Although ON-time can be increased to maximum value and obtain the acceptable Ra.

Figure 15, with R^2 0.9485 and 0.9810 for AMMC and Al 6061 respectively, shows the effects of OFF-time on machining time of AMMC and Al 6061. Time for machining AMMC is longer than that of Al 6061 when the OFF-time increases from $3\mu\text{s}$ to $96\mu\text{s}$. In EDM all work is done only during ON-time. The shorter OFF-time makes machining faster.

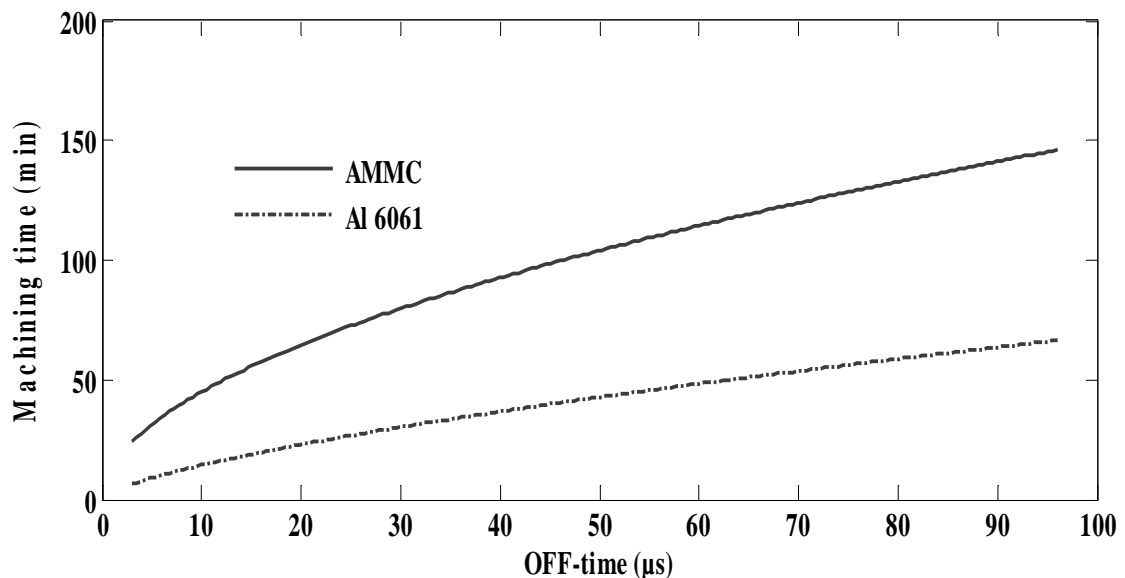


Figure 4.15: Variation in machining time versus OFF-time (Peak current: 15A, ON-time: $16\mu\text{s}$)

4.2.4 Analysis of EDM Parameters on MRR Using Design Expert Software

Appendix B-5, B-6, B-7 and B-8 present the sequential and ANOVA tables for MRR of AMMC and Al 6061.

4.2.4.1 Analysis on AMMC

Figure 4.16 presents the perturbation plot and it shows the intersection of the three lines at the reference points and the actual conditions for the three parameters. It shows the changes in MRR due to variations in peak current (A), ON-time (B) and OFF-time (C). When peak current and ON-time increase, the MRR increases due to an increase in spark energy.

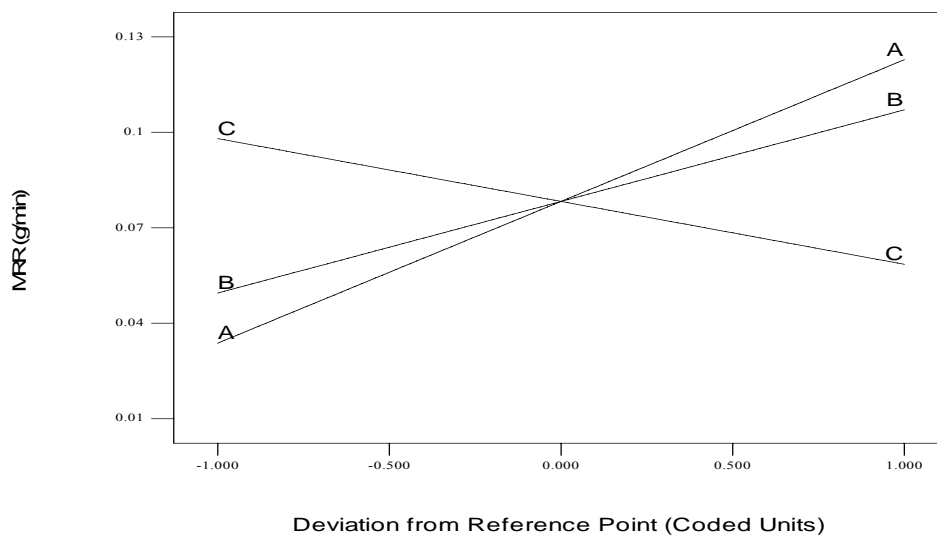


Figure 4.16: Perturbation plot Vs. deviation from reference point for MRR of AMMC

A two-dimensional contour plot for MRR versus peak current and ON-time with keeping OFF-time at 25.5 μ s is presented in Figure 4.17. It can be observed that MRR is higher at high peak current and ON-time due to an increase in size of spark energy.

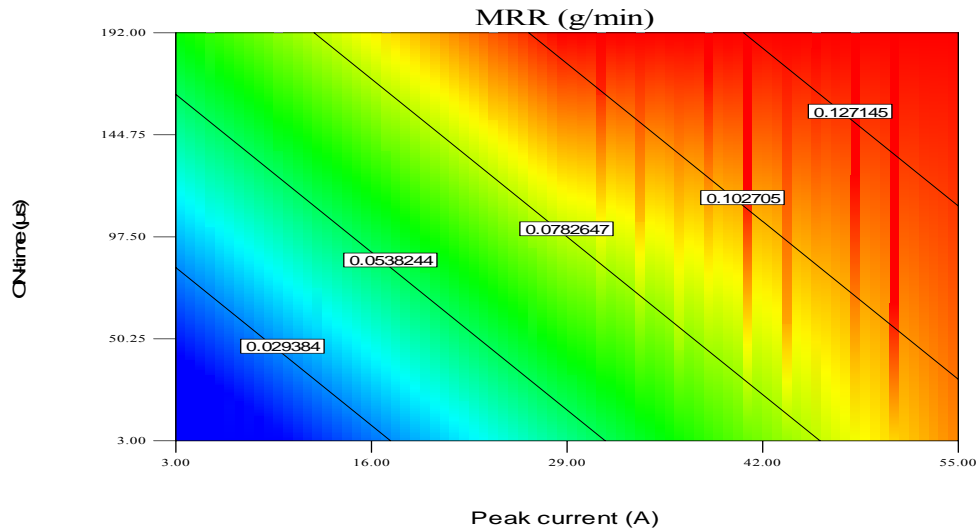


Figure 4.17: Contour plot Vs. parameters for MRR of AMMC

Figure 4.18 presents a 3-D graph for MRR of AMMC versus peak current and OFF-time while OFF-time is kept constant at 25.5μs. It can be seen from Figure 4.18 that MRR increases with increasing in peak current and ON-time.

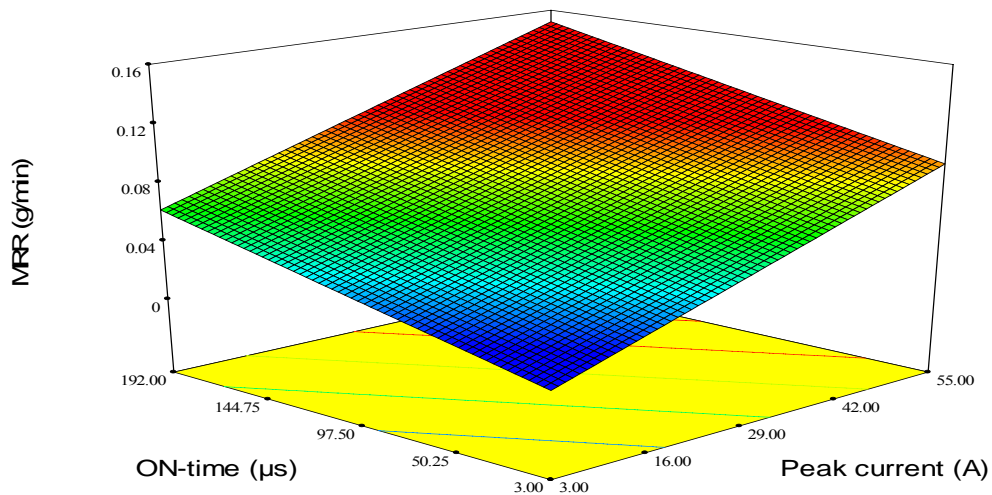


Figure 4.18: 3-D graph for MRR of AMMC

A mathematical model as given in Equation (4.3) is obtained by performing linear regression analysis on the collected data using Design Expert software. The final expression with R^2 equals 0.9150 for material removal rate is:

$$\text{MRR} = 0.017 + 1.787 \times 10^{-3} A + 2.366 \times 10^{-4} B - 5.305 \times 10^{-4} C \quad (4.3)$$

Where, MRR is material removal rate, A is peak current, B is ON-time and C is OFF-time.

4.2.4.2 Analysis on Al 6061

Figure 4.19 shows a perturbation plot that compares the effects of the three parameters on MRR. The results indicate that Peak current (A), Pulse On-time (B) and OFF-time (C) have a significant effect on Ra. The value of Ra increases when either peak current or ON-time increases. However, the Ra decreases when OFF-time increases.

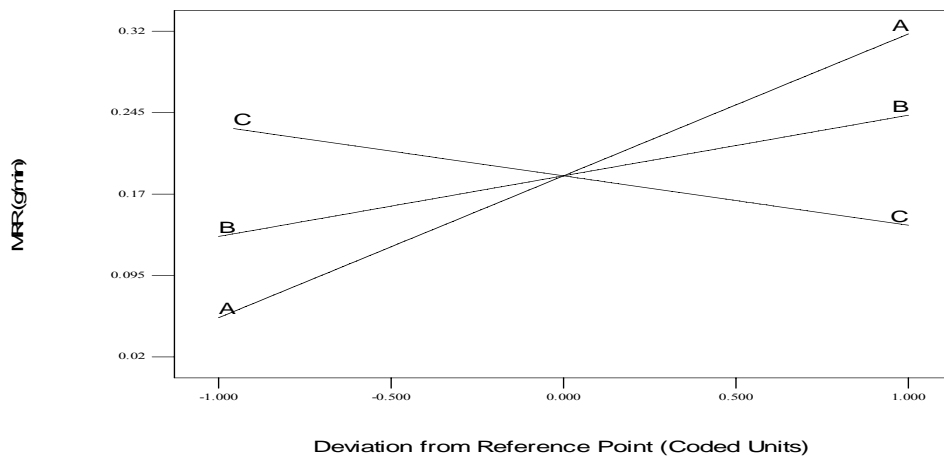


Figure 4.19: Perturbation plot Vs. deviation from reference point for MRR of Al 6061

Figure 4.20 shows the effect of peak current and ON-time on MRR of Al 6061 while the OFF-time remains constant at value 25.5 μ s. It can be observed from Figure 4.16 that the increase in peak current and ON-time leads to an increase in MRR. Both peak current and ON-time have nearly the same effect on the increase of MRR.

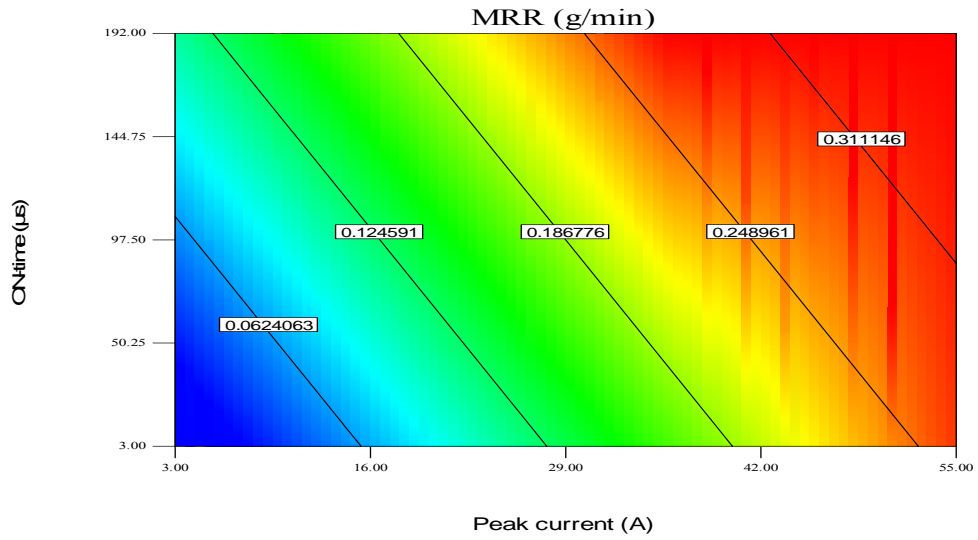


Figure 4.20: Contour plot Vs. parameters for MRR of Al 6061

Figure 4.21 presents the three-dimension graph of MRR for Al 6061. It shows the effects of peak current and ON-time while OFF-time is kept constant at 25.5 μ s. The graph shows that MRR increases with increasing peak current and ON-time.

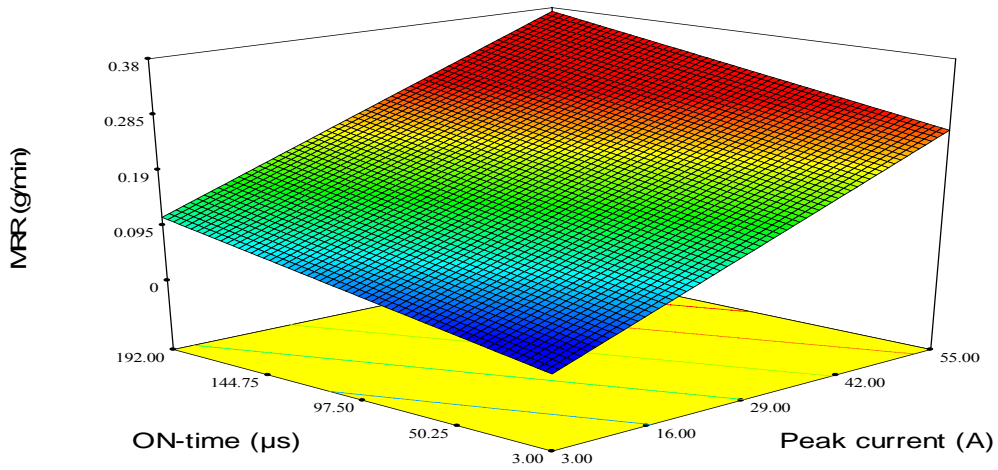


Figure 4.21: 3-D graph for MRR of Al 6061

The final mathematical equation with R^2 equals 0.8624 of MRR for Al 6061 is:

$$\text{MRR} = 0.019 + 5.34 \times 10^{-3}A + 4.783 \times 10^{-4}B - 1.083 \times 10^{-3}C \quad (4.4)$$

Where, MRR is material removal rate, A, the peak current, B, ON-time and C, is OFF-time.

4.3 Effects of EDM Parameters on Tool Wear Ratio

Electrode wear is the result of either electron or positive ion bombardment. When the electrode is positive, it is bombardment by electrons. The effects of EDM parameters on tool wear ratio were recorded and are presented in Appendix A-7, A-8 and A-9.

4.3.1 Effects of Peak Current on Tool Wear Ratio

The influence of peak current on tool wear ratio was investigated by keeping constant ON-time and OFF-time at $16\mu\text{s}$ and $8\mu\text{s}$ respectively. The peak current is varied from 3A to 55A as shown in Figure 4.22 with R^2 0.5221 and 0.9538 for AMMC and Al 6061 respectively. TWR of Al 6061 is higher at low peak current and it decreases when the peak current increases. Khanra et al [68] found that volumetric wear ratio decreases with the increase in peak current. Minimal TWR of AMMC and Al 6061 can be achieved at higher peak current. The current passes through the electrode to the workpiece. When the electrical energy discharges, it ionizes a part through the dielectric fluid and vaporizes an area on the workpiece.

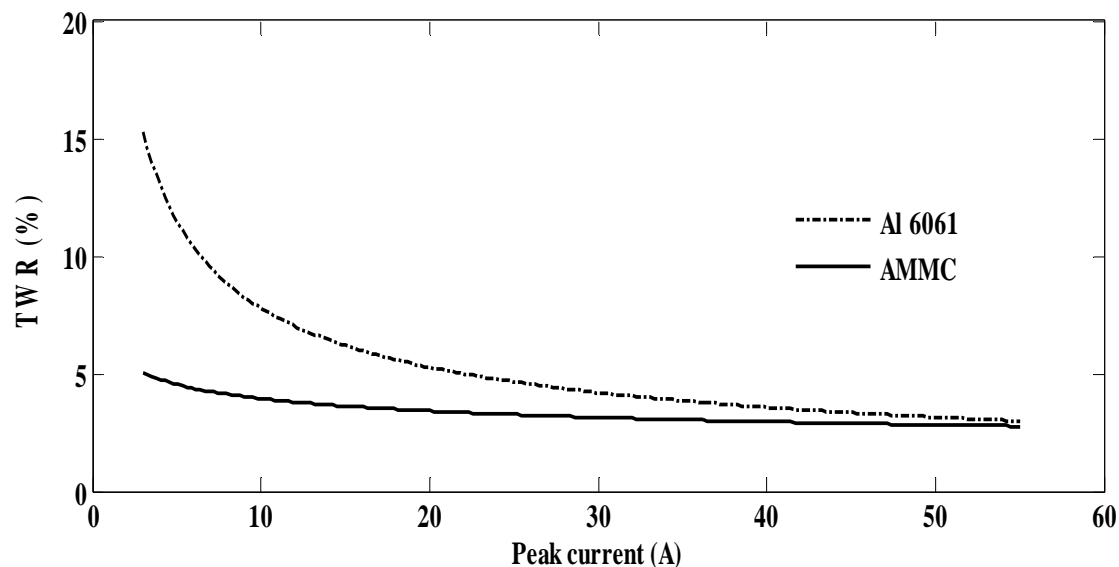


Figure 4.22: Variation in TWR due to changes in peak current (ON-time: $16\mu\text{s}$, OFF-time: $8\mu\text{s}$)

4.3.2 Effects of ON-time on Tool Wear Ratio

The effect of keeping peak current and OFF-time at 15A and 8 μ s respectively and varying ON-time is presented in Figure 4.23 with R^2 0.9556 and 0.9936 for AMMC and Al 6061 respectively.

The ON-time is varied from 3 μ s to 192 μ s. As it can be observed from Figure 4.23, at short ON-time below 12 μ s, more material is removed from the tool for AMMC. When the ON-time is longer than 12 μ s, TWR of both AMMC and Al 6061 becomes lower.

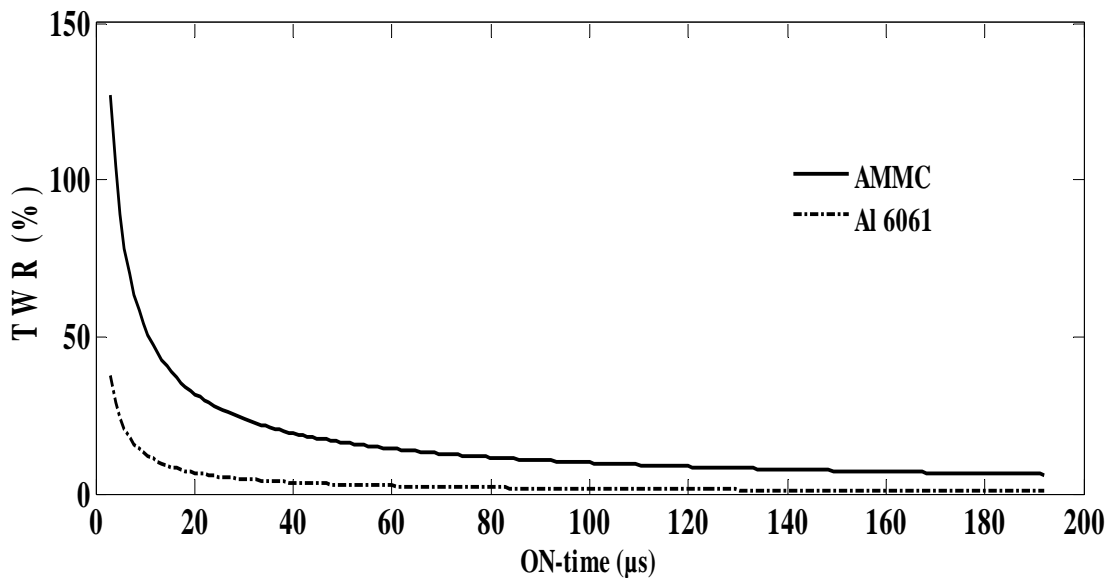


Figure 4.23: Variation in TWR due to changes in ON-time (Peak current: 15A, OFF-time: 8 μ s)

The decreasing TWR with increasing ON-time was also observed by Marafona et al. [76]. Minimal TWR of AMMC and Al 6061 can be achieved at shorter ON-time.

4.3.3 Effects of OFF-time on Tool Wear Ratio

The influence of varying OFF-time, by keeping peak current and ON-time, on TWR was recorded and is presented in Figure 4.24 with R^2 0.8980 and 0.9918 for AMMC and Al 6061 respectively.

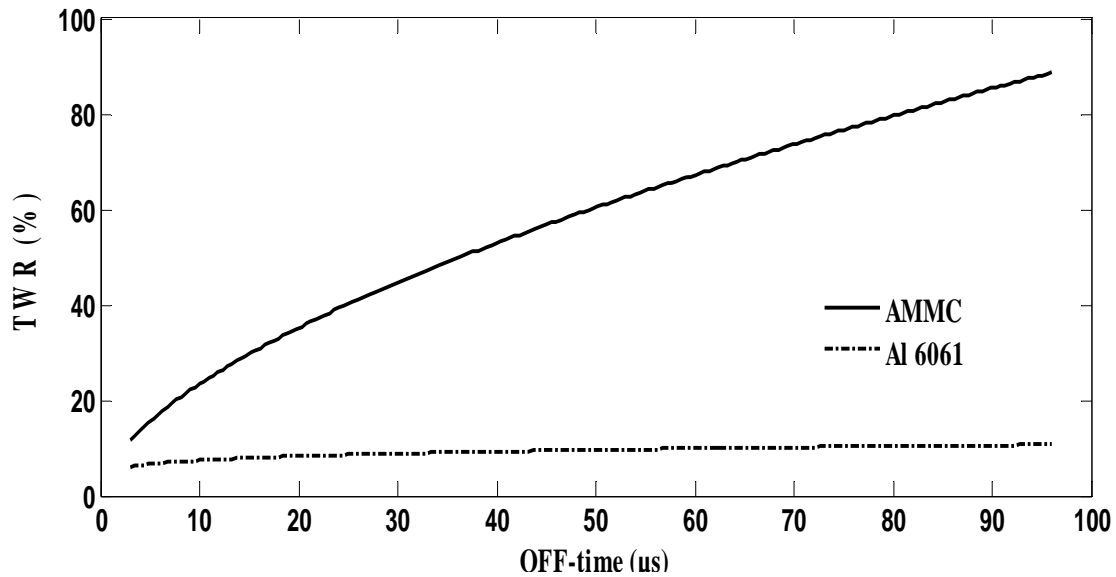


Figure 4.24: Variation in TWR due to changes in OFF-time
(Peak current: 15A, ON-time: 16μs)

As indicated in the graph, the OFF-time varies from 3μs to 96μs, the TWR of Al 6061 remains closely constant around 10%, but that of AMMC is best at short OFF-time. For OFF-time 12μs, TWR of AMMC is about five times greater than that of Al 6061. Short OFF-time increases the machining efficiency since more sparks occur in a given time. Minimal TWR of AMMC and Al 6061 can be achieved at shorter OFF-time.

4.3.4 Analysis of EDM Parameters on TWR using Design Expert Software

Appendix B-9, B-10, B-11 and B-12 present the sequential and ANOVA tables for Ra of AMMC and Al 6061.

4.3.4.1 Analysis on AMMC

Figure 4.25 shows the perturbation plot versus deviation from reference point for TWR. It compares the effect of all the parameters at a particular point in the design space. The plot indicates that when the peak current (A) and ON-time (B) increase, the TWR tend to decrease. When the OFF-time (C) increases, TWR increases.

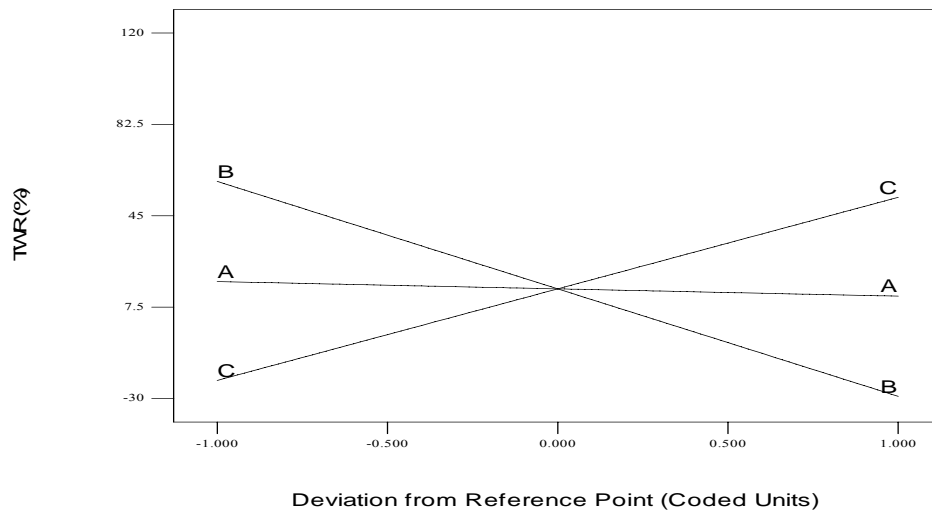


Figure 4.25: Perturbation plot Vs. deviation from reference point for TWR of AMMC

Figure 4.26 is the contour plot versus parameters for TWR. It can be observed that the TWR is higher for low peak current and short ON-time.

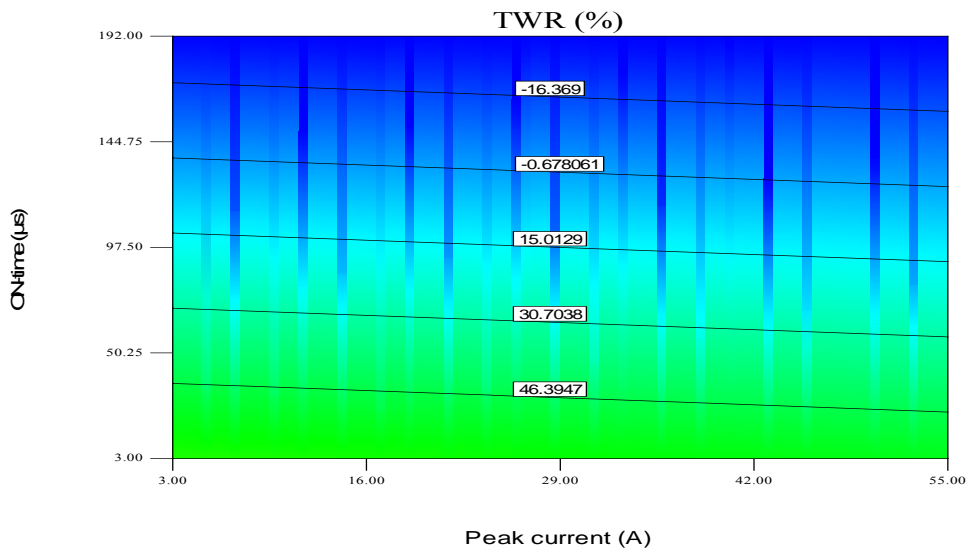


Figure 4.26: Contour plot Vs. parameters for TWR of AMMC

Figure 4.27 presents 3-D graph for TWR of AMMC. At low peak current and short ON-time, TWR is higher and it decreases with increasing of peak current and ON-time.

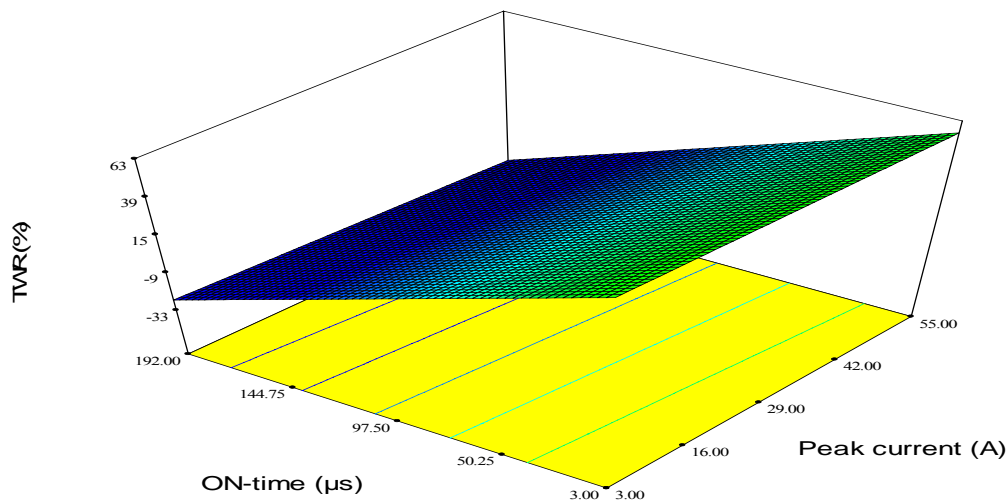


Figure 4.27: 3-D graph for TWR of AMMC

A linear regression analysis was performed on the collected data using Design Expert software and a mathematical model of the following expression with R^2 equals 0.5246 for TWR is obtained:

$$\text{TWR} = 35.057 - 0.841A - 0.217B + 0.769C \quad (4.5)$$

Where, TWR is the tool wear rate, A is peak current, B is ON-time and C is OFF-time.

4.3.4.2 Analysis on Al 6061

Figure 4.28 shows the effects of the three parameters on TWR of Al 6061. It indicates the influence of peak current (A), ON-time (B) and OFF-time (C) on TWR. As it can be observed when the peak current and ON-time increase, the TWR decreases. However, when OFF-time increases, the TWR increases.

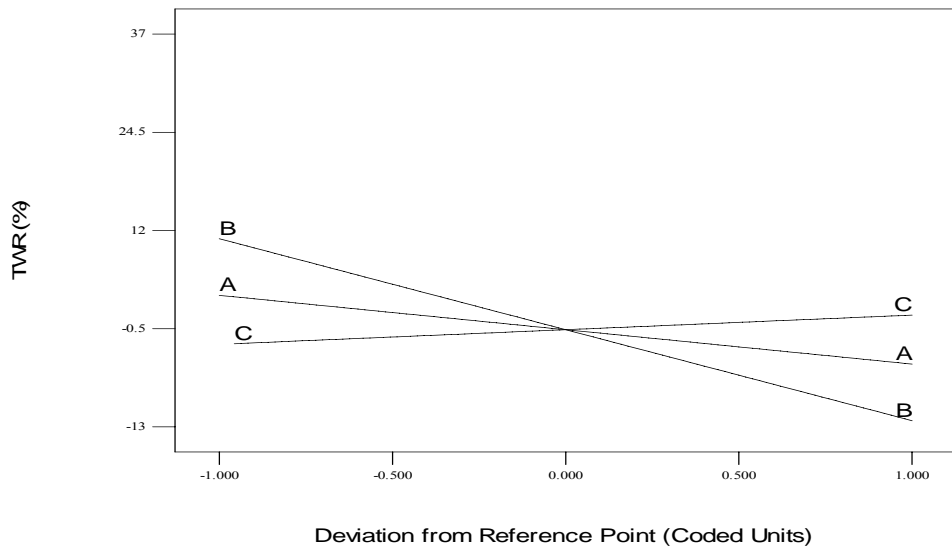


Figure 4.28: Perturbation plot Vs. deviation from reference point for TWR of Al 6061

Figure 4.29 presents the contour plot of TWR of Al 6061.

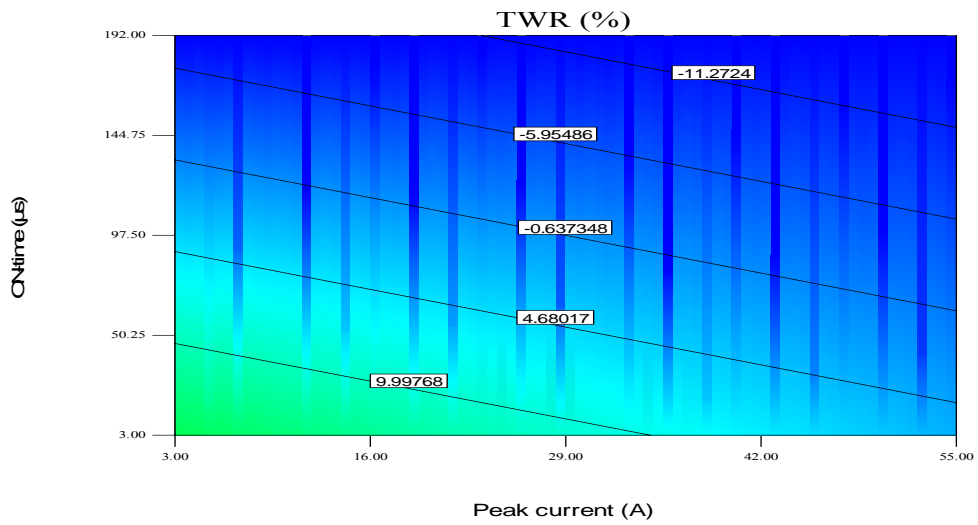


Figure 4.29: Contour plot Vs. parameters for TWR of Al 6061

The effects of peak current and ON-time on TWR are shown while the OFF-time is keeping at 25.5 μ s. As it can be seen, TWR is higher at low peak current and short ON-time.

The effects of EDM parameters on TWR of Al 6061 are shown in three dimensional from Figure 4.30.

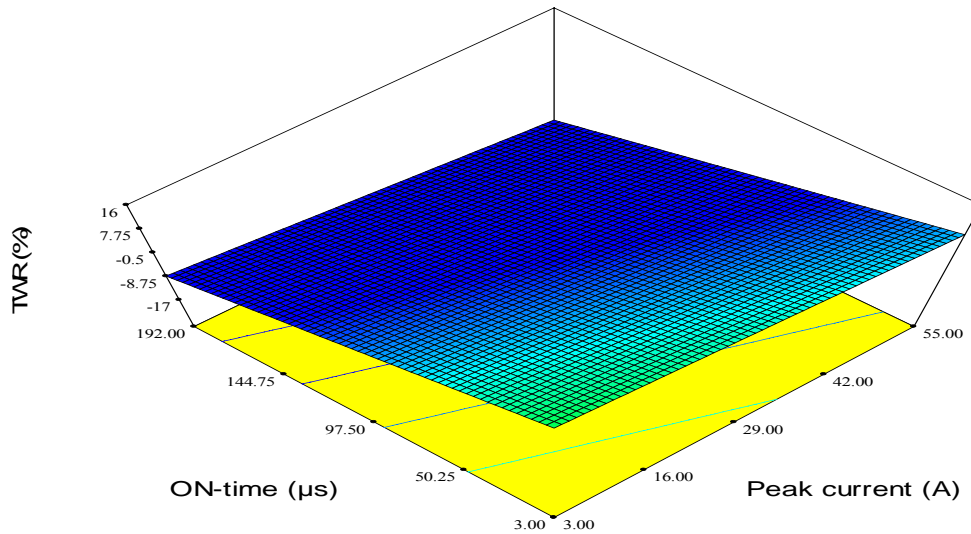


Figure 4.30: 3-D graph for TWR of Al 6061

The final mathematical model with R^2 equals 0.9285 of TWR for Al 6061 is expressed as in the following equation:

$$\text{TWR} = 15.835 - 0.294A - 0.071B + 0.033C \quad (4.6)$$

Where, TWR is the tool wear ratio, A is peak current, B is ON-time and C is OFF-time.

4.4 Effects of EDM Parameters on Overcut

Overcut is the gap distance between the electrode and workpiece produced by sparking. This per-side dimension must be taken into consideration when designing the electrode for EDM die-sinking [3]. The result of EDM parameters on overcut were recorded and are presented in Appendix A-10, A-11 and A-12.

4.4.1 Effects of Peak Current on Overcut

The influence of varying peak current from 3A to 55A and keeping ON-time and OFF-time at $6\mu\text{s}$ and $8\mu\text{s}$ respectively is plotted in Figure 4.31, with R^2 0.9453 and 0.9497 for AMMC and Al 6061 respectively. It can be seen in Figure 4.31 that overcut of both AMMC and Al 6061 increase with increasing the peak current, but at

different rates. At low peak current, the OC of AMMC is about two times higher than that of Al 6061. But for peak current beyond 25A the OC of AMMC is about three times higher than that of Al 6061. The increase of peak current increases the spark energy and this leads to the creation of big craters on the cavity. The size of cavity increases with the increase of spark energy. Khanra et al. [68] have shown that when the spark energy increases the electron bombardment from the side wall of tool increased, which led to more overcut. Minimal overcut can be obtained at lower peak current.

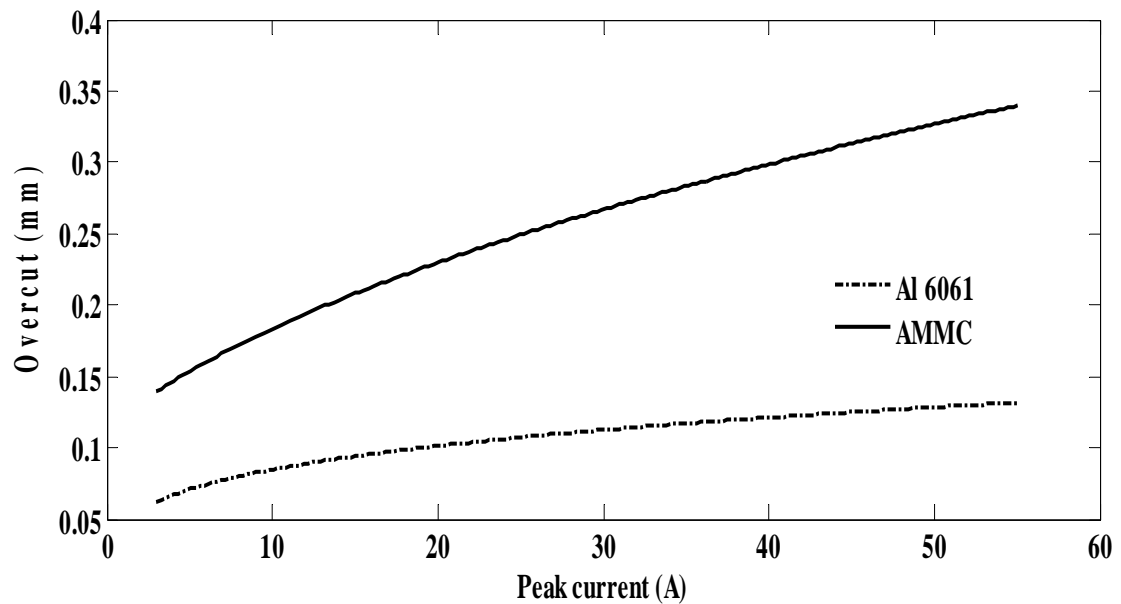


Figure 4.31: Variation in overcut due to changes in peak current (ON-time: 16 μ s, OFF-time: 8 μ s)

4.4.2 Effects of ON-time on Overcut

The influence of varying ON-time from 3 μ s to 192 μ s and keeping peak current and OFF-time at 15A and 8 μ s respectively is plotted in Figure 4.32, with R^2 0.9734 and 0.9829 for AMMC and Al 6061 respectively. It can be seen that overcut of both AMMC and Al 6061 increases but at different rates. The overcut of AMMC is about two times higher than that of Al 6061. Increasing ON-time leads to increasing spark energy and a larger overcut is expected as observed by Khanra et al. [68]. Minimal overcut can be obtained at shorter ON-time.

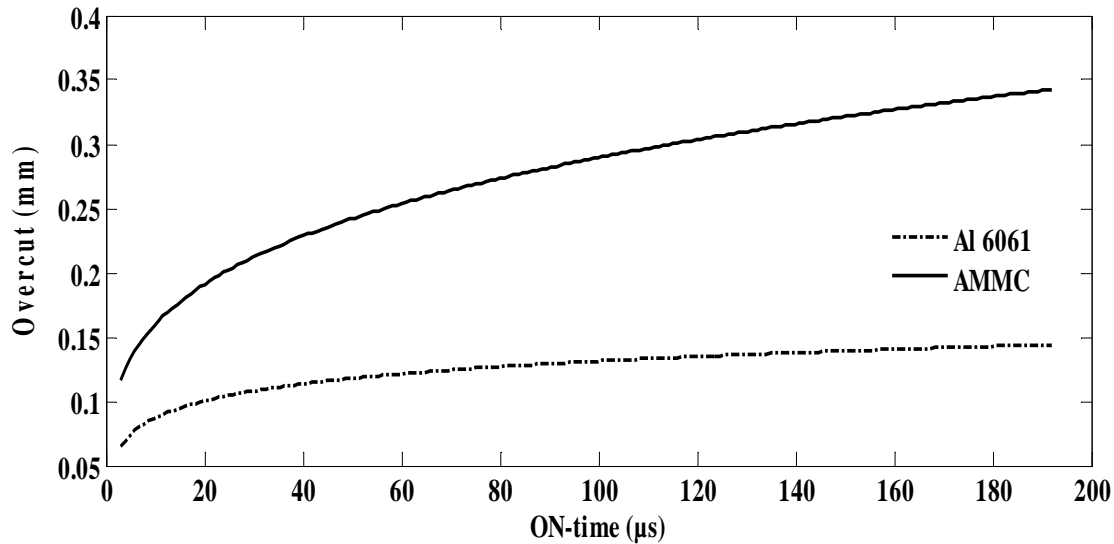


Figure 4.32: Variation in overcut due to change in the ON-time (Peak current: 15A, OFF-time: 8μs)

4.4.3 Effects of OFF-time on Overcut

The effect of keeping peak current and ON-time constant at 15A and 8μs and varying OFF-time is shown in Figure 4.33, with R^2 0.9234 and 0.9449 for AMMC and Al 6061 respectively. At short OFF-time, the overcut of both AMMC and Al 6061 is larger but at different rates. Overcut of AMMC is about two times higher than that of Al 6061. The overcut decreases with increasing OFF-time. Longer OFF-time reduces the spark energy and therefore minor overcut is expected. Minimal overcut can be obtained at longer OFF-time.

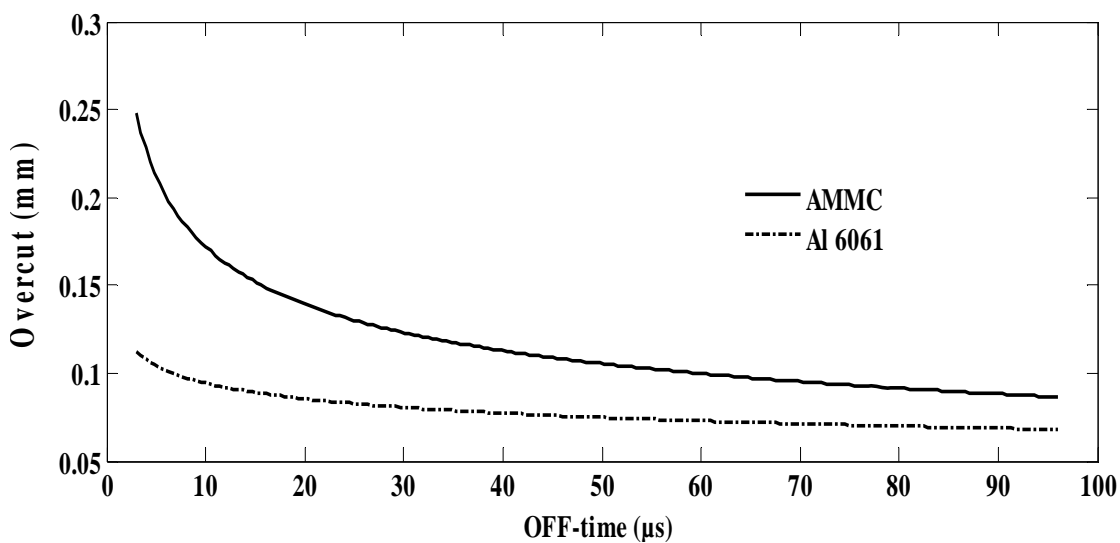


Figure 4.33: Variation in overcut due to changes in OFF-time (Peak current: 15A, ON-time: 16μs)

4.4.4 Analysis of EDM parameters on Overcut using Design Expert Software

Appendix B-13, B-14, B-15 and B-16 present the sequential tables and the ANOVA tables for Ra of AMMC and Al 6061.

4.4.4.1 Analysis on AMMC

Figure 4.34 presents the perturbation plot versus deviation from reference point for OC. The curves indicate the influence of par parameters overcut. Curves A and B indicate increasing overcut when peak current and ON-time increase, while curve C indicates the decrease of overcut when OFF-time increases.

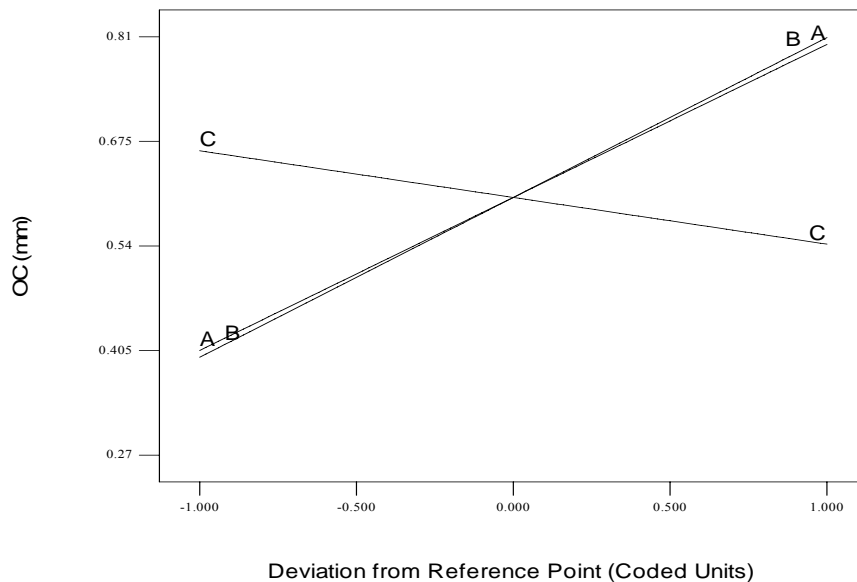


Figure 4.34: Perturbation plot Vs. deviation from reference point for OC of AMMC

Figure 4.35 shows a two-dimensional contour plot where a high overcut is observed at high values of peak current and longer ON-time.

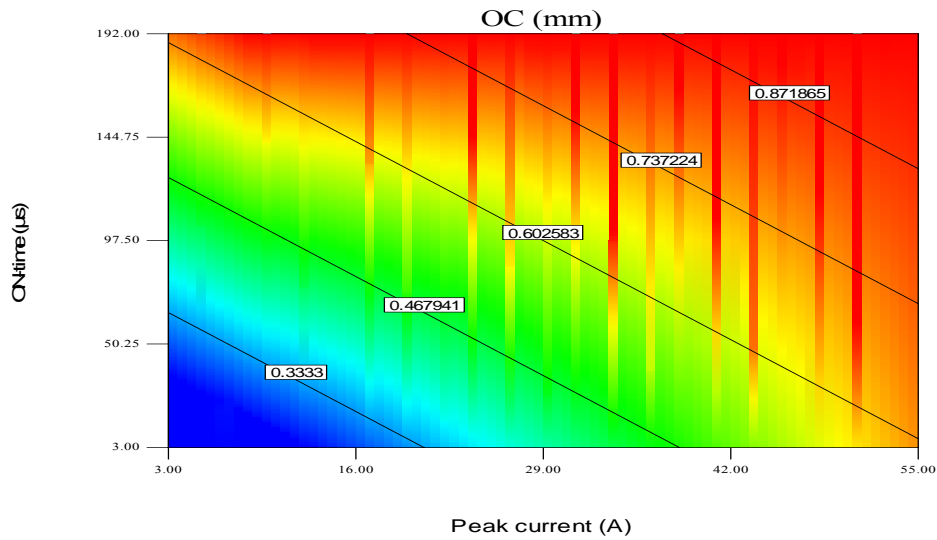


Figure 4.35: Contour plot Vs. parameters for OC of AMMC

Figure 4.36 presents the 3-D graph for overcut of AMMC. A higher overcut is obtained at higher peak current and ON-time, while OFF-time is kept constant at $25.5\mu\text{s}$.

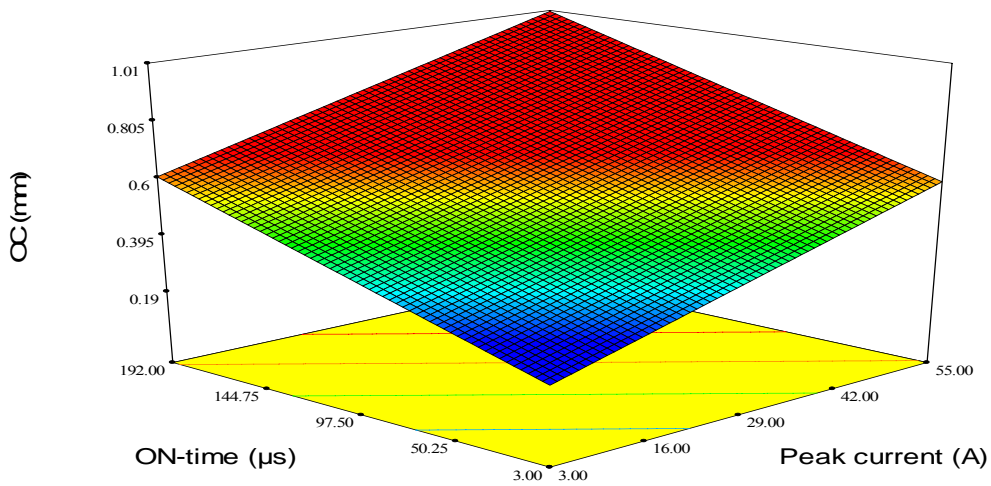


Figure 4.36: 3-D graph for OC of AMMC

A linear regression analysis on the collected data using Design Expert software generates a mathematical model with R^2 equals 0.8352 for overcut as expressed in Equation (4.7):

$$\text{OC} = 0.119 + 4.394 \times 10^{-3} A + 9.329 \times 10^{-4} B - 1.506 \times 10^{-3} C \quad (4.7)$$

Where, OC is the overcut, A is peak current, B is ON-time and C is OFF-time.

4.4.4.2 Analysis on Al 6061

Figure 4.37 shows the perturbation plot for Al 6061. It shows the effects of peak current, ON-time and OFF-time on overcut. The results indicate that the parameters Peak current (A), Pulse On-time (B) and OFF-time (C) have a significant effect on the overcut. Overcut increases with the increase of peak current and ON-time. However, overcut decreases when OFF-time (C) increases.

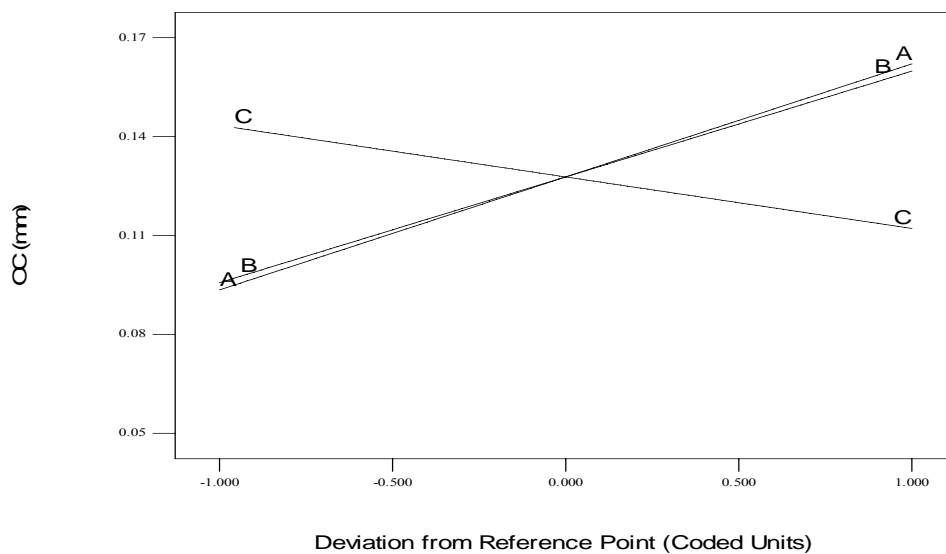


Figure 4.37: Perturbation plot Vs. deviation from reference point for OC of Al 6061

The Figure 4.38 shows the effect of peak current and ON-time on overcut, while OFF-time remains constant at 25.5 μ s. It can be observed that the increase of peak current and ON-time leads to increase the overcut.

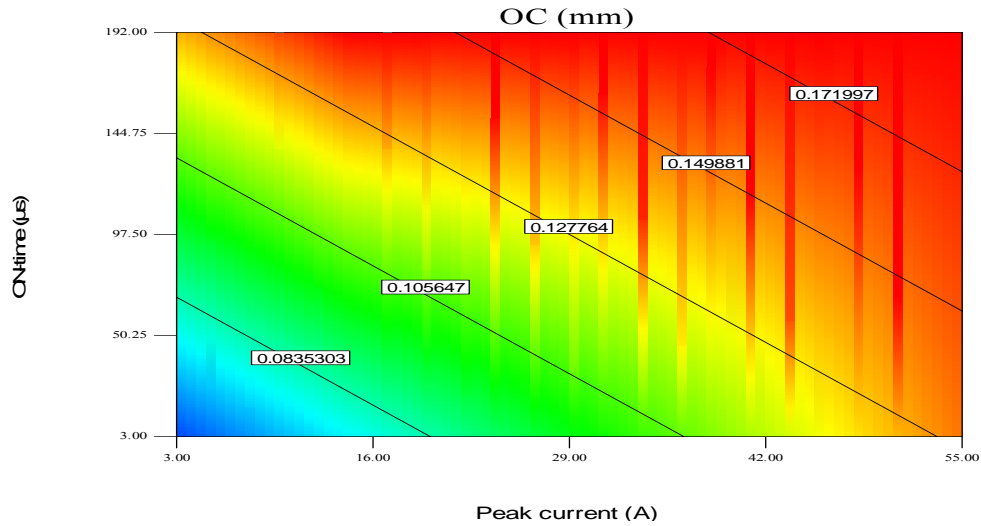


Figure 4.38: Contour plot Vs. parameters for OC of Al 6061

Figure 4.39 presents the 3-D graph for overcut of Al 6061. It shows the effects of peak current and ON-time, while OFF-time is kept constant at 25.5μs. As can be seen in the graph, overcut increases when peak current and ON-time increase.

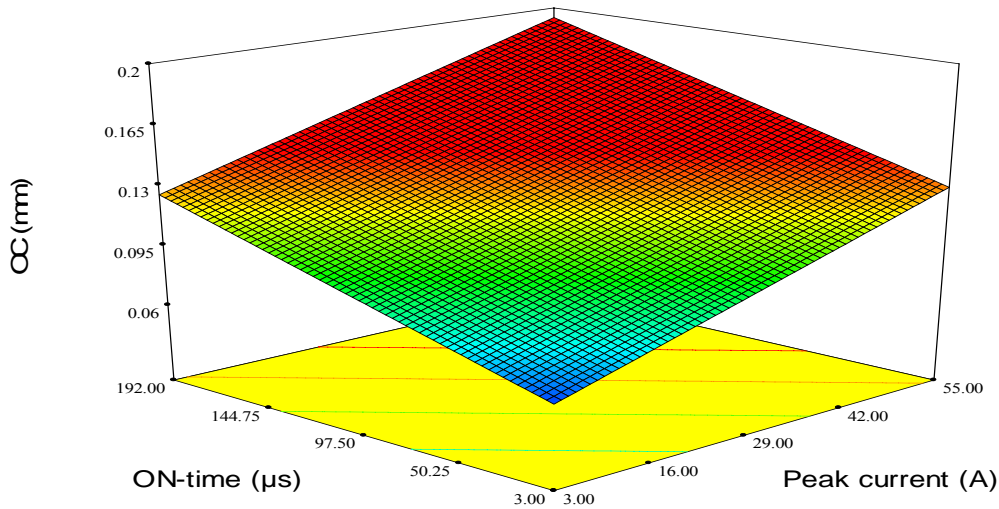


Figure 4.39: 3-D graph for OC of Al 6061

The final mathematical equation with R^2 equals 0.7568 for overcut of Al 6061 is:

$$OC = 0.074 + 1.241 \times 10^{-3} A + 2.778 \times 10^{-4} B - 5.19243 \times 10^{-4} C \quad (4.8)$$

Where, OC is the overcut, A is peak current, B is ON-time and C is OFF-time.

4.5 Effects of EDM Parameters on Surface Morphology of AMMC

EDM process creates alterations layer on the machined surface. The alterations on the surface layers vary according to the machining parameters setting. These damages layers are formed in relation to the surface roughness of the workpiece. The depth and characteristics of surface morphology are studied using SEM for some selected parameter setting. Effects of EDM parameters on surface morphology of Al 6061 are presented in Appendix C-1, C-2 and C-3.

4.5.1 Effect of Peak Current on Surface Morphology of AMMC

Figure 4.40a, Figure 4.40b and Figure 4.40c show SEM view of machined surfaces of AMMC as the result of changes in peak current. Craters and micro-cracks can be seen especially for samples machined at high peak current. It can be observed that the surface becomes rougher with an increase in peak current while ON-time and OFF-time are kept constant at $16\mu\text{s}$ and $8\mu\text{s}$ respectively.

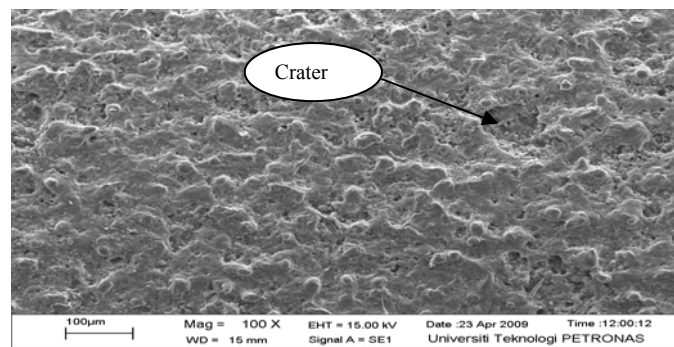


Figure 4.40a: SEM micrograph of machined surface due to change in ON-time. (Peak current: 10A, ON-time: $16\mu\text{s}$, OFF-time: $8\mu\text{s}$)

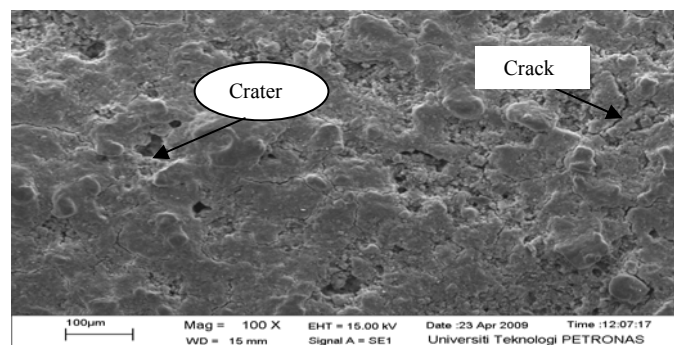


Figure 4.40b: SEM micrograph of machined surface due to change in ON-time. (Peak current: 15 A, ON-time: $16\mu\text{s}$, OFF-time: $8\mu\text{s}$)

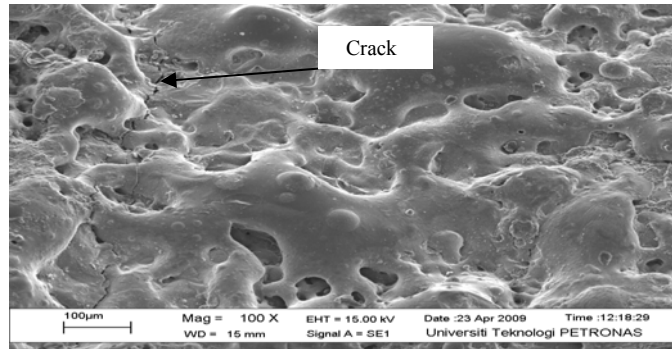


Figure 4.40c: SEM micrograph of machined surface due to change in ON-time. (Peak current: 35A, ON-time: 16 μ s, OFF-time: 8 μ s)

Figure 4.40a shows a SEM micrograph at low peak current, which shows a less rough surface. While Figure 4.41c shows a surface more rough at high peak current. Figures 4.40a, 4.40b and 4.40c present further evidence of increasing in surface roughness when peak current increases as shown in Figure 4.1. G. Chrishna et al [67], showed the influence of machining parameters on EDM of maraging steels where cracks were formed due to high thermal energy.

4.5.2 Effect of ON-time on Surface Morphology of AMMC

Figure 4.41a, Figure 4.41b and Figure 4.41c show the SEM view of machined surfaces of AMMC by varying ON-time. It can be seen in Figure 4.41a that the surface is less rough at short ON-time compared to Figure 4.41c which is at longer ON-time. It can be observed that when ON-time increases the spark erosion time increases, making more craters on the machined surface. Figure 4.41a Figure 4.41b and Figure 4.41c explain the increase of surface roughness observed in Figure 4.2.

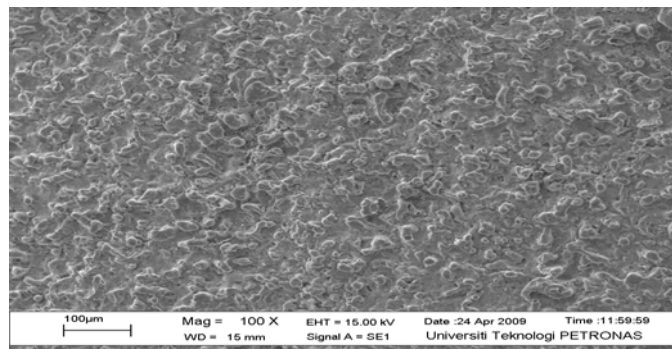


Figure 4.41a: SEM micrograph of machined surface due to change in ON-time. (Peak current: 15A, ON-time: 3 μ s, OFF-time: 8 μ s)

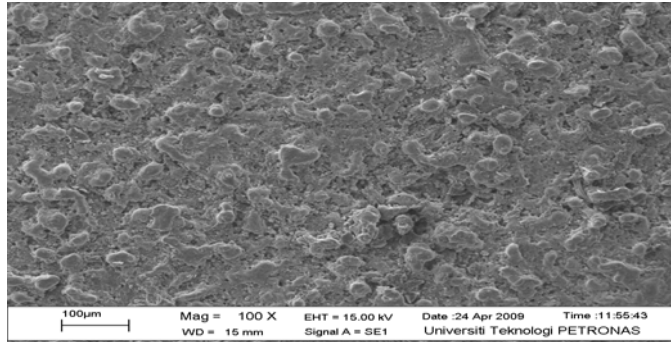


Figure 4.41b: SEM micrograph of machined surface due to change in ON-time. (Peak current: 15A, ON-time: 12 μ s, OFF-time: 8 μ s)

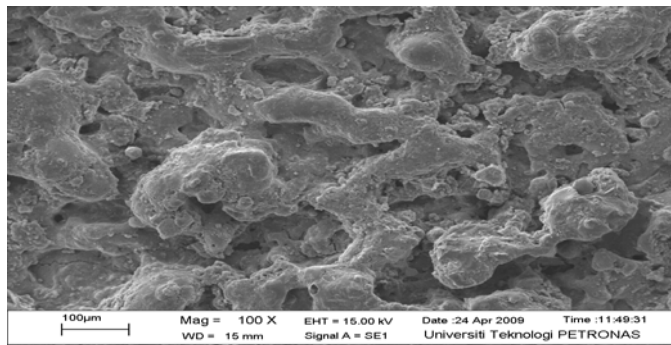


Figure 4.41c: SEM micrograph of machined surface due to change in ON-time. (Peak current: 15A, ON-time: 48 μ s, OFF-time: 8 μ s)

4.5.3 Effect of OFF-time on Surface Morphology of AMMC

Figure 4.42a, Figure 4.42b and Figure 4.42c present the SEM view of machined surfaces of AMMC with change in OFF-time, while keeping peak current and ON-time constant at 15A and 16 μ s respectively. Figure 4.42a shows the SEM micrograph at short value of OFF-time; and it can be seen that the machined surface is rougher compared to Figure 4.42c, where the OFF-time is increased. When OFF-time is increased the machined surface becomes fine, this explains the decrease of surface roughness presented in Figure 4.3.

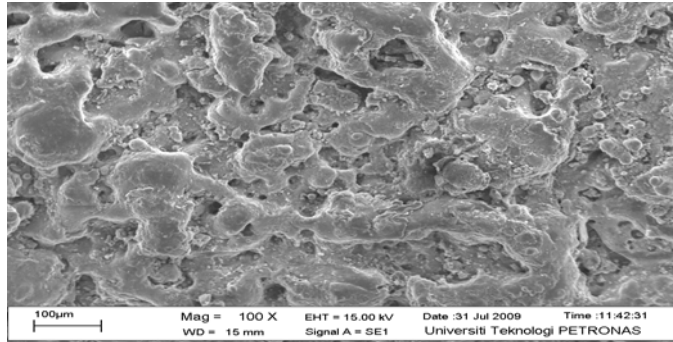


Figure 4.42a: SEM micrograph of machined surface due to change in OFF-time (Peak current: 15A, ON-time: 16µs, OFF-time: 3µs)

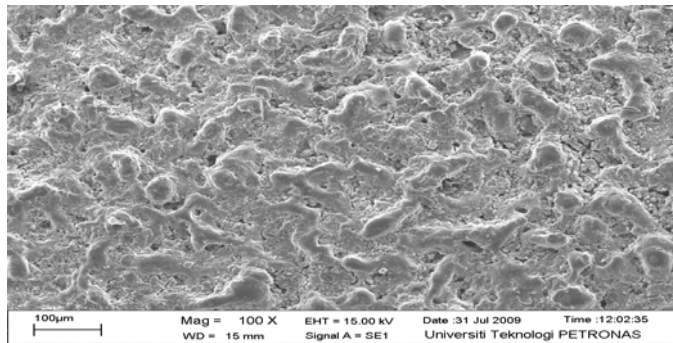


Figure 4.42b: SEM micrograph of machined surface due to change in OFF-time (Peak current: 15A, ON-time: 16µs, OFF-time: 12µs)

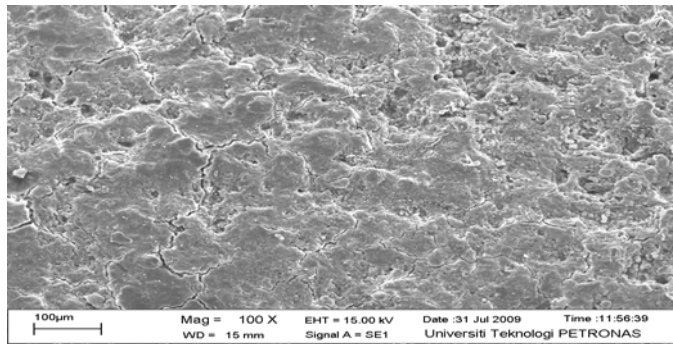


Figure 4.42c: SEM micrograph of machined surface due to change in OFF-time. (Peak current: 15A, ON-time: 16µs, OFF-time: 48µs)

4.6 Affected Layer of AMMC

The cross-sectional SEM views of machined surface are presented for some selected parameter setting.

4.6.1 Effect of Peak Current on Affected Layer of AMMC

Figure 4.43 illustrates the variation in thickness of affected layer due to change in peak current. As it can be seen from the graph, peak current has a significant influence on thickness of affected layer. The thickness of affected layer increases as the peak current increases.

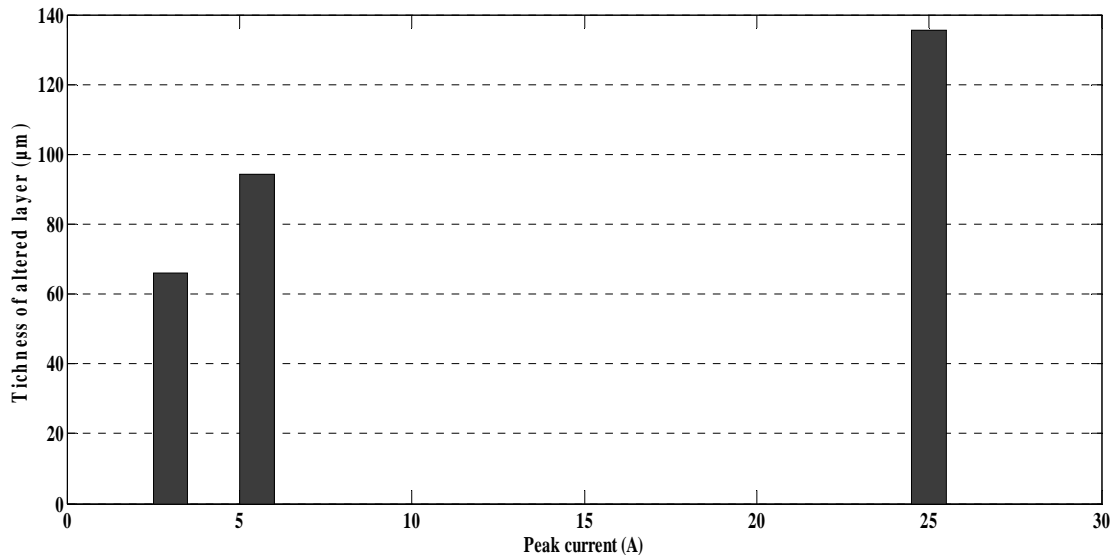


Figure 4.43: Thickness of affected layer Vs. peak current

Figures 4.44a, 4.44b and 4.44c show the cross-sectional SEM views of machined surfaces when the peak current increases. The results show that the thermal energy causes local evaporation of material on the machined surface. This happens because more heat is transferred into the sample when peak current is increased. Consequently, this increases the thickness of the affected layer. Micro-cracks are also observed in the cross-sectional views.

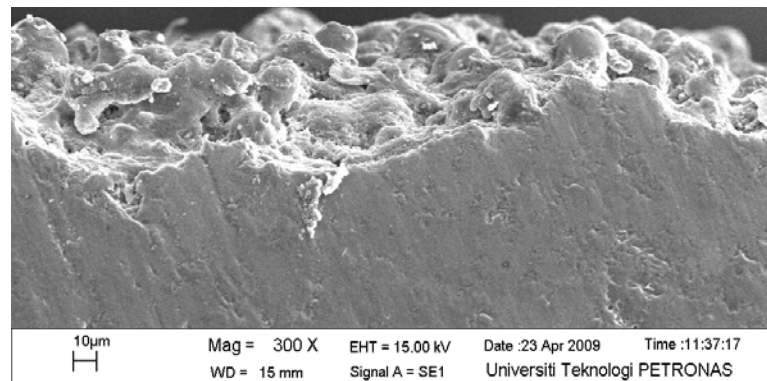


Figure 4.44a: SEM cross-sectional micrograph of machined surface due to change in peak current (Peak current: 3A, ON-time: 16µs, OFF-time: 8µs)

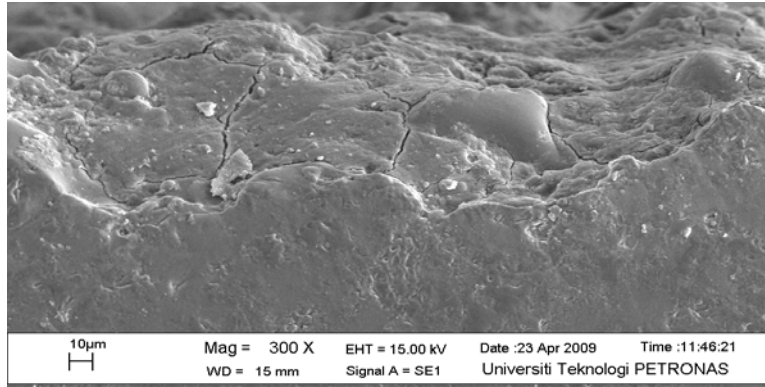


Figure 4.44b: SEM cross-sectional micrograph of machined surface due to Change in peak current. (Peak current: 5.5A, ON-time: 16 μ s, OFF-time: 8 μ s)

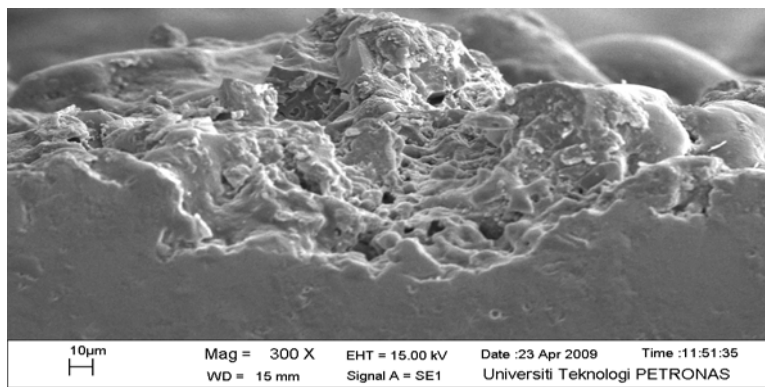


Figure 4.44c: SEM cross-sectional micrograph of machined surface due to change in peak current (Peak current: 25A, ON-time: 16 μ s, OFF-time: 8 μ s)

4.6.2 Effect of ON-time on Affected Layer of AMMC

Figure 4.45 shows the thickness of affected surface layer versus ON-time. The effects of ON-time are similar to the effects of peak current. When ON-time increases, the thickness of affected layer increases due to increasing thermal heat.

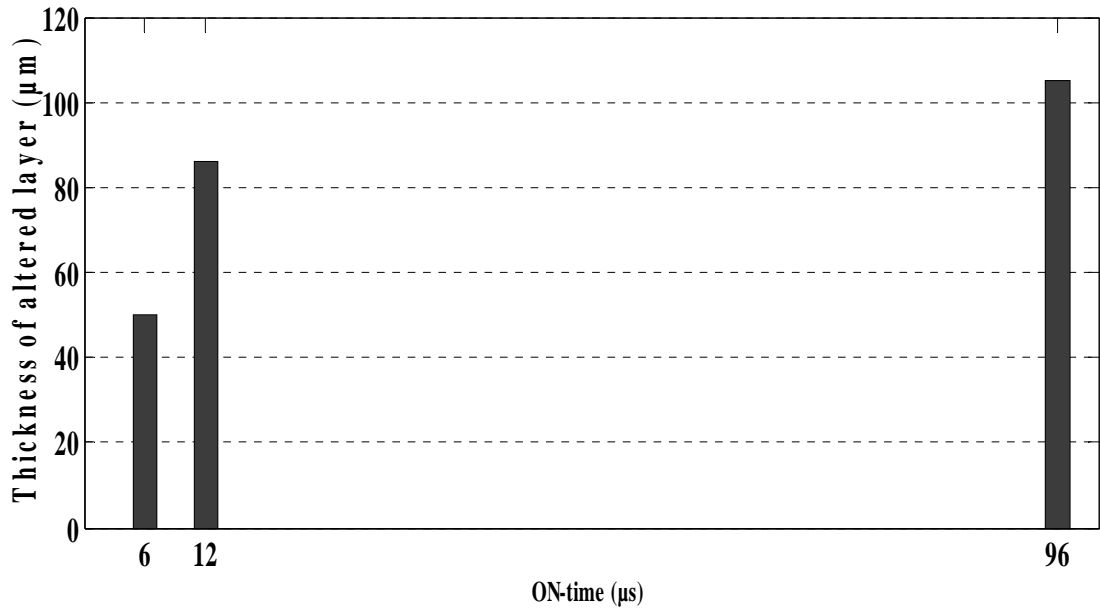


Figure 4.45: Thickness of affected layer Vs. ON-time

Figures 4.46a, 4.46b and 4.46c show the cross-sectional views at increased ON-time. It can be observed in these figures, the affected layer has different metallographic and micro-structural characteristics than the bulk material, which can be observed in the same figures.

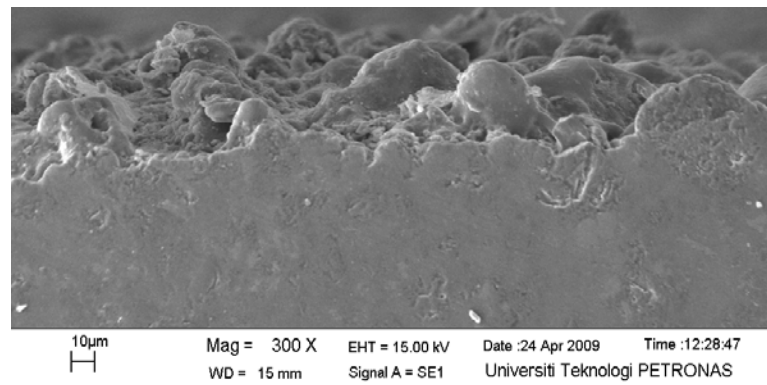


Figure 4.46a SEM cross-sectional micrograph of machined surface due to change in ON-time (Peak current: 15A, ON-time: 6 μs , OFF-time: 8 μs)

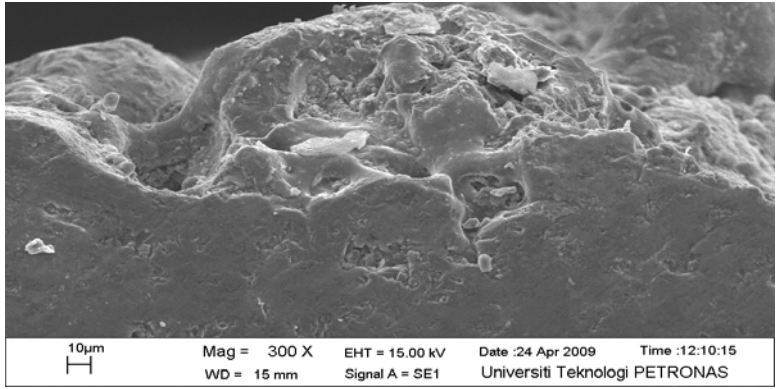


Figure 4.46b: SEM cross-sectional micrograph of machined surface due to change in ON-time (Peak current: 15A, ON-time: 12 μ s, OFF-time: 8 μ s)

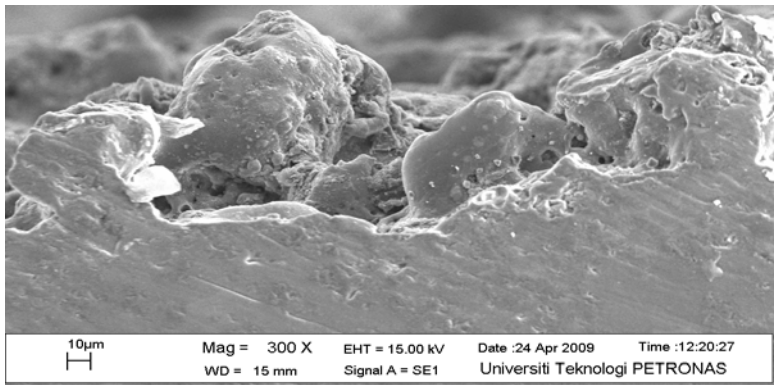


Figure 4.46c: SEM cross-sectional micrograph of machined surface due to change in ON-time (Peak current: 15A, ON-time: 96 μ s, OFF-time: 8 μ s)

4.6.3 Effect of OFF-time on Affected Layer of AMMC

Figure 4.47 illustrates the effect of OFF-time on thickness of affected layer. The thickness of affected layer decreases with increasing OFF-time.

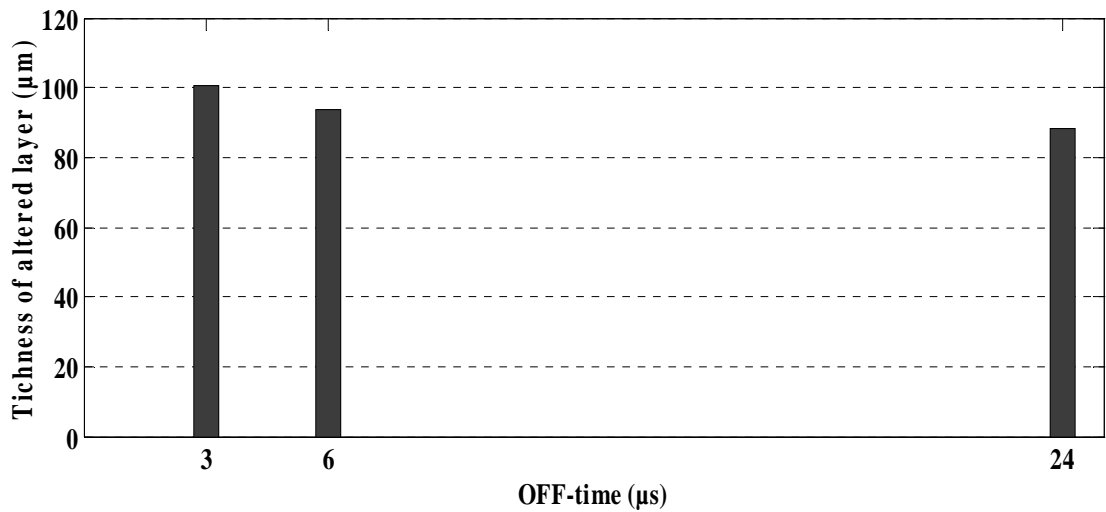


Figure 4.47: Thickness of affected layer versus OFF-time

Figures 4.48a, 4.48b and 4.48c show the SEM cross-sectional views when OFF-time increased. Presence of some micro-cracks is detected in the cross-sectional view.

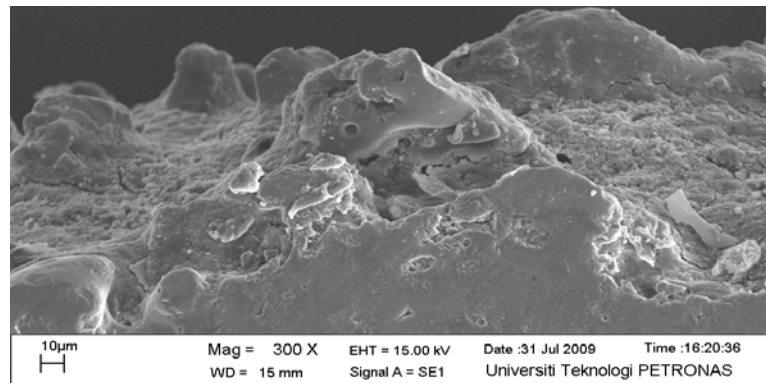


Figure 4.48a: SEM cross-sectional micrograph of machined surface due to Change in OFF-time (Peak current: 15A, ON-time: 16µs, OFF-time: 3µs)

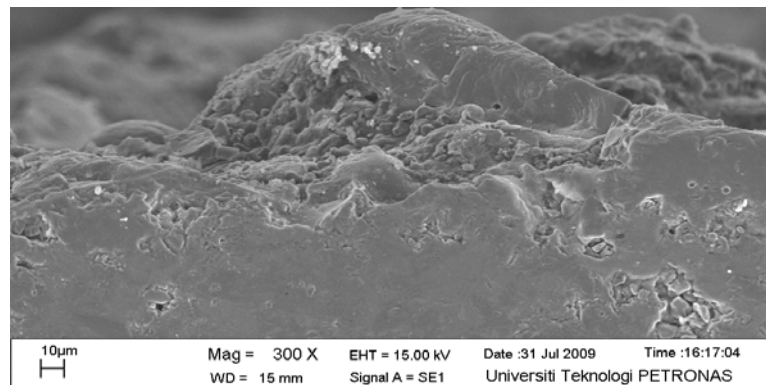


Figure 4.48b: SEM cross-sectional micrograph of machined surface due to change in OFF-time (Peak current: 15A, ON-time: 16µs, OFF-time: 6µs)

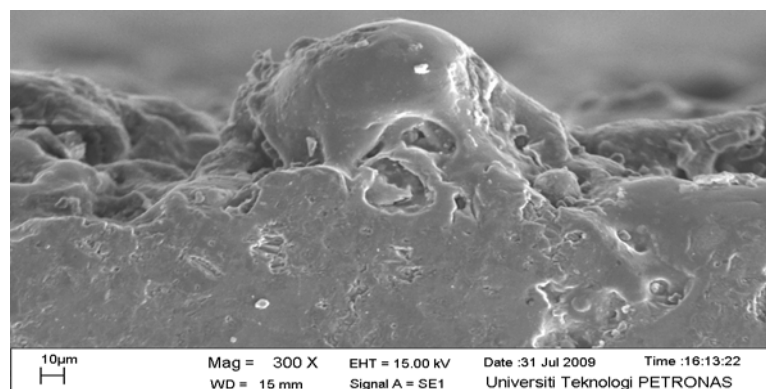


Figure 4.48c: SEM cross-sectional micrograph of machined surface due to change in OFF-time (Peak current: 15A, ON-time: 16µs, OFF-time: 24µs)

4.7 Validation Test

To verify the accuracy of the developed models (Equation 4.1 to Equation 4.8), four validation test were conducted. The parameters selected for validation test corresponding to Ra, MRR, TWR and OC were generated using Design Expert software.

4.7.1 Validation Test for AMMC

Table 4.1 presents the example of output by the point prediction tool based on the models that have been developed for AMMC. The predicted and actual values from confirmation runs were compared by calculating the percentage of error. The error is by Equation 4.9.

$$Error (\%) = \frac{Actual\ value - Predicted\ value}{Actual\ value} \quad (4.9)$$

Table 4.1: Example of output from the point prediction for AMMC

Factor	Name	Level	Low	High
A	Peak current (A)	29.00	3.00	55.00
B	ON-time (μs)	97.50	3.00	192.00
C	OFF-time (μs)	49.50	3.00	96.00
Response		Prediction		
Ra(μm)		27.980		
MRR (g/min)		0.066		
TWR (%)		26.261		
OC (mm)		0.262		

Table 4.2: Analysis of validation test for Ra of AMMC

No	Peak current (A)	ON-time (μs)	OFF-time (μs)	Predicted Ra(μm)	Actual Ra (μm)	Error (%)
1	29.00	97.50	49.50	27.98	30.182	7.29
2	29.00	3.00	3.00	24.2113	24.056	-0.64
3	55.00	97.50	49.50	44.2584	43.007	-2.91
4	3.00	192.00	96.00	15.4703	16.866	8.27

Table 4.3: Analysis of validation test for MRR of AMMC

No	Peak current (A)	ON-time (μ s)	OFF-time (μ s)	Predicted MRR (g/min)	Actual MRR (g/min)	Error (%)
1	29.00	97.50	49.50	0.066	0.071	7.11
2	29.00	3.00	3.00	0.068	0.071	3.68
3	55.00	97.50	49.50	0.113	0.111	-1.48
4	3.00	192.00	96.00	0.017	0.018	6.79

Table 4.4: Analysis of validation test for TWR of AMMC

No	Peak current (A)	ON-time (μ s)	OFF-time (μ s)	Predicted TWR (%)	Actual TWR (%)	Error (%)
1	29.00	97.50	49.50	26.261	24.846	-5.70
2	29.00	3.00	3.00	13.626	14.311	4.78
3	55.00	97.50	49.50	1.286	1.402	8.28
4	3.00	192.00	96.00	63.871	68.320	6.51

Table 4.5: Analysis of validation test for OC of AMMC

No	Peak current (A)	ON-time (μ s)	OFF-time (μ s)	Predicted OC (μ m)	Actual OC (μ m)	Error (%)
1	29.00	97.50	49.50	0.262	0.287	8.71
2	29.00	3.00	3.00	0.244	0.223	-9.42
3	55.00	97.50	49.50	0.377	0.416	9.37
4	3.00	192.00	96.00	0.166	0.175	5.14

Analyses of the validation experiments show that the actual values of Ra, MRR, TWR and OC are within 95% of the prediction interval. This indicates that the empirical models developed in this work are reasonably reliable for prediction of Ra, MRR, TWR and OC according to acceptable error.

4.7.2 Validation Test for Al 6061

Table 4.6 presents the example of output by the point prediction tool based on the models that have been developed for Al 6061. The predicted and actual values from confirmation runs were compared by calculating the percentage of error. These values are presented in Table 4.7 to Table 4.10.

Table 4.6: Example of output from the point prediction for Al 6061

Factor	Name	Level	low	high
A	Peak current (A)	29.00	3.00	55.00
B	ON-time (μ s)	97.50	3.00	192.00
C	OFF-time (μ s)	49.50	3.00	96.00
Response		Prediction		
Ra(μ m)		10.989		
MRR (g/min)		0.167		
TWR (%)		2.058		
OC (mm)		0.111		

Table 4.7: Analysis of validation test for Ra of Al 6061

No	Peak current (A)	ON-time (μ s)	OFF-time (μ s)	Predicted Ra(μ m)	Actual Ra (μ m)	Error (%)
1	29.00	97.50	49.50	10.989	12.182	9.79
2	29.00	3.00	3.00	8.87692	8.216	-8.04
3	55.00	97.50	49.50	15.8715	16.207	2.07
4	3.00	192.00	96.00	8.21845	9.057	9.25

Table 4.8: Analysis of validation test for MRR of Al 6061

No	Peak current (A)	ON-time (μ s)	OFF-time (μ s)	Predicted MRR (g/min)	Actual MRR (g/min)	Error (%)
1	29.00	97.50	49.50	0.167	0.180	7.17
2	29.00	3.00	3.00	0.1727	0.193	10.33
3	55.00	97.50	49.50	0.306	0.318	3.88
4	3.00	192.00	96.00	0.022	0.023	4.93

Table 4.9: Analysis of validation test for TWR of Al 6061

No	Peak current (A)	ON-time (μ s)	OFF-time (μ s)	Predicted TWR (%)	Actual TWR (%)	Error (%)
1	29.00	97.50	49.50	2.058	2.2846	9.92
2	29.00	3.00	3.00	7.265	8.0305	9.53
3	55.00	97.50	49.50	5.412	5.1121	-5.87
4	3.00	192.00	96.00	4.32	4.1988	-2.89

Table 4.10: Analysis of validation test for OC of Al 6061

No	Peak current (A)	ON-time (μ s)	OFF-time (μ s)	Predicted OC (μ m)	Actual OC (mm)	Error (%)
1	29.00	97.50	49.50	0.111	0.124	10.48
2	29.00	3.00	3.00	0.109	0.113	3.54
3	55.00	97.50	49.50	0.144	0.136	-5.88
4	3.00	192.00	96.00	0.0815	0.0782	-4.22

Analysis of the confirmation experiments show that the actual values of Ra, MRR, TWR and OC are within 95% of the prediction interval. This indicates that the empirical models developed in this work are acceptable for prediction of Ra, MRR, TWR and OC.

4.8 Optimization of Machining Performance

4.8.1 Optimization for AMMC

Process optimization is a method to find the minimum or maximum output parameters by choosing the setting of input parameters. The optimization criterion is listed in Table 4.11. The output parameters to be optimized are called objective functions. In this research, the objective functions to be predicted are surface roughness, material removal rate, tool wear ratio and overcut.

Table 4.11: Optimization criteria for AMMC

Constraints			
		Lower	Upper
Name	Goal	Limit	Limit
Peak current (A)	is in range	3	55
ON-time (μ s)	is in range	3	192
OFF-time (μ s)	is in range	3	96
Ra (μ m)	Minimize	7.39	37.95
MRR (g/min)	Maximize	0.017	0.106
TWR (%)	Minimize	0.084	117.55
OC (mm)	Minimize	0.135	0.325

The prediction of optimal parameters for minimum surface roughness, maximum material removal rate, minimum tool wear ratio and minimum overcut are established using the Design Expert software and the four confirmation test were conducted on samples for 30% Al₂O₃ reinforced AMMC and Al 6061 due to limitation of AMMC material. Table 4.11 shows the criteria setting of the parameters.

The possible optimal solutions suggested by Design Expert software are given in Table 4.12 in terms of predicted values for the responses including the desirability index.

Table 4.12: Possible optimal solution for AMMC

Solutions								
No	Peak current (A)	ON-time (μ s)	OFF-time (μ s)	Ra (μ m)	MRR (g/min)	TWR (%)	OC (mm)	Desirability
1	17.08	3.00	3.00	15.990	0.049	22.916	0.194	0.614
2	17.46	3.00	3.00	16.208	0.049	22.873	0.196	0.614
3	16.67	3.00	3.00	15.757	0.048	22.964	0.193	0.614
4	17.86	3.00	3.00	16.437	0.050	22.826	0.197	0.614
5	16.62	4.40	3.00	15.962	0.048	22.314	0.194	0.614
6	16.30	5.47	3.00	15.955	0.048	21.856	0.194	0.614
7	16.41	6.53	3.00	16.190	0.049	21.346	0.196	0.613
8	17.13	3.00	3.35	15.930	0.049	23.488	0.194	0.613
9	18.82	3.00	3.00	16.978	0.052	22.717	0.201	0.613
10	19.16	3.00	3.00	17.172	0.052	22.677	0.202	0.613
11	14.99	3.00	3.00	14.803	0.045	23.159	0.186	0.613
12	14.31	8.92	3.00	15.393	0.046	20.474	0.190	0.612
13	16.68	3.00	3.79	15.557	0.047	24.287	0.191	0.612
14	17.49	3.00	4.26	15.893	0.048	24.971	0.193	0.611
15	13.28	18.79	3.00	16.433	0.047	15.990	0.197	0.610
16	4.05	50.42	3.00	16.402	0.041	2.295	0.197	0.595

Tables 4.13 to 4.17 present the validation test for Ra, MRR, TWR and OC. Based on the validation test, it can be concluded that the optimal solution is acceptable.

Table 4.13: Validation test for optimal for Ra of AMMC

No	Peak current (A)	ON-time (μ s)	OFF-time (μ s)	Predicted Ra(μ m)	Actual Ra (μ m)	Error (%)
1	17.08	3.00	3.00	15.990	16.615	3.76
2	16.30	5.47	3.00	15.955	16.350	2.42
3	14.31	8.92	3.00	15.393	16.237	5.20
4	17.49	3.00	4.26	15.893	16.572	4.10

Table 4.14: Validation test for optimal for MRR of AMMC

No	Peak current (A)	ON-time (μ s)	OFF-time (μ s)	Predicted MRR (g/min)	Actual MRR (g/min)	Error (%)
1	17.08	3.00	3.00	0.049	0.054	9.26
2	16.30	5.47	3.00	0.048	0.052	7.69
3	14.31	8.92	3.00	0.046	0.051	9.80
4	17.49	3.00	4.26	0.048	0.043	-11.63

Table 4.15: Validation test for optimal for TWR of AMMC

No	Peak current (A)	ON-time (μ s)	OFF-time (μ s)	Predicted TWR (%)	Actual TWR (%)	Error (%)
1	17.08	3.00	3.00	22.88	21.01	-8.90
2	16.30	5.47	3.00	19.39	18.77	-3.30
3	14.31	8.92	3.00	17.19	18.26	5.86
4	17.49	3.00	4.26	28.66	26.97	-6.27

Table 4.16: Validation test for optimal for OC of AMMC

No	Peak current (A)	ON-time (μ s)	OFF-time (μ s)	Predicted OC (μ m)	Actual OC (μ m)	Error (%)
1	17.08	3.00	3.00	0.194	0.203	4.43
2	16.30	5.47	3.00	0.194	0.188	-3.19
3	14.31	8.92	3.00	0.190	0.186	-2.15
4	17.49	3.00	4.26	0.193	0.189	-2.12

4.8.2 Optimization for Al 6061

The optimization criterion is listed in Table 4.17. The predicted optimal parameters for minimum surface roughness, maximum material removal rate, minimum tool wear ratio and minimum overcut are established using the Design Expert software and the validation test was conducted on four setting for Al 6061. Table 4.17 shows the preferred setting of the factors that will give up the desired responses.

Table 4.17: Optimization criteria for Al 6061

Constraints			
		Lower	Upper
Name	Goal	Limit	Limit
Peak current (A)	is in range	3.00	55.00
ON-time (μs)	is in range	3.00	192.00
OFF-time (μs)	is in range	3.00	96.00
Ra (μm)	minimize	3.355	12.506
MRR (g/min)	maximize	0.0216	0.276
TWR (%)	minimize	0.0403	15.487
OC (mm)	minimize	0.11	0.28

The possible optimal solutions suggested by Design Expert software are given in Table 4.18 in terms of predicted values for the responses including the desirability index.

Table 4.18: Possible optimal solution for Al 6061

Solutions								
No	Peak current (A)	ON-time (μs)	OFF-time (μs)	Ra (μm)	MRR (g/min)	TWR (%)	OC (mm)	Desirability
1	11.47	9.82	3.00	5.895	0.089	2.983	0.180	0.5496
2	11.68	7.49	3.00	5.860	0.089	3.150	0.179	0.5496
3	11.48	11.11	3.00	5.938	0.090	2.934	0.180	0.5496
4	11.39	13.04	3.00	5.981	0.090	2.822	0.181	0.5496
5	11.85	4.99	3.00	5.812	0.089	3.308	0.178	0.5496
6	12.04	5.60	3.00	5.868	0.090	3.346	0.179	0.5496
7	11.98	3.73	3.00	5.796	0.089	3.402	0.178	0.5495
8	10.81	16.17	3.00	5.972	0.088	2.503	0.181	0.5495
9	10.19	22.86	3.00	6.069	0.088	2.022	0.183	0.5491
10	10.00	23.53	3.00	6.054	0.087	1.932	0.183	0.5490
11	9.02	29.29	3.00	6.055	0.085	1.376	0.184	0.5481
12	8.12	42.37	3.00	6.301	0.086	0.536	0.189	0.5463
13	8.04	53.64	3.00	6.645	0.091	0.041	0.195	0.5436

Tables 4.19 to 4.22 present the confirmation test for Ra, MRR, TWR and OC. Based on the confirmation test, it can be concluded that the optimal solution is acceptable.

Table 4.19: Validation test for optimal for Ra of Al 6061

No	Peak current (A)	ON-time (μ s)	OFF-time (μ s)	Predicted Ra(μ m)	Actual Ra (μ m)	Error (%)
1	11.47	9.82	3.00	5.895	5.445	-8.26
2	12.04	5.60	3.00	5.868	6.312	7.03
3	10.19	22.86	3.00	6.069	6.634	8.52
4	8.12	42.37	3.00	6.301	6.873	8.32

Table 4.20: Validation test for optimal for MRR of Al 6061

No	Peak current (A)	ON-time (μ s)	OFF-time (μ s)	Predicted MRR (g/min)	Actual MRR (g/min)	Error (%)
1	11.47	9.82	3.00	0.089	0.0928	4.09
2	12.04	5.60	3.00	0.090	0.102	11.76
3	10.19	22.86	3.00	0.088	0.0925	4.86
4	8.12	42.37	3.00	0.086	0.094	8.51

Table 4.21: Validation test for optimal for TWR of Al 6061

No	Peak current (A)	ON-time (μ s)	OFF-time (μ s)	Predicted TWR (%)	Actual TWR (%)	Error (%)
1	11.47	9.82	3.00	2.983	3.214	7.19
2	12.04	5.60	3.00	3.346	3.812	12.22
3	10.19	22.86	3.00	2.022	2.251	10.17
4	8.12	42.37	3.00	0.536	0.605	11.40

Table 4.22: Validation test for optimal for OC of Al 6061

No	Peak current (A)	ON-time (μ s)	OFF-time (μ s)	Predicted OC(mm)	Actual OC (mm)	Error (%)
1	11.47	9.82	3.00	0.180	0.175	-2.86
2	12.04	5.60	3.00	0.179	0.182	1.65
3	10.19	22.86	3.00	0.183	0.169	-8.28
4	8.12	42.37	3.00	0.189	0.202	6.44

CHAPTER FIVE

CONCLUSION

5.1 Conclusion

Electro discharge machining (EDM) on 30% alumina reinforced aluminium metal matrix composite has been conducted to investigate the machinability of the material. The output responses such as surface roughness (Ra), material removal rate (MRR), tool wear ratio (TWR), overcut (OC), surface morphology and thickness of affected layer were analyzed and the results were compared to EDM on Al 6061. Analysis based on Central Composite Design (CCD) tool provides mathematical models of output responses, plots the experimental graphs and identifies process optimization. The following conclusions can be drawn from this research.

- This research have established that of 30% alumina reinforced aluminium metal matrix composite can be machined using EDM with copper electrode with acceptable result on Ra, MRR, TWR and OC at identified machining parameters. However, EDM performance of machining Al 6061 is better than that of AMMC due the presence of alumina in AMMC and good electrical and thermal conductivities of Al 6061 than that of AMMC.
- It was shown that peak current, pulse duration and pause durations directly affect AMMC surface roughness, surface morphology and thickness of affected layer. These machining parameters also affect the material removal rate, tool wear ratio and overcut. The recorded quantitative data can be utilized for identifying suitable EDM parameters for the desired end result.

- Optimal EDM parameters for machining 30% alumina reinforced AMMC have been identified by inserting EDM experimental data into a Design Expert software. The reliability of the optimal EDM parameters were tested and validated by conducting validation test using EDM.
- Mathematical models of output responses from Design Expert software with respect to peak current, pulse duration and pause duration can be used to identify various machining output response by varying input parameters with reasonable accuracy within the limits of the parameters ranges used.

5.2 Recommendation for Further Work

Observations of the results obtained from this research lead to recommendations for future work.

- The current research established reasonably well that EDM machining parameters influence on the surface roughness, the material removal rate, tool wear ratio and overcut of AMMC. Further EDM experiment can be conducted to study the influence of EDM process parameters such as dielectric type, flushing pressure, voltage, polarity on AMMC in order to improve the machinability.
- The current research was done based on varying one parameter while keeping others parameters at constant values. It would be interesting to vary simultaneously all the process parameters and investigate the effects of EDM parameters combination on alumina reinforce AMMC.
- EDM experiment can be conducted on the same material but with different percentages in volume of reinforcing phases (alumina) in AMMC in order to investigate the effect of varying alumina volumes on the machinability of AMMC.

REFERENCES

- [1] F. C. Campbell, “*Manufacturing Technology for Aerospace Structure*”, ELSERVIER, London, 2006.
- [2] R. Teti, “*Machining of Composite Materials*”, CIRP Annals- Manuf. Tech., vol. 51, Issue 2, p 611-634, 2002.
- [3] E. C. Jameson, “*Electrical-Discharge Machining*”, Soc. of Manuf. Eng. (SME), 2001.
- [4] J. Dwight, “*Aluminium Design and Construction*”, London: E & FN Spon, 1998.
- [5] K. Dmitri, “*Substech*”, <http://www.substech.com>. Retrieved on August 2009.
- [6] J. R. Kissell and O. L. Ferry, “*Aluminum Structures: A Guide to Their Specifications and Design*”, JOHN WILEY & SONS, New York 2002.
- [7] E. J. Barbero, “*Introduction to Composite Materials Design*”, New York, Taylor & Francis, pp. 2-25, 1998.
- [8] M. S. Chawartz, “*Composite Materials: Properties, Non destructive Testing and Repair*”, New Jersey: Prentice Hallpp, vol. 1 pp. 2-4, 1996.
- [9] F. L. Matthews and R. D. Rawlings, “*Composite Materials: Eng. and Sci.*”, England, Woodhead, Publish. pp .5-79, 1999.
- [10] V. K. Choo, “*Introductions to Composite Material: Fundamentals of Composite Materials*”, Depart. of Mech., New Mexico State University, USA.
- [11] S. T. Mileiko, “*Composite Materials Series: Metal and Ceramic Based Composites*”, ELSEVIER, vol. 12, New York, 1997.
- [12] M. Kathiresan and T. Sornakumar, “*EDM Studies on Aluminum Alloy Silicon Carbide Composites Developed by Vortex Technique and Pressure Die Casting*”, J. of Miner. & Mat. Charact. & Eng., vol. 9, No.1, pp. 79-88, 2010.
- [13] R. Karthikeyan, P. R. Lakshmi Narayanan and R. S. Naagarazan, “*Mathematical Modelling for Electric Discharge Machining of Aluminium– Silicon Carbide Particulate Composites*”, J. of Mat. Process. Tech., vol. 87, pp. 59–63, 1999.

- [14] A. K. Kaw, “*Mechanic of Composite Materials*”, Taylor & Francis, 2005.
- [15] N. F. Petrofes: PhD Thesis, Texas A. & M. Univ., 1989.
- [16] D. A. Lucca and E. Brinksmeier: “*Progress in Assessing Surface and Subsurface Integrity*”, Ann. CIRP, vol. 47, Issue 2, pp. 669–693, 1998.
- [17] T. R. Swanson, “*Advanced Composite Materials*”, Prentice Hall, Upper Saddle River, NJ, pp6-101, 997.
- [18] W.S. Lau, M. Wang and W.B. Lee, “*Electrical Discharge Machining of Carbon Fibre Composite Materials*”, Int. J. of Mach. Tools and Manuf., vol. 30, Issue, pp. 297-3082, 1990.
- [19] T. L. Richardson, “*Composites: A design Guide*”, New York, Ind. Press Inc, pp7-11, 1987.
- [20] A. B. Strong, “*Fundamentals of Composites Manufacturing Materials, Methods and Applications*”, Michigan: Soc. of Manuf. Engineers, pp. 47-70, 1989.
- [21] B Cantor Dunne, F. P. E. and Stone, I. C., “*Metal and Ceramic Matrix Composites: Series in Materials Science and Engineering*”, IOP Bristol, 2004. pp.16-20.
- [22] S. Demarker, “*Metal Matrix Composites*”, Metals and Materials, pp.144-146, Mar. 1986.
- [23] R. L. Trumper, “*Metal Matrix Composites - Applications and Prospects*”, Met. and Mat., pp.662-667, Nov. 1987.
- [24] N. Chawla and K. Chawla, “*Metal Matrix Composite*”, Springer, New York, pp. 67-83, 2006.
- [25] M. K. Surappa, “*Aluminium Matrix Composites: Challenges and Opportunities*”, Sadhana, vol. 28, Parts 1 & 2, Feb. 2003, pp. 319–334.
- [26] S. K. Mazumdar, “*Composites Manuf.: Material, Product and Process Eng.*”, CRC Press LLC, Florida, pp.332-333, 2002.
- [27] F. Muller and J. Monagahn, “*Non-Conventional Machining of Particle Reinforced Metal Matrix Composites*”, J. of Mat. Process. Tech., vol. 118, pp.278-285, 2001.
- [28] S. Kannana and H. A. Kishaw, “*Surface Characteristics of Machined Aluminium Metal Matrix Composites*”, Int. J. of Mach. Tools and Manuf., vol. 46, Issue 15, pp.2017-2025, Dec. 2006.

- [29] Fast EDM, <http://www.fastedm.com/WhatisEDM.htm>. Retrieved on Oct. 2009.
- [30] H. A. El-Hofy, “*Advanced Machining Process*”, Mc Graw-Hill Mech. Eng., New York, pp.147-159, 2005.
- [31] ANSI/ASME B 46.1, Amer. Soc. of Mech. Eng., 1985.
- [32] http://www.bobcad.com/images/What_is_EDM.pdf. Retrieved on Dec. 2009.
- [33] E. B. Guitrau, “*The Electrical Discharge Machining Handbook*”, Cincinnati: Hanser Gardner Publica., 1997.
- [34] R. Dorf and A. Kusiak, “*Handbook of Design, Manufacturing and Automation*”, New York, John Weley & Sons, 1994.
- [35] H. A. Youssouf and H. El-Hofy, “*Machining Technology, machine tools and Operation*”, New York, Taylor & Francis Group, 2008.
- [36] A. J. Lissaman and S. J. Martin, “*Principles of Eng. Production*”, Hodder and Stoughton Educ., London, UK, 1982.
- [37] Scott F. Millera, Chen-C. Koa, Albert J. Shiha, and Jun Qu, “*Investigation of Wire Electrical Discharge Machining of Thin Cross-sections and Compliant Mechanisms*”, Int. J. of Mach. Tools and Manuf., vol. 45, Issue 15, pp. 1717-1725, Dec. 2005.
- [38] R. Kern, “Sinker electrode selection”, EDM Today, Jul. 2008, <http://www.edmtodaymagazine.com>.
- [39] Sanjeev Kumara, Rupinder Singh, T.P. Singh and B.L. Sethid, “*Surface modification by Electrical Discharge Machining: A Review*”, J. of Mat. Process. Tech. vol. 209 pp.3675–3687, 2009.
- [40] S. Norasetthekul, P. T. Eubank, W. L. Bradley, B. Bozkur, “*Use of Zirconium Diboride-Copper as an Electrode in Plasma Applications*”, J. of Mat. Sci., vol.34, Issue 6, pp. 1261-127, 1999.
- [41] M. Kathiresan and T. Sornakumar, “*EDM Studies on Aluminum Alloy-Silicon Carbide Composites Developed by Vortex Technique and Pressure Die Casting*”, J. of Minerals & Mat. Characterization & Eng., vol. 9, No.1, pp.79-88, 2010.
- [42] B. Griffiths, “*Manufacturing Surface Technology*”, 2001, Penton Press

- [43] S.H. Tomadi, M.A. Hassan, Z. Hamedon, R. Daud, A.G. Khalid, “*Analysis of the Influence of EDM Parameters on Surface Quality, Material Removal Rate and Electrode Wear Rate of Tungsten Carbide*”, Int. Multi-Conf. of Eng. and Comput. Sci. (IMECS), Hong Kong, vol. 2, 2009.
- [44] Khan Ahsan Ali, Mohd Ali Munira, Mohd ShaffiarNorhashimah, “*Relationship of Surface Roughness with Current and Voltage during WEDM*”, J. of Appl. Sci., vol. 6, Issue 10, pp. 2317-2320, 2006.
- [45] S. H. Lee and X. P. Li, “*Study of the Effect of Machining Parameters on the Machining Characteristics in Electrical Discharge Machining of Tungsten Carbide*”, J. of Mat. Process. Tech., vol. 115, Issue 3, pp.344-358, 24 Sep. 2001.
- [46] M. R. Delpreti, “*Physical and Chemical Characteristics of Super Facial Layers*”, Proc. of ISEM-5, pp.209–212, 1977.
- [47] M. Motoki and C. Lee, “*Electro Spark Machining Using Trapezoidal Power Supply*,” Electroch. Eng., Japan, vol. 8, Issue 3, pp.12–20, 1968.
- [48] P. Narender Singh, K. Raghukandan, M. Rathinasabapathi and B. C. Pai, “*Electric Discharge Machining of Al-10%SiC as-Cast Metal Matrix Composites*”, J. of Mat. Process. Tech, pp. 1653-1657, 2004.
- [49] F. Kolahan and M. Bironro, “*Modelling and Optimization of Process Parameters in PMEDM by Genetic Algorithm*”, World Acad. of Sci., Eng. and Tech., vol. 48, 2008.
- [50] M. R. Shabgard and R. M. Shotorbani, “*Mathematical Modelling of Machining Parameters in Electrical Discharge Machining of FW4 Welded Steel*”, World of Sci. and Tech., vol. 52, 2009.
- [51] A. Hascalik and U. Cayday, “*Electrical-Discharge Machining of Titanium Alloy (Ti-6Al-4V)*”, Appl. Surf. Sci., vol. 253, Issue 22, p.9007-9016, May 2007.
- [52] A. Rooks, “*Dress for Success*”, vol. 60, issue 10, Oct. 2008.
- [53] Complete EDM Handbook: Overcut, www.ReliableEDM.com.
- [54] M. Boujelbene et al., “*Influence of Machining Parameters on the Surface Integrity in Electrical Discharge Machining*”, Archiv. of Mat. Sci. and Eng. 37/2, pp.110-116, 2009.

- [55] G. Levy Et al., “WED Machinability Comparison of Different Steel Grades”, Ann of CIRP, vol. 39 Issue 1, pp.183–186, 1990.
- [56] R. H. Lochner and J. E. Matar, “*Designing for quality; an introduction to the best of Taguchi and Western methods of statistical experiment design*”, Chapman and Hall, New York 1990.
- [57] W. J. Diamond, “*Practical experiment design for engineers and scientists*”, 3th ed. John Wiley & Sons. New York, 2001.
- [58] D. C. Montgomery, “*Design and Analysis of Experiments*” NJ: John Wiley & Sons, 2005.
- [59] G. Tosun and M. Muratoglu, “*The Drilling of an Al/SiCp Metal-Matrix Composites. Part I: Microstructure*”, Compo. Sci. and Tech., vol. 64, Issue 2, pp. 299-308, Feb. 2004.
- [60] H. Persson, “*Machining guidelines of Al/SiC particulate MMC*”, MMC-Assess Consortium, vol. 6, Jul. 2001.
- [61] M. Kiyaka and O. Çakır, “*Examination of Machining Parameters on Surface Roughness in EDM of Tool Steel*”, J. of Mat. Process. Tech., vol. 191, Issues 1-3, pp. 141-144, 1 Aug. 2007.
- [62] Y. H. Guu H. Hocheng, C. Y. Chou and C. S. Deng, “*Effect of Electrical Discharge Machining on Surface Characteristics and Machining Damage of AISI D2 tool steel*”, Mat. Sci. and Eng. A358, pp. 37-43, 2003.
- [63] Biing Hwa Yan, Hsien Chung Tsai, Fuang Yuan Huang and Long Chorng Lee, “*Examination of Wire Electrical Discharge Machining of Al₂O₃p/6061Al Composites*”, Int. J. of Mach. Tools and Manuf. vol. 45, Issue 3, Mar. 2005, pp. 251-259.
- [64] Shruti Mehta, Avadhoot Rajurkarand Jignesh Chauhan, “*A Review on Current Research Trends in Die-Sinking Electrical Discharge Machining of Conductive Ceramics*”, Int. J. of Recent Trends in Eng., vol. 1, No. 5, May 2009.
- [65] B. Mohana, A. Rajaduraib and K.G. Satyanarayana, “*Electric discharge machining of Al–SiC metal matrix composites using rotary tube electrode*”, Journal of Materials Processing Technology Volumes 153-154, 10 November 2004, Pages 978-985.

- [66] P. Cichosz and P. Karolczak, “*Sinker EDM of Aluminum Metal Matrix Composite*”, *Inst. of Prod. Eng. & Automa.*, vol. 26, No 3, 2008.
- [67] G. Krishna Mohana Rao, S. Satyanarayana, M Praveen, “*Influence of Machining Parameters on Electric Discharge Machining of Maraging Steels– An Experimental Investigation*”, *Proc. of the World Congr. on Eng.*, vol. 2, WCE, London, U.K, 2008.
- [68] Khanra A K and Pathak, L.C. and Godkhindi M.M., “*Application of new Tool Material for Electrical Discharge Machining (EDM)*”, *Bull. Mat. Sci.*, vol. 32, pp. 401–405, Aug. 2009.
- [69] P. Janmanee and A. Muttamara, “*Performance of Difference Electrode Materials in Electrical Discharge Machining of Tungsten Carbide*”, *Energ. Resear. J.* 1 (2): 87-90, 2010.
- [70] M. Kumar P. and C. B. Kumar, “*Modelling of Machining Parameters for MRR in EDM using Response Surface Methodology*”, *Proc. of NCMSTA’08 Conf.* Nov. 13-14, 2008.
- [71] Mitsubishi Electric Corporation, *Operation and Maintenance Manual*, EA Series NC-EDM System, 2001.
- [72] D. C. Montgomery, “*The Design and Analysis of Experiments*”, 4th Ed. New York: John Wiley and Sons, 1997.
- [73] W. M. Peter, “*Statistical Design and Analysis of Experiment*”, New York: Macmillan, 1971.
- [74] Design-Expert Software, Version 7.1, *User’s Guide, Technical Manual*, Stat-Ease Inc., Minneapolis, MN 55413-2726, 2007.
- [75] H. Singh and R. Gar, “*Effects of Process Parameters on Material Removal Rate in WEDM*”, *J. of Achiev. in Mat. and Manuf. Eng.*, vol. 32, Issue 1, Jan. 2009.
- [76] J. Marafona and C. Wykes, “*New Method of Optimization Material Removal Rate Using EDM with Copper-Tungsten Electrodes*”, *Int. J. of Mach. & Manuf.*, vol. 40, pp. 153-164, 2000.

APPENDIXES

Appendix A: Results Recorded on AMMC and Al 6061

Appendix A-1: Result on Ra due to change in peak current

Run No	Parameters			Responses	
	Peak current (A)	ON-time (μ s)	OFF-time (μ s)	Ra (μ m)	
				AMMC	Al 6061
Peak current varies, ON-time and OFF-time are fixed					
1	3	16	8	9.92	3.36
2	5.5	16	8	10.15	3.94
3	10	16	8	12.28	4.81
4	15	16	8	13.43	6.59
5	25	16	8	24.59	9.06
6	35	16	8	30.87	10.88
7	55	16	8	36.41	12.51

Appendix A-2: Result on Ra due to change in ON-time

Run No	Parameters			Responses	
	Peak current (A)	ON-time (μ s)	OFF-time (μ s)	Ra (μ m)	
				AMMC	Al 6061
ON-time varies, peak current and OFF-time are fixed					
1	15	3	8	7.39	3.93
2	15	6	8	8.13	4.87
3	15	12	8	9.16	5.91
4	15	24	8	19.16	7.93
5	15	48	8	22.6	9.02
6	15	96	8	32.53	11.30
7	15	192	8	37.95	11.76

Appendix A-3: Result on Ra due to change in OFF-time

Run No	Parameters			Responses	
	Peak current (A)	ON-time (μ s)	OFF-time (μ s)	Ra (μ m)	
				AMMC	Al 6061
OFF-time varies, peak current and ON-time are constant					
1	15	16	3	34.42	8.05
2	15	16	4	21.68	7.36
3	15	16	6	18.52	7.17
4	15	16	12	11.51	6.99
5	15	16	24	10.59	6.86
6	15	16	48	9.36	6.08
7	15	16	96	7.99	5.84

Appendix A-4: Result on MRR due to change in peak current

Run No	Parameters			Responses			
	Peak current (A)	ON-time (μ s)	OFF-time (μ s)	MRR (g/min)		Machining time (min)	
				AMMC	Al 6061	AMMC	Al 6061
Peak current varies, ON-time and OFF-time are constant							
1	3	16	8	0.017	0.022	119.20	68.35
2	5.5	16	8	0.020	0.023	110.05	65.55
3	10	16	8	0.037	0.067	60.28	22.46
4	15	16	8	0.050	0.167	42.31	18.12
5	25	16	8	0.068	0.169	36.28	8.9
6	35	16	8	0.079	0.223	32.66	6.78
7	55	16	8	0.106	0.276	29.92	5.38

Appendix A-5: Result on MRR due to change in ON-time

Run No	Parameters			Responses			
	Peak current (A)	ON-time (μ s)	OFF-time (μ s)	MRR (g/min)		Machining time (min)	
				AMMC	Al 6061	AMMC	Al 6061
ON-time varies, peak current and OFF-time are constant							
1	15	3	8	0.026	0.04	53.08	33.55
2	15	6	8	0.034	0.06	43.70	24.3
3	15	12	8	0.044	0.09	42.43	16.33
4	15	24	8	0.045	0.12	40.03	12.06
5	15	48	8	0.052	0.14	39.55	10.68
6	15	96	8	0.068	0.15	37.18	10.56
7	15	192	8	0.09	0.17	29.92	9.05

Appendix A-6: Result on MRR due to change in OFF-time

Run No	Parameters			Responses			
	Peak current (A)	ON-time (μ s)	OFF-time (μ s)	MRR (g/min)		Machining time (min)	
				AMMC	Al 6061	AMMC	Al 6061
OFF-time varies, peak current and ON-time are constant							
1	15	16	3	0.073	0.131	38.15	11.58
2	15	16	4	0.063	0.124	39.18	12.18
3	15	16	6	0.052	0.110	45.78	13.63
4	15	16	12	0.037	0.100	49.16	15.82
5	15	16	24	0.035	0.070	50.51	21.56
6	15	16	48	0.02	0.040	85.28	36.68
7	15	16	96	0.01	0.020	160.65	69.86

Appendix A-7: Result on TWR due to change in peak current

Run No	Parameters			Responses	
	Peak current (A)	ON-time (μ s)	OFF-time (μ s)	TWR (%)	
				AMMC	Al 6061
Peak current varies, ON-time and OFF-time are fixed					
1	3	16	8	2.103	15.49
2	5.5	16	8	2.979	10.60
3	10	16	8	11.034	9.28
4	15	16	8	7.625	3.53
5	25	16	8	1.64	4.99
6	35	16	8	0.231	3.54
7	55	16	8	0.19	4.61

Appendix A-8: Result on TWR due to change in ON-time

Run No	Parameters			Responses	
	Peak current (A)	ON-time (μ s)	OFF-time (μ s)	TWR (%)	
				AMMC	Al 6061
ON-time varies, peak current and OFF-time are constant					
1	15	3	8	117.550	36.620
2	15	6	8	97.801	22.84
3	15	12	8	34.331	10.210
4	15	24	8	33.832	4.250
5	15	48	8	0.156	2.310
6	15	96	8	0.107	0.140
7	15	192	8	0.084	0.580

Appendix A-9: Result on TWR due to change in OFF-time

Run No	Parameters			Responses	
	Peak current (A)	ON-time (μ s)	OFF-time (μ s)	TWR (%)	
				AMMC	Al 6061
OFF-time varies, peak current and ON-time are constant					
1	15	16	3	0.251	6.240
2	15	16	4	0.937	6.300
3	15	16	6	0.522	6.510
4	15	16	12	33.448	7.890
5	15	16	24	56.237	8.390
6	15	16	48	70.777	9.790
7	15	16	96	77.826	10.540

Appendix A-10: Result on OC due to change in peak current

Run No	Parameters			Responses	
	Peak current (A)	ON-time (μ s)	OFF-time (μ s)	Overcut (mm)	
				AMMC	Al 6061
Peak current varies, ON-time and OFF-time are constant					
1	3	16	8	0.150	0.060
2	5.5	16	8	0.160	0.080
3	10	16	8	0.170	0.080
4	15	16	8	0.175	0.090
5	25	16	8	0.270	0.110
6	35	16	8	0.315	0.120
7	55	16	8	0.320	0.130

Appendix A-11: Result on OC due to change in ON-time

Run No	Parameters			Responses	
	Peak current (A)	ON-time (μ s)	OFF-time (μ s)	Overcut (mm)	
				AMMC	Al 6061
ON-time varies, peak current and OFF-time are constant					
1	15	3	8	0.135	0.055
2	15	6	8	0.145	0.080
3	15	12	8	0.150	0.091
4	15	24	8	0.165	0.113
5	15	48	8	0.255	0.120
6	15	96	8	0.320	0.125
7	15	192	8	0.325	0.140

Appendix A-12: Result on OC due to change in OFF-time

Run No	Parameters			Responses	
	Peak current (A)	ON-time (μ s)	OFF-time (μ s)	Overcut (mm)	
				AMMC	Al 6061
OFF-time varies, peak current and ON-time are constant					
1	15	16	3	0.275	0.112
2	15	16	4	0.215	0.103
3	15	16	6	0.175	0.100
4	15	16	12	0.150	0.097
5	15	16	24	0.140	0.095
6	15	16	48	0.135	0.075
7	15	16	96	0.075	0.058

Appendix B: Sequential and ANOVA Tables for AMMC and Al 6061

Appendix B-1: Sequential model for Ra of AMMC

Sequential Model: Ra						
Source	Sum of Squares	df	Mean Square	F Value	p-value Prob > F	
Mean Vs. Total	6732.98	1	6732.98			
Block Vs. Mean	54.12	2	27.06			
Linear Vs. Block	1678.73	3	559.58	17.23	< 0.0001	Suggested
2FI Vs. Linear	0.000	0				Aliased
Quadratic Vs. 2FI	196.33	3	65.44	2.79	0.0906	Aliased
Cubic Vs. Quadratic	155.18	3	51.73	4.01	0.0517	Aliased
Residual	103.25	8	12.91			
Total	8920.59	20	446.03			

Appendix B-2: Sequential model for RA of Al 6061

Sequential Model: Ra						
Source	Sum of Squares	df	Mean Square	F Value	p-value Prob > F	
Mean Vs. Total	1078.3	1	1078.39			
Block Vs. Mean	8.41	2	4.21			
Linear Vs. Block	113.02	3	37.67	29.24	< 0.0001	Suggeste
2FI Vs. Linear	0.000	0				Aliased
Quadratic Vs. 2FI	14.32	3	4.77	14.12	0.0004	Aliased
Cubic Vs. Quadratic	2.67	3	0.89	6.81	0.0136	Aliased
Residual	1.05	8	0.13			
Total	1217.8	20	60.89			

Appendix B-3: ANOVA table for Ra of AMMC

Response 1 : Ra						
Source	Sum of Squares	df	Mean Squares	F Value	Prob Value>F	
Block	54.12	2	27.06			
Model	1678.73	3	559.58	17.23	< 0.0001	Significant
A: Peak current	819.37	1	819.37	25.22	0.0002	
B: ON-time	426.80	1	426.80	13.14	0.0028	
C: OFF-time	190.52	1	190.52	5.87	0.0296	
Residual	454.76	14	32.48			
Cor. Total	2187.61	19				
Std. Dev.	5.70	R-Squared	0.7868			
Mean	18.35	Adj R-Squared	0.7412			
C.V. %	31.06	Pred R-Squared	0.3096			
PRESS	1472.98	Adeq Precision	11.830			

Where:

Cor. Total: total corrected to the mean

Std. Dev.: standard deviation

C.V. %: coefficient of variation

PRESS: predicted error of sum of squared

R-Squared: regression squared

Adj R-Squared: adjusted squared

Adeq Precision: adequate precision

Appendix B-4: ANOVA table for Ra of Al 6061

Response 1 : Ra						
Source	Sum of Squares	df	Mean Squares	F Value	Prob Value>F	
Block	8.41	4.21	37.67			
Model	113.02	73.71	28.7	29.24	< 0.0001	significant
A: Peak current	73.71	2.6	1.29	57.22	< 0.0001	
B: ON-time	28.7	4.21	37.67	22.28	0.0003	
C: OFF-time	2.6	73.71	28.7	2.02	0.1771	
Residual	18.04	2.6	1.29			
Cor. Total	139.47	19				
Std. Dev.	1.14	R-Squared	0.8624			
Mean	7.34	Adj R-Squared	0.8329			
C.V. %	15.46	Pred R-Squared	0.3894			
PRESS	80.02	Adeq Precision	15.24			

Appendix B-5: Sequential table for MRR of AMMC

Sequential model: MRR						
Source	Sum of Squares	df	Mean Square	F Value	p-value Prob > F	
Mean Vs. Total	0.046	1	0.046			
Block Vs. Mean	1.080x10 ⁻⁴	2	5.4x10 ⁻⁵			
Linear Vs. Block	0.011	3	3.82x10 ⁻³	50.21	< 0.0001	Suggested
2FI Vs. Linear	0.000	0				Aliased
Quadratic Vs. 2FI	4.908x10 ⁻⁴	3	1.63x10 ⁻⁴	3.13	0.0697	Aliased
Cubic Vs. Quadratic	2.991x10 ⁻⁴	3	9.96x10 ⁻⁵	2.89	0.1021	Aliased
Residual	2.758x10 ⁻⁴	8	3.44x10 ⁻⁵			
Total	0.059	20	2.95x10 ⁻³			

Appendix B-6: Sequential table for MRR of AI 6061

Sequential model: MRR						
Source	Sum of Squares	df	Mean Square	F Value	p-value Prob > F	
Mean Vs. Total	0.24	1	0.24			
Block Vs. Mean	1.75x10 ⁻³	2	8.75x10 ⁻⁴			
Linear Vs. Block	0.079	3	0.026	30.58	< 0.0001	Suggested
2FI Vs. Linear	0.000	0				Aliased
Quadratic Vs. 2FI	6.044x10 ⁻³	3	2.01x10 ⁻³	3.65	0.0480	Aliased
Cubic Vs. Quadratic	3.215x10 ⁻³	3	1.07x10 ⁻³	2.99	0.0956	Aliased
Residual	2.865x10 ⁻³	8	3.58x10 ⁻⁴			
Total	0.33	20	0.017			

Appendix B-7: ANOVA table for MRR of AMMC

Response 2: MRR						
Source	Sum of Squares	df	Mean Square	F Value	p-value Prob > F	
Block	1.08x10 ⁻⁴	2	5.4x10 ⁻⁵			
Model	0.011	3	3.822x10 ⁻³	50.21	< 0.0001	significant
A-Peak current	6.67x10 ⁻³	1	6.678x10 ⁻³	87.74	0.0001	
B-ON-time	1.55x10 ⁻³	1	1.551x10 ⁻³	20.37	0.0005	
C-OFF-time	1.82x10 ⁻³	1	1.828x10 ⁻³	24.01	0.0002	
Residual	1.06x10 ⁻³	14	7.612x10 ⁻⁵			
Cor. Total	0.013	19				
Std. Dev.	8.725x10 ⁻³		R-Squared	0.9150		
Mean	0.048		Adj R-Squared	0.8967		
C.V. %	18.12		Pred R-Squared	0.7265		
PRESS	3.42710 ⁻³		Adeq Precision	22.396		

Appendix B-8: ANOVA table for MRR of Al 6061

Response 2: MRR						
Source	Sum of Squares	df	Mean Square	F Value	p-value Prob > F	
Block	1.75x10 ⁻³	2	8.751x10 ⁻⁴			
Model	0.079	3	0.026	30.58	< 0.0001	significant
A-Peak current	0.060	1	0.060	69.07	0.0001	
B-ON-time	6.33x10 ⁻³	1	6.334x10 ⁻³	7.31	0.0171	
C-OFF-time	7.61x10 ⁻³	1	7.618x10 ⁻³	8.80	0.0102	
Residual	0.012	14	8.660x10 ⁻⁴			
Cor. Total	0.093	19				
Std. Dev.	0.029	R-Squared	0.8676			
Mean	0.11	Adj R-Squared	0.8392			
C.V. %	26.91	Pred R-Squared	0.6118			
PRESS	0.036	Adeq Precision	18.058			

Appendix B-9: Sequential model table for TWR of AMMC

Sequential Model: TWR						
Source	Sum of Squares	df	Mean Square	F Value	p-value Prob > F	
Mean Vs. Total	13093.07	1	13093.07			Suggested
Block Vs. Mean	4328.09	2	2164.04			
Linear Vs. Block	8655.28	3	2885.09	5.15	<0.0132	Suggested
2FI Vs. Linear	0.000	0				Aliased
Quadratic Vs. 2FI	3959.64	3	1319.88	3.74	0.0450	Aliased
Cubic Vs. Quadratic	2687.64	3	895.88	5.99	0.0192	Aliased
Residual	1196.83	8	149.60			
Total	33920.54	20	1696.03			

Appendix B-10: Sequential model table for TWR of Al 6061

Sequential Model: TWR						
Source	Sum of Squares	df	Mean Square	F Value	p-value Prob > F	
Mean Vs. Total	1590.44	1	1590.44			Suggested
Block Vs. Mean	175.65	2	87.82			
Linear Vs. Block	361.76	3	120.59	2.13	0.1425	Suggested
2FI Vs. Linear	0.000	0				Aliased
Quadratic Vs. 2FI	265.18	3	88.39	1.84	0.1981	Aliased
Cubic Vs. Quadratic	367.54	3	122.51	6.10	0.0183	Aliased
Residual	160.59	8	20.07			
Total	2921.15	20	146.06			

Appendix B-11: ANOVA table for TWR of AMMC

Response 2: MRR						
Source	Sum of Squares	df	Mean Square	F Value	p-value Prob > F	
Block	4859.237	2	2429.61			
Model	10433.93	3	3477.97	75.2991	< 0.0001	significant
A: Peak current	27.67226	1	27.6722	139.377	0.0001	
B:ON-time	6181.902	1	6181.90	59.9422	0.0001	
C: OFF-time	4224.363	1	4224.36	26.5782	0.0001	
Residual	8761.268	14	625.804			
Cor. Total		19				
Std. Dev.	23.67	R-Squared	0.5246			
Mean	25.59	Adj R-Squared	0.4227			
C.V. %	92.51	Pred R-Squared	-0.5346			
PRESS	25319.48	Adeq Precision	8.183			

Appendix B-12: ANOVA table for TWR of AI 6061

Response 2: MRR						
Source	Sum of Squares	df	Mean Square	F Value	p-value Prob > F	
Block	246.67	2	123.34			
Model	123.37	3	41.12	60.64	< 0.0001	significant
A: Peak current	113.58	1	113.58	167.48	< 0.0001	
B:ON-time	9.923x10 ⁻³	1	9.923x10 ⁻³	0.015	0.9054	
C: OFF-time	9.78	1	9.78	14.43	0.0020	
Residual	9.49	14	0.68			
Cor. Total	379.54	19				
Std. Dev.	0.82	R-Squared	0.9285			
Mean	4.90	Adj R-Squared	0.9132			
C.V. %	16.82	Pred R-Squared	0.8734			
PRESS	16.82	Adeq Precision	33.767			

Appendix B-13: Sequential table for OC of AMMC

Sequential model: OC						
Source	Sum of Squares	df	Mean Square	F Value	p-value Prob > F	
Mean Vs. Total	0.80	1	0.80			
Block Vs. Mean	4.185x10 ⁻⁴	2	2.09x10 ⁻⁴			
Linear Vs. Block	0.095	3	0.032	23.65	< 0.0001	Suggested
2FI Vs. Linear	0.000	0				Aliased
Quadratic Vs. 2FI	9.158x10 ⁻³	3	3.05x10 ⁻³	3.49	0.0536	Aliased
Cubic Vs. Quadratic	5.029x10 ⁻³	3	1.67x10 ⁻³	2.92	0.1002	Aliased
Residual	4.591x10 ⁻³	8	5.73x10 ⁻⁴			
Total	0.92	20	0.046			

Appendix B-14: Sequential table for OC of AI 6061

Sequential model: OC						
Source	Sum of Squares	df	Mean Square	F Value	p-value Prob > F	
Mean Vs. Total	4.24x10 ⁻⁴	2	2.12x10 ⁻⁴			
Block Vs. Mean	8.752x10 ⁻³	3	2.91x10 ⁻³	18.64	< 0.0001	Suggested
Linear Vs. Block	0.000	0				Aliased
2FI Vs. Linear	1.186x10 ⁻³	3	3.95x10 ⁻⁴	4.32	0.0304	Aliased
Quadratic Vs. 2FI	6.737x10 ⁻⁴	3	2.24x10 ⁻⁴	5.41	0.0251	Aliased
Cubic Vs. Quadratic	3.320x10 ⁻⁴	8	4.15x10 ⁻⁵			
Residual	0.20	20	9.94x10 ⁻³			
Total	4.243x10 ⁻⁴	2	2.12x10 ⁻⁴			

Appendix B-15: ANOVA table for overcut of AMMC

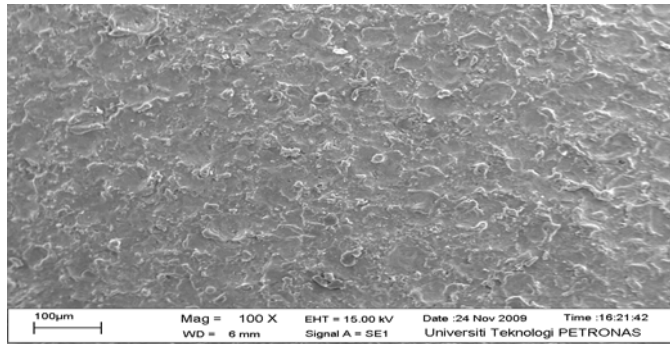
Response 4 : Overcut						
Source	Sum of Squares	df	Mean Square	F Value	p-value Prob > F	
Block	4.18x10 ⁻⁴	2	2.09x10 ⁻⁴			
Model	0.095	3	0.032	23.65	< 0.0001	significant
A: Peak current	0.040	1	0.040	30.10	0.0001	
B: ON-time	0.024	1	0.024	17.97	0.0008	
C: OFF-time	0.015	1	0.015	10.99	0.0051	
Residual	0.019	14	1.34x10 ⁻³			
Cor. Total	0.11	19				
Std. Dev.	0.037	R-Squared	0.8352			
Mean	0.20	Adj R-Squared	0.7999			
C.V. %	18.29	Pred R-Squared	0.3797			
PRESS	0.071	Adeq Precision	14.796			

Appendix B-16: ANOVA table for overcut of Al 6061

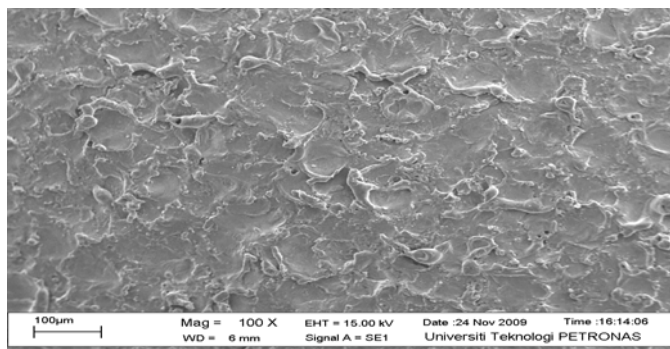
Response 4 : Overcut						
Source	Sum of Squares	df	Mean Square	F Value	p-value Prob > F	
Block	4.243x10 ⁻⁴	2	2.12x10 ⁻⁴			
Model	8.752x10 ⁻³	3	2.91x10 ⁻³	18.64	< 0.0001	significant
A: Peak current	3.223x10 ⁻³	1	3.22x10 ⁻³	20.58	0.0005	
B: ON-time	2.137x10 ⁻³	1	2.13x10 ⁻³	13.65	0.0024	
C: OFF-time	1.751x10 ⁻³	1	1.75x10 ⁻³	11.18	0.0048	
Residual	2.192x10 ⁻³	14	1.56x10 ⁻⁴			
Cor. Total	0.011	19				
Std. Dev.	0.013		R-Squared	0.7997		
Mean	0.097		Adj R-Squared	0.7568		
C.V. %	12.92		Pred R-Squared	0.3567		
PRESS	7.04X10 ⁻³		Adeq Precision	13.803		

Appendix C: Effects of EDM on Surface Morphology of Al 6061

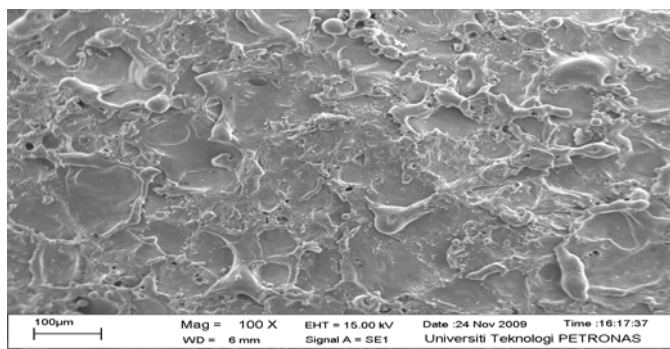
Appendix C1- Effect of Peak Current on Surface Morphology



SEM micrograph of machined surface
(Peak current: 3A, ON-time: 3µs, OFF-time: 8µs)

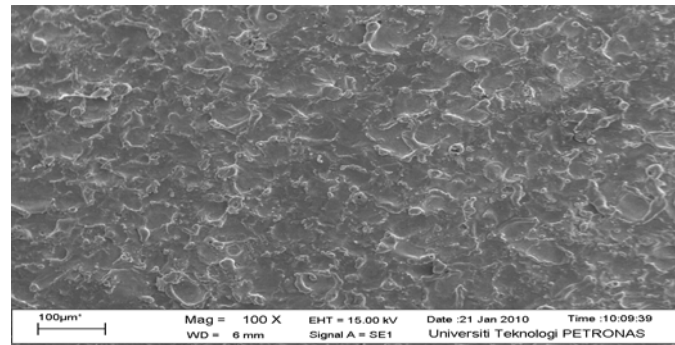


SEM micrograph of machined surface
(Peak current: 10A, ON-time: 12µs, OFF-time: 8µs)

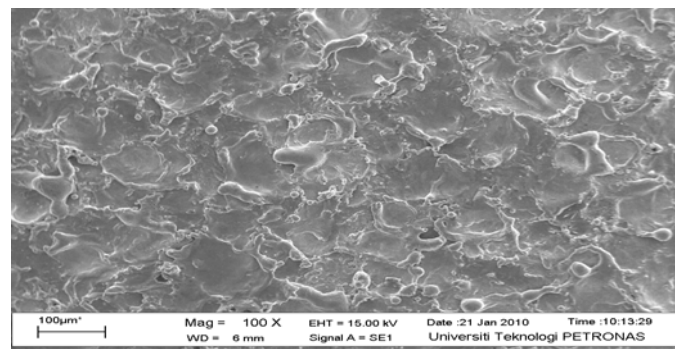


SEM micrograph of machined surface
(Peak current: 25A, ON-time: 48µs, OFF-time: 8µs)

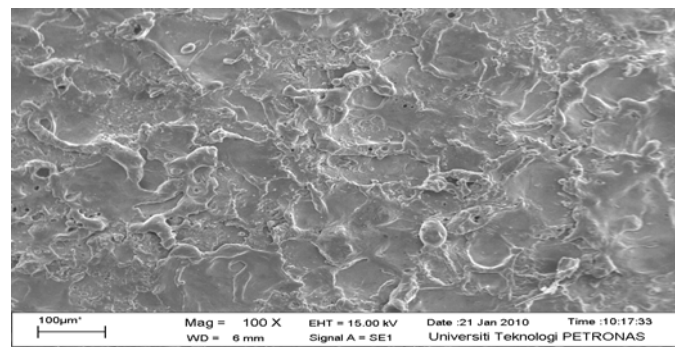
Appendix C2- Effect of ON-time on Surface Morphology



SEM micrograph of machined surface
(Peak current: 15A, ON-time: 3 μ s, OFF-time: 8 μ s)

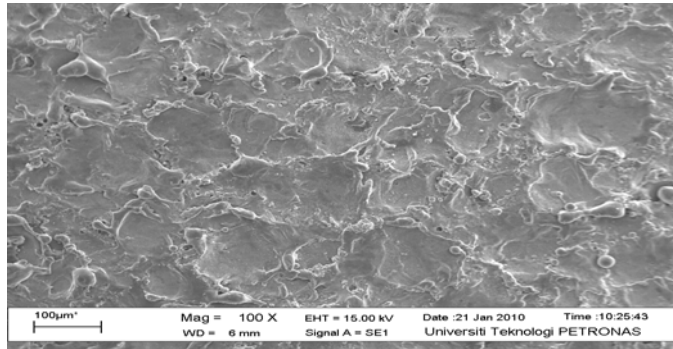


SEM micrograph of machined surface
(Peak current: 15A, ON-time: 12 μ s, OFF-time: 8 μ s)



SEM micrograph of machined surface
(Peak current: 15A, ON-time: 48 μ s, OFF-time: 8 μ s)

Appendix C3- Effect of OFF-time on Surface Morphology



SEM micrograph of machined surface
(Peak current: 15A, ON-time: 16µs, OFF-time: 3µs)

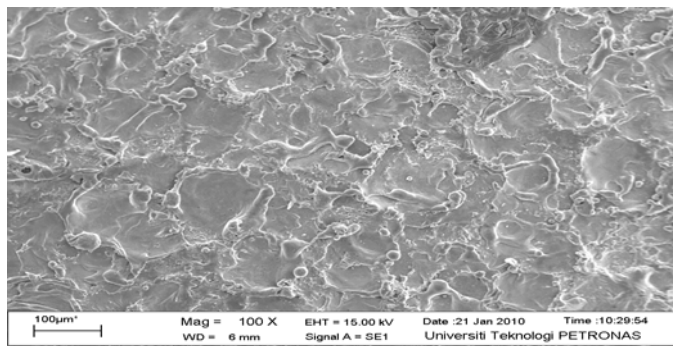


Figure C5: SEM micrograph of machined surface.
(Peak current: 15A, ON-time: 16µs, OFF-time: 6µs)

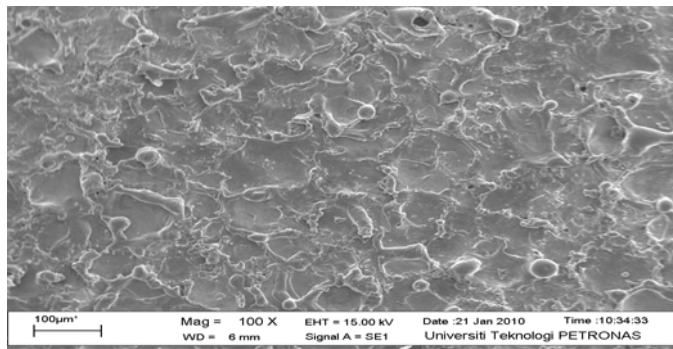


Figure C6: SEM micrograph of machined surface.
(Peak current: 15A, ON-time: 16µs, OFF-time: 24µs)